SULFUR POISONING OF HYDROCARBON OXIDATION BY PALLADIUM

by

Arthur James Baumgartner

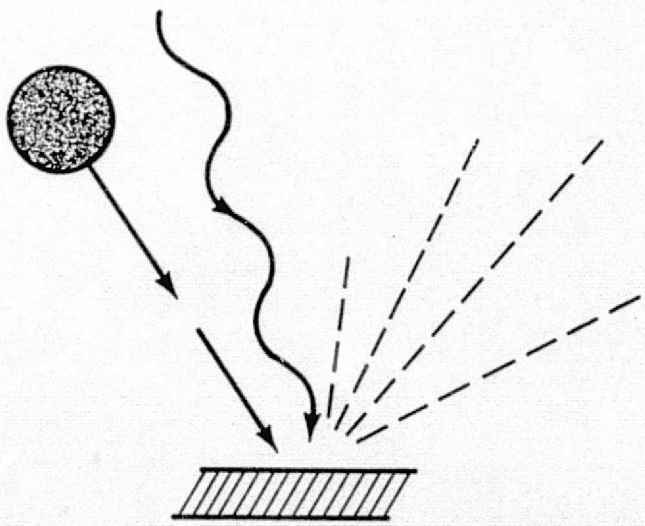

Sulfur Poisoning of Hydrocarbon Oxidation by Palladium

By

Arthur James Baumgartner

B.S. (California State University, Bakersfield) 1974

THESIS

Submitted in partial satisfaction of the requirements for the degree of

MASTER OF SCIENCE

in

Chemical Engineering

in the

GRADUATE DIVISION

of the

UNIVERSITY OF CALIFORNIA, BERKELEY

Approved:

Robert P. Merrill

Robert J. Sawyer

Clayton J. Radke

Committee in Charge

.....

Abstract

Using a differential bed recycle reactor the oxidation of ethane ∿(200-320°C) and diethyl ketone ∿(110-190°C) by a Pd catalyst has been studied at the 0-30 ppm level in air. In both cases first order kinetics were observed. The ethane oxidation rate was characterized in the Arrhenius form by a pre-exponential of 1.0×10^8 cm/sec and an E_a of 27 kcal/mole. The diethyl ketone oxidation rate was characterized by a pre-exponential of 5.7×10^3 cm/sec and and E_a of 14 kcal/mole.

Poisoning of ethane oxidation was also investigated (250-310°C), by hydrogen sulfide and to a smaller extent by the refrigerants Freon 22 and Gentron 142-B at ∿ 247°C. Poisoning by Gentron 142-B was much more severe than by hydrogen sulfide. Kinetic experiments indicated that only the pre-exponential was changing. Low pressure CO adsorption measurements after each of the hydrogen sulfide poisoning experiments showed that the pre-exponential was dependent upon the clean Pd surface area.

Acknowledgement

The author wishes to acknowledge the assistance and encouragement of Professor Robert P. Merrill who directed this study.

This research project was funded by a grant from the National Aeronautics and Space Administration (Grant #NASA NGR 05-003-478).

Table of Contents

Page number

Introduction 1
Background 2
Apparatus and Procedures 6
Procedures 12
Kinetic Experiments 14
I. Concentration Dependence 14
II. Temperature Dependence 16
Preliminary Sulfur Adsorption and Reaction Experiments 16
Surface Area Measurements 18
Adsorption Calculations 19
I. N_2 Adsorption 19
II. CO Adsorption 19
Results 21
I. Ethane Oxidation Kinetics 21
II. Diethyl Ketone Oxidation Kinetics 30
III. Hydrogen Sulfide Poisoning 35
Discussion 55
I. Intrinsic Kinetics 55
1. Ethane Oxidation 55
2. Diethyl Ketone Oxidation 57
3. Comparsion of Ethane and Diethyl Ketone Oxidation Rates 58
4. Mechanism and Predicted Pre-exponentials of Hydrocarbon Oxidation on Noble Metals 59
II. Hydrogen Sulfide Poisoning 60
1. First Catalyst Load 60
2. Second Catalyst Load 64
3. Comparsion of Hydrogen Sulfide Poisoning Observed in This Work with Other Work in This Laboratory 67
4. Comparsion of Freon and Hydrogen Sulfide Poisoning of the First Catalyst Load 69
References 72

Appendix 1.
Tracer Experiments..... 75
Appendix 2.
Thermal Conductivity Cell Response..... 78
Appendix 3.
Flame Photometric Dectector Response..... 82
Appendix 4.
Equations Used in Calculations..... 88
Appendix 5.
Adsorption of Ethane on the Catalyst..... 96
Appendix 6.
Hydrogen Sulfide Oxidation and Removal by the Apparatus..... 103
Low Level Hydrogen Sulfide Oxidation..... 103
Low Level Hydrogen Sulfide Removal by the Reactor Feed Tubing..... 103
Appendix 7.
Poisoning of the Ethane Oxidation Reaction by Halogenated Hydrocarbons..... 108
Poisoning of Ethane Oxidation by Freon 22..... 108
Poisoning of Ethane Oxidation by Gentron 142B.. 113
Appendix 8.
Oxidation and Removal of Ethane and Hydrogen Sulfide by the Catalyst Support..... 119
Ethane Removal..... 119
Hydrogen Sulfide Oxidation..... 122
Appendix 9.
Diffusion Limitations..... 124
Appendix 10.
Reaction Heating of the Catalyst Pellets..... 129
Appendix 11.
Description of Catalyst and Gases 131
Appendix 12
Gas Chromatograph Data 133

List of Figures

Figure Number	Title	Page Number
1	Overall equipment schematic.	7
2	Recycle reactor.	8
3	Steady state reaction order runs, first catalyst load, 200-300°C.	22
4	Arrhenius plot of the lower activity data presented in figure 3.	25
5	Arrhenius plot of data taken before the hydrogen sulfide poisoning.	26
6	Arrhenius plot, 210-300°C on 0.17 grams of catalyst.	28
7	Unsteady state reaction order runs on the second catalyst load, 1.66 grams, mole fraction ethane versus time.	29
8	Self poisoning of diethyl ketone oxidation, first order rate coefficient vs time.	32
9	Diethyl ketone oxidation at 137°C.	33
10	Arrhenius plot for diethyl ketone oxidation.	34
11	Hydrogen sulfide poisoning of the first catalyst load.	38
12	Unsteady state behavior of third poisoning series for 59 μ mole injections.	39
13	Unsteady state behavior of the first injection on the fourth poisoning series 184.1 μ mole injection.	40
14	Adsorption-desorption of CO after third poisoning series and before high temperature outgassing.	45
15	Sulfur dioxide desorption rate in flowing helium, 0.40 cm^3/sec.	46

List of Figures (continued)

Figure Number	Title	Page Number
16	Sulfur dioxide desorption during high temperature oxygen treatment.	47
17	Arrehenius plot for data on catalyst loads one and two, prior to hydrogen sulfide injections.	49
18	Hydrogen sulfide poisoning of the second catalyst load, 1.66 grams.	50
19	Unsteady state behavior, second catalyst load, after 1326 μ mole hydrogen sulfide injection.	53
20	Unsteady state behavior, second catalyst load, after 184 μ mole hydrogen sulfide injection.	54
21	Tracer experiments.	76
22	Thermal conductivity cell calibration for air-He mixtures.	80
23	Thermal conductivity cell calibration for CO-He mixtures.	81
24	Hydrogen sulfide calibration of flame photometric detector.	84
25	Flame photometric detector calibration.	86
26	Nonsteady state reaction order run, second catalyst load.	95
27	First ethane breakthrough on the first catalyst load, 1.1 grams.	97
28	Second ethane breakthrough on the first catalyst load, 1.1 grams.	98
29	Temperature programmed ethane desorption.	101
30	Hydrogen sulfide oxidation and removal in the reactor with no catalyst.	104

List of Figures (continued)

Figure Number	Title	Page Number
31	Hydrogen sulfide removal in reactor feed tubing.	105
32	First order plot of hydrogen sulfide removal in reactor feed tubing.	107
33	Arrehenius plot of data taken on the first catalyst load before and after the catalyst was poisoned by halogenated hydrocarbons.	110
34	Freon 22 poisoning of the first catalyst load.	112
35	Unsteady state behavior after a 13.6 μ mole Freon 22 injection.	114
36	Gentron 142B poisoning of the first catalyst load.	115
37	Unsteady state behavior after a 64.2 μ mole Gentron 142B injection.	117
38	Log plot of concentration vs reaction rate for ethane removal over the catalyst support at 502°C.	120
39	Arrehinus plot of data for the removal of ethane over the catalyst support 423-513°C.	121
40	Oxidation of a 15.1 μ mole hydrogen sulfide injection over 1.11 grams of the γ Al_2O_3 catalyst support.	123

Introduction

Adsorption and catalytic oxidation have been widely used to reduce impurities in gas streams.

These methods have been applied to effect the removal of a wide range of atmospheric trace contaminants present in the closed environments of submarines and space capsules. In space capsules, sorption and oxidation beds are arranged so that those molecules which do not adsorb pass through to the catalyst bed and the oxidation products are later adsorbed.

It is possible that this method of adsorption and oxidation can be exploited employing only one bed, a large bed of catalyst whose support acts as a sorption bed. This design requires an adsorptive support with a distribution of active metal in the bed or in each pellet such that catalytic poisons are adsorbed before they can cause serious deactivation of the bed.

One type of catalyst that is widely used for catalytic oxidation consists of a noble metal(s) supported on porous γ alumina pellets. This catalyst is very attractive because of (1) high activity, (2) stability, (3) ability to oxidize a wide range of contaminants, (4) the profile of the active metal can be adjusted during impregnation to minimize poisoning and mass transfer limitations, and (5) high adsorptivity, both for hydrocarbons and oxidation products as well as catalytic poisons. The catalyst investigated in this work was Pd on

γ alumina pellets and was prepared by Universal Oil Products Research Laboratory.

A knowledge of the kinetics governing the oxidation of individual contaminates as well as any kinetic interactions present during the simultaneous oxidation of a wide variety of compounds is needed for the design of a catalytic oxidizer. Evaluation of a suitable catalyst requires an investigation of its adsorptivity and the effect of the catalyst impregnation profile on activity and poisoning.

The oxidation rates of small molecular weight hydrocarbons, which are common trace contaminants, offer a convenient measure of catalyst oxidation activity and poisoning, since stable high oxidation rates can be achieved with these compounds. Much of the published data concerning the poisoning of hydrocarbon oxidation has been generated from integral catalyst beds. There are substantial difficulties and approximations in calculating intrinsic reaction rates from such data (1). Often little attention has been focused on the impregnation profile of the active metal or the surface area of the catalyst. It has been the approach of this work to measure the intrinsic oxidation kinetics of a simple hydrocarbon, ethane, and the effect of typical poisons on it using a catalyst whose surface area and impregnation profile are known. In a previous work in this laboratory by D.T. Rabb (2) an integral bed reactor was used to investigate the poisoning of a

commercial Pd on γ Al_2O_3 catalyst by hydrogen sulfide and ethyl mercaptan. Rabb also studied the adsorption and catalytic oxidation of ethane and diethyl ketone. In this work, as in Rabbs work, the rate of ethane oxidation was chosen as a measure of catalyst oxidation activity and poisoning. Catalyst poisoning in this work was investigated chiefly with hydrogen sulfide which was chosen as a representative sulfur containing air contaminant. The refrigerants Freon 22 and Gentron 142-B were selected as representive halocarbon air contaminants and catalyst poisoning by these compounds was investigated to a much lesser extent. In addition the oxidation kinetics of diethyl ketone, which was selected as a typical partially oxidized air contaminant, were investigated for comparison to ethane oxidation kinetics.

The experiments were performed with a differential bed recycle reactor equipped to carry out in situ surface area measurements. High gas recirculation ratios and a very shallow catalyst bed were used to attain continous flow stirred tank reactor, CFSTR, performance and eliminate concentration gradients in the catalyst bed.

Background

The most widely studied hydrocarbon for complete oxidation is methane, the reason being that it is the most difficult simple hydrocarbon to adsorb or oxidize . In one investigation (3), 26 catalysts were evaluated for

their effectiveness in oxidizing methane, palladium and platinum were found to be the most active. The scope of the literature on noble metal oxidation of methane includes kinetic data on low (4) and high (5) concentrations as well as poisoning by sulfur (6) and halogen (7) compounds.

To date many experimental approaches have been used to study systematically the kinetics and poisoning of one reaction, usually methane oxidation, over a variety of catalysts. Albeit there has been little published work done to elucidate a general reactivity pattern for hydrocarbon oxidation at low concentrations. Wise (8) systematically studied the oxidation of a wide variety of hydrocarbons over Pt and Pd at ~ 2 vol. % hydrocarbon and 20-40 vol. % oxygen at a total pressure of one atmosphere. The general empirical picture that emerges for the compounds studied is that the apparent activation energy, E_a, is controlled by the struture of the hydrocarbon such that for paraffins the E_a depends only on the most highly branched part of the molecule. The E_a decreases in order: primary > secondary > tertiary carbon. There is also an increase in the preexponential with increasing chain length. Oxygenated functional groups (-OH, C=O) tend to mask the carbon structure effect on the E_a and result in reaction rates much larger than their paraffinic

analogues*. Oxidation of all hydrocarbons using Pd exhibited first order kinetics.

*It should be mentioned that Wise didn't report the kinetics of methane oxidation and that the literature value of ~20 kcal/mole (3-5) doesn't fit into his pattern of E_a although the reactivity pattern remains the same due to a low preexponential.

Apparatus and Procedure

The equipment used for this work is represented in fig. 1. All catalytic measurements were made using a differential bed recycle reactor (fig. 2).

A constant volumetric feed rate to the reactor was established by throttling the gas flow from high pressure gas cylinders equipped with pressure regulators. Flows were metered through capillaries fitted with manometers. The pressure drops across the capillaries were linear with volumetric flowrate as predicted for laminar flow (9). The flowrate of each gas used was calibrated for pressure drop across a given capillary since the Hagen-Poiseuille equation (9) for laminar flow did not always give the correct magnitude for the measured flow rate. The manometer fluid was a silicon base oil, Dow Corning 704, which had been distilled in a diffusion pump before use. The residual vapor pressure of the oil at 25°C is reported to be 2×10^{-8} Torr (10).

Absolute pressures were measured by three detectors: (1) Bourdon tube gauge ($1\text{-}10^{3}$ Torr); (2) thermal conductivity gauge (10^{-3}-1 Torr); and (3) ion gauge (10^{-8}-10^{-3} Torr).

The valves, the pumping chamber and most of the tubing in the recycle loop were stainless steel. The reactor and gas preheater sections were quartz. The quartz and stainless steel sections were connected with pyrex glass tubing. Graded glass was used for pyrex-quartz transitions and Kovar for pyrex-stainless steel transitions. The valves and other

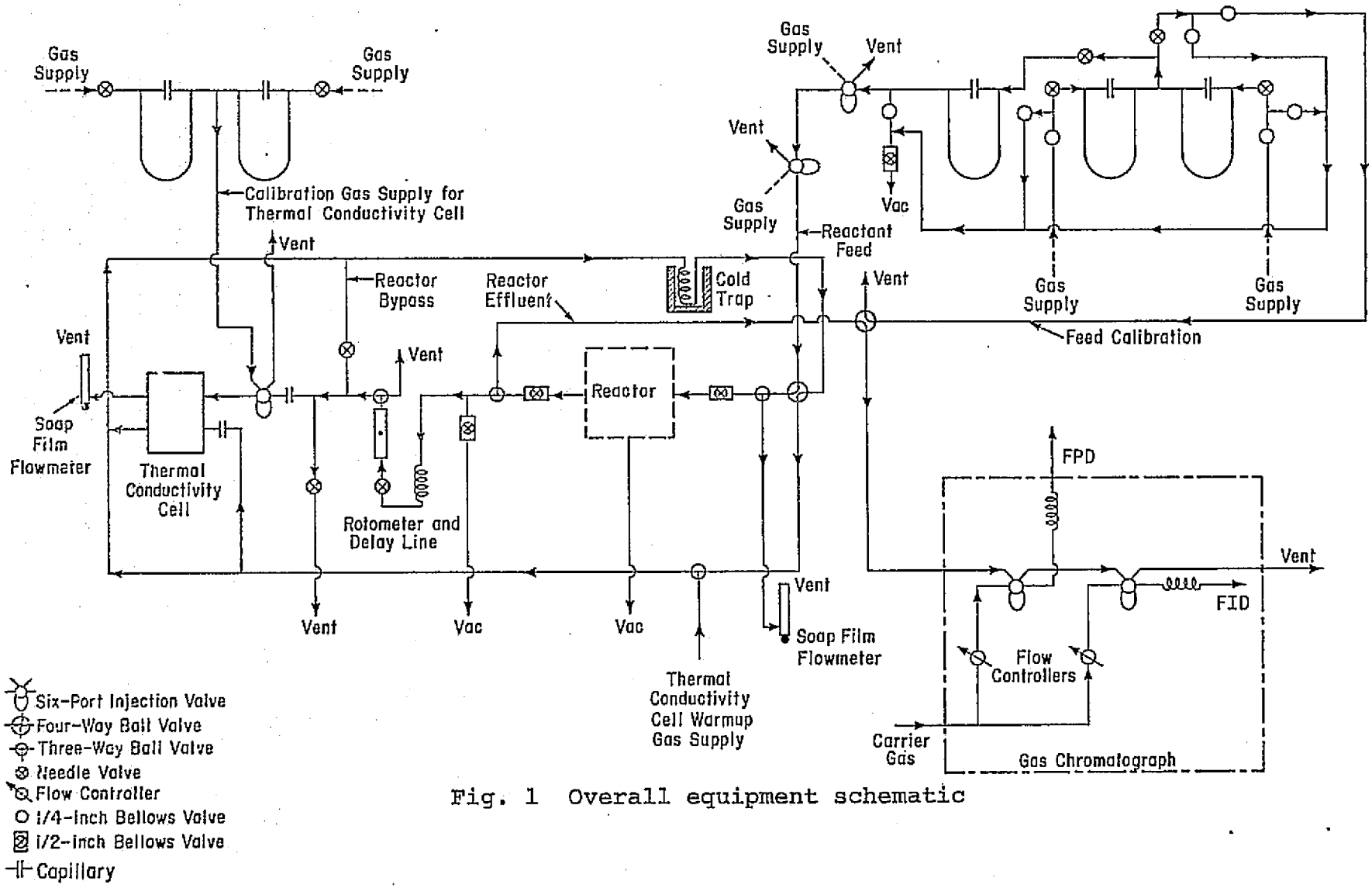

Fig. 1 Overall equipment schematic

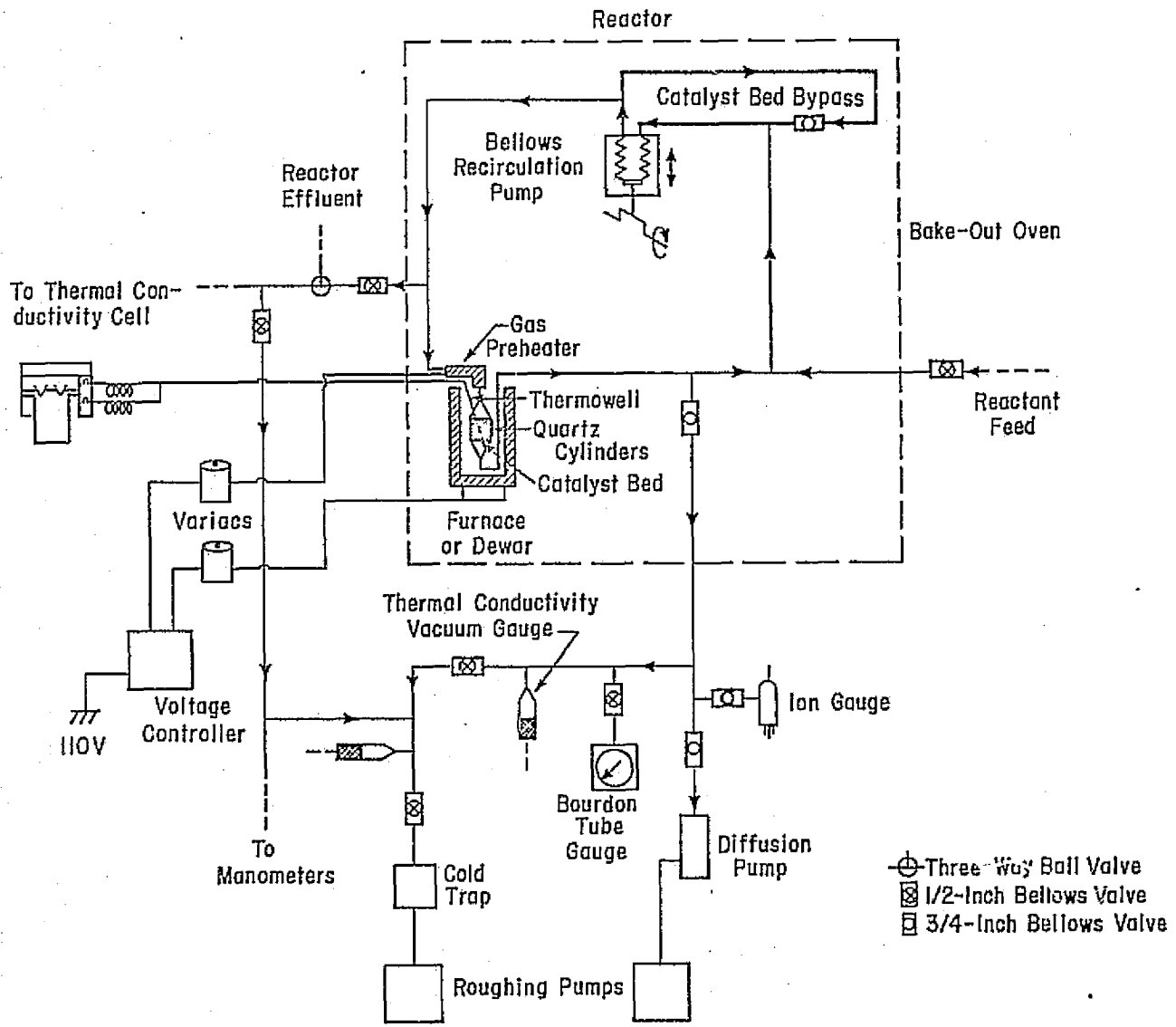

Fig. 2 Recycle reactor

stainless steel components that were not welded were connected with high vacuum flanges. Gold-plated gaskets were used to avoid undesirable corrosion by sulfurous gases.

The recycle pump was a bellows pump modified for vacuum use. The whole reactor system was encased in an oven that could be baked to 200°C.

The catalyst consisted of 2-3 layers of $\frac{1}{8}$" catalyst pellets and was supported on a quartz mesh. Quartz packing that consisted of $\frac{1}{4}$" dia. x $\frac{1}{4}$" long quartz cylinders was loaded on top of the pellets to distribute the gas flow and heat evenly.

To maintain a constant temperature across the quartz packing and catalyst bed it was necessary to preheat the gas before it entered the reactor section. The reactor was heated by two elements of a 500 watt ceramic furnace and a 175 watt gas preheater. The maximum reactor temperature of this arrangement was $\sim$ 600°C.

Reactor temperature was measured by two chromel-alumel thermocouples inserted into a quartz thermowell. The thermowell was placed diagonally across the reaction section. One thermocouple was located at the level of the catalyst bed in the center of the quartz tube that made up the reactor section, the other was placed at the top of the quartz packing. Excellent temperature stability was obtained by using a voltage regulator on the power source for the variacs that controlled the furnace and preheater.

During an experiment the variacs were adjusted so that the thermocouple voltages registered within 1-2 degrees and the voltage of the lower thermocouple as measured by a potentiometer (using an ice-water slush reference junction) was taken to indicate the reaction temperature.

All reaction rate measurements were done at a total pressure of 750-760 Torr (room pressure).

Reactor feed gas of a low ppm* hydrocarbon (20-30) was obtained from commercial sources and their analyses of the compositions were used in treating the data.

It is very important in catalytic combustion to avoid high reactant concentrations because of the high rate of heat production and thus danger of catalyst sintering resulting from the exothermic combustion reactions. However it was necessary in some experiments to introduce large concentrations of reactants and/or poisons into the reactor loop. This was accomplished by injecting a sample loop of a small volume of high concentration gas from a six-way injection valve into the gas flow feeding the reactor loop. The recycle tubing was designed to avoid initial localized regions of high concentrations on the order of the injection concentration. This was done by including a catalyst bed bypass loop in the reactor recycle loop (fig. 2). The flow resistance caused by the quartz mesh, catalyst pellets and quartz packing in the reactor section together with the

*ppm is based on volume, ppm=mole fraction x 10^6

larger diameter tubing used in the bypass increase the internal recycle through the bypass and thereby increase the instantaneous mixing performance of the reactor recycle loop. A valve was included in the catalyst bed bypass loop to control the bypass flow if needed. In the kinetic experiments the reactor feed rate was slow enough for it to be left open. It was, however, necessary to close it for the surface area measurements and temperature programmed desorptions that will be mentioned later.

Calibrations of the pressure drop around the recycle loop indicate that the flow through the reactor with the bypass open was in excess of 20 liters per minute. High flowrates and the shallow bed used in this work gave very small space times and very small conversions per pass. Carberry (11) has shown that for very small conversions involving a first order reaction recycle ratios of 1:20 will exhibit CFSTR, continuous flow stirred tank reactor, behavior. In all experiments the recycle ratios based upon reactor loop pressure drop correlations were kept in excess of 1:20. In addition some tracer experiments with air and helium were performed to study the mixing phenomena of this reactor at high reactor loop feed rates and to calculate the kinetic volume of the reactor. The mixing performance of the reactor loop with the catalyst bed bypass valve open was investigated over low and moderate flowrates and two very high flowrates. CFSTR behavior was observed at flows of 38.1-361.4 cm^3/min. with the calculated reactor loop volume

of ∿ 630 cm^3. Mixing behavior at higher flowrate which were well beyond those used in the reaction rate measurements, 1019 and 2035 cm^3/min., progressively exhibited large deviations from CFSTR performance. A graphical representation of these results and a tentative explanation for the high flow deviations is included in Appendix 1.

Concentrations in the catalyst surface area measurements and in the tracer experiments were measured by a hot wire thermal conductivity cell. The cell response was calibrated by injecting gas mixtures supplied by calibrated capillaries into the cell flow immediately before the cell to obtain a square-wave concentration input. The cell performance is described in Appendix 2.

Hydrocarbon concentrations were measured by a flame ionization detector. The linearity of this detector is well documented (12). The sulfur concentrations were measured by a flame photometric detector. The detector performance is in fair agreement with published calibrations (13). The flame photometric calibrations are given in Appendix 3.

Procedures

For brevity a generalized description of the procedures used in this work are given below. When appropriate the specific details are presented in an appendix or as a preface to work reported in the results section.

Due to the possibility of sintering, temperatures above 400°C (14) were avoided in all procedures. The temperature

of ∿ 380°C (2) was generally chosen as the maximum usable temperature.

The general preparation procedure involved 4 steps: (1) clean up the catalyst by outgassing to ∿ 10^{-6} Torr at 380°C; (2) oxidize at 380°C to burn off any residual adsorbed impurities; (3) reduce at 380°C; and (4) outgas at 380°C to remove adsorbed hydrogen from the palladium (15). During the oxidation and reduction periods the oxygen and hydrogen pressures are kept to a few Torr and the temperature is slowly raised (∿ 5°C/min maximum) to avoid a high exothermic surface reaction rate with surface species, which could lead to catalyst sintering (14).

Throughout this work a major problem was encountered in separating the catalytic phenomena from the adsorption phenomena, since both the combustion products and the reactants adsorb strongly on the catalyst support. Since in these experiments only ethane concentrations were monitored, catalytic experiments were made particularly difficult in the are 0-30 ppm concentration range because it was found that the adsorption and reaction rates could be of the same magnitude. For instance in one experiment it took approximately 33 hours to saturate the ethane adsorption on the catalyst support and thereby obtain a steady state ethane conversion, based on ethane disappearance, which was due to ethane oxidation. Specific details of this and one other adsorption experiment are given in Appendix 5.

Initially the isothermal reaction rate was investigated for concentration dependence in the temperature range ∿200-270°C. Because of the slow rate of ethane adsorption at low ppm relatively high ethane concentrations ∿ 4000 ppm were introduced into the reactor loop at ∿ 60 cm^3/min for extended periods ∿ 2 hrs. in these runs. This procedure saturated the adsorption of ethane but resulted in catalyst deactiviation and was not used in further kinetic investigations.

Another method used to saturate the adsorption on the catalyst involved dosing the catalyst with a hydrocarbon by means of injections in the reactor as previously mentioned. This gave brief periods of high concentration as would be expected in a well mixed vessel. Deactivation of the catalyst, if any, appeared to be negligible and was generally within experimental error. In any case this method gave by far the best results in terms of obtaining a stable catalyst in a short period of time.

Kinetic Experiments

I. Concentration Dependence

The objective of these experiments was to determine the dependence of the reaction rate on the concentration of the hydrocarbon reactant. The data, taken isothermally, were fit to the general form:

$$R = kC^n$$

The CFSTR equations used in these calculations appear in Appendix 4. Experiments with ethane oxidation showed that some methane is simultaneously produced, indicating that some ethane disappearance is due to cracking to methane. Since the rate of oxidation of ethane is much greater than that of methane and the apparent cracking is much less than ethane oxidation, it was assumed that the cracking rate can be directly subtracted from the rate of ethane disappearance to give the rate of ethane oxidation.

The reaction order experiments were of two kinds.

(1) Steady state experiments with low reactor concentrations ($\sim$0-30 ppm). In these experiments a constant reactor loop feed concentration was used and the concentration in the reactor, which was monitored isothermally, was varied by changing the volumetric reactor loop feed rate. The log-slope of the reaction rate vs concentration is the apparent reaction order.

(2) Non-steady state experiments. Here large concentrations are introduced into the reactor loop and the concentration decay is measured. A reaction order is assumed and the solution to the differential equation is arranged in such a way that by plotting the appropriate function of concentration versus time linear plots are obtained if the assumed kinetics are correct. The most obvious case is the

test for first order decay in a well mixed vessel where ln(concentration) is linear with time.

II. Temperature Dependence

The temperature dependence of the reaction rate is characterized by the Arrhenius form:

$$k = k_o \exp[-E_a/RT]$$

E_a is the apparent activation energy for the reaction.

The general procedure in these experiments (to avoid dosing the catalyst repeatedly) was to establish a steady state adsorption at low temperature by dosing the catalyst and then to raise the catalyst temperature without dosing. Presumably this resulted in a fast desorption of reactant from the alumina base to establish the new steady state.

Preliminary Sulfur Adsorption and Reaction Experiments

Introduction of a steady known concentration (ppm levels) of H_2S in the feed to the reactor proved to be a problem. Premixed gases, ppm of SO_2 and H_2S in N_2, with concentration analysis supplied by Matheson Gas were not accurate at the time they were used in this work. Calibration mixtures from a two stage dilution of H_2S gas showed that a H_2S tank was 2.3 ppm rather than the listed 18 ppm and a SO_2 tank was 3.0 ppm not the reported 9.9 ppm.

These low values are not surprising since the gas mixtures were stored in steel cylinders and large losses of ppm H_2S and SO_2 have been reported on metal and glass surfaces (13).

During an attempt to calibrate the FPD detector it was found that the irreversible removal of H_2S by stainless steel tubing follows approximately first order kinetics and the removal rates are stable in excess of 50 hrs. This corresponds to well beyond monolayer coverage of the inside walls of the tubing.

Because of the reported ease of oxidation of H_2S (16) and the known removal behavior by a small amount of stainless steel tubing the oxidation and removal of H_2S by the reactor without a catalyst was investigated.

Flows from the 2.3 ppm H_2S tank and an air tank were mixed to give a total volumetric flow rate of 246 cm^3/min with pressures of 100 Torr O_2 and 7×10^{-4} Torr (0.86 ppm) H_2S. A temperature of 46°C results in removal of 56% of the H_2S input with 8% being detected as SO_2. At 141°C no H_2S could be detected and 42% of the input sulfur was detected as SO_2. A graphical representation of all of the data for these calibrations is given in Appendix 6.

Poisoning Experiments

The method used to poison the catalyst was first to establish a stable catalyst at the desired reaction temperature and generally at about 50% conversion. Then the

catalytic poison was introduced via a six way injection valve as previously mentioned. The kinetic response of the catalyst was then measured. This method of introducing the poison is very useful in establishing measureable reactor poison concentrations when using poisons such as H_2S at temperatures where the gas phase oxidation of H_2S competes with its catalytic oxidation.

Surface Area Measurements

The methods used to measure surface areas involve measuring the amount of an adsorbate desorbed or adsorbed in a flowing carrier gas sweeping the catalyst bed with the catalyst bed bypass valve closed. Flow through the bellows pump is prevented by check valves in the exhaust and intake.

There was some adsorbate dispersion due to diffusion into the dead spaces and segregated flow in the large tubing used for the recycle loop, but this dispersion was minimized by adjusting the carrier gas flow.

Total catalyst surface areas were measured by nitrogen adsorption at low temperature. The general method was similar to that used by Nelsen and Eggertsen (17). To cool the catalyst a dewar was inserted in place of the furnace. Nitrogen pressures were obtained by mixing helium and nitrogen flows using the reactor feed manometers. Since the adsorption was slow only desorption could be accurately measured.

Palladium surface areas were measured by CO adsorption. Two methods were used: (1) adsorption at low pressure $\sim$ 10

Torr and subsequent desorption at high temperature in a helium carrier; and (2) low temperature adsorption from CO injections in a helium carrier. This second method is similar to that used by Gruber (18) to measure platinum surface areas. Some measurements of high temperature H_2 desorption in a N_2 carrier were also done.

Adsorption Calculations

I. N_2 Adsorption

Total surface areas were measured by physical adsorption of N_2 at 77°K. The well-known BET equation (19) was used to calculate the surface area.

II. CO Adsorption

Pallidium surface areas were measured by CO chemisorption at 25°C. No uniform method has been adopted to calculate palladium surface area from CO adsorption. Ertl (20) has reported the maximum coverage, i.e., CO/Pd ratio, on four different crystal planes. They are: 0.5(111), 0.7(100), 1.0(110), and 1.5 (210). From the data of Ertl the surface area per CO molecule on each plane can be calculated: (111) 13.1 A^2; (100) 10.7 A^2; (110) 10.6 A^2; (210) 12.6 A^2. The average of the three most stable planes, (111), (100), and (110), is 11.5 A^2. This value corresponds to 3.1 [m^2 Pd/cm^3 CO (STP)], the maximum variations in the values of the different planes reported is $\sim \pm 0.4$ m^2/cm^3. Scholten

and Van Montfoort (21) have obtained value of 3.2 m^2 Pd/cm^3 CO (STP). They compared CO chemisorption to BET surface areas on Pd black and Pd sponge. The value of 3.1 was used throughout this work.

Ertl has suggested that "maximum coverage is given by the tendency to find a compromise between the formation of a close packed adsorbate layer (which is determined by the size of the CO molecule) and with the periodicity of the surface." This structure interpretation offers a rough check on the above assumed CO average surface area of 11.5 A^2.

Values listed by Hirschfelder (22) of the collision diameter from kinetic theory all give values of the molecular cross-sectional area within the range 10.1-12.3 A^2.

Results

I. Ethane Oxidation Kinetics

The kinetics of ethane oxidation was initially investigated using 1.1 grams of catalyst.*

The catalyst load was pretreated as mentioned in the apparatus and procedure section. As shown by the ethane adsorption breakthrough in Appendix 5 the initial activity of this catalyst load at 197°C was very low. The corresponding first order pre-exponential** assuming an E_a of 27 kcal/mole was 0.81×10^{11} $cm^3/(sec \cdot g)$. The initial breakthrough after a second oxidation and reduction gave a pre-exponential of 3.0×10^{11} $cm^3/(sec \cdot g)$. Two subsequent oxidation treaments (380°C in air for 8-10 hours) resulted in essentially the same pre-exponential. After a third oxidation treatment a series of steady-state experiments (200-270°C) were performed to investigate the concentration dependence of the oxidative reaction rate. The first run, at 197°C is shown in Figure 3 along with some other runs which are described later. Plotted in Figure 3 are the $\log_{10}$ coordinates of the oxidative reaction rate in moles/(sec·g) vs. the ethane reactor

*The surface area of this catalyst was not measured until the H_2S poisoning experiments.

**Pre-exponentials quoted on this first catalyst load are evaluated using first order kinetics and an E_a of 27 kcal/mole. Subsequent reaction order and E_a determinations have shown these to be good values.

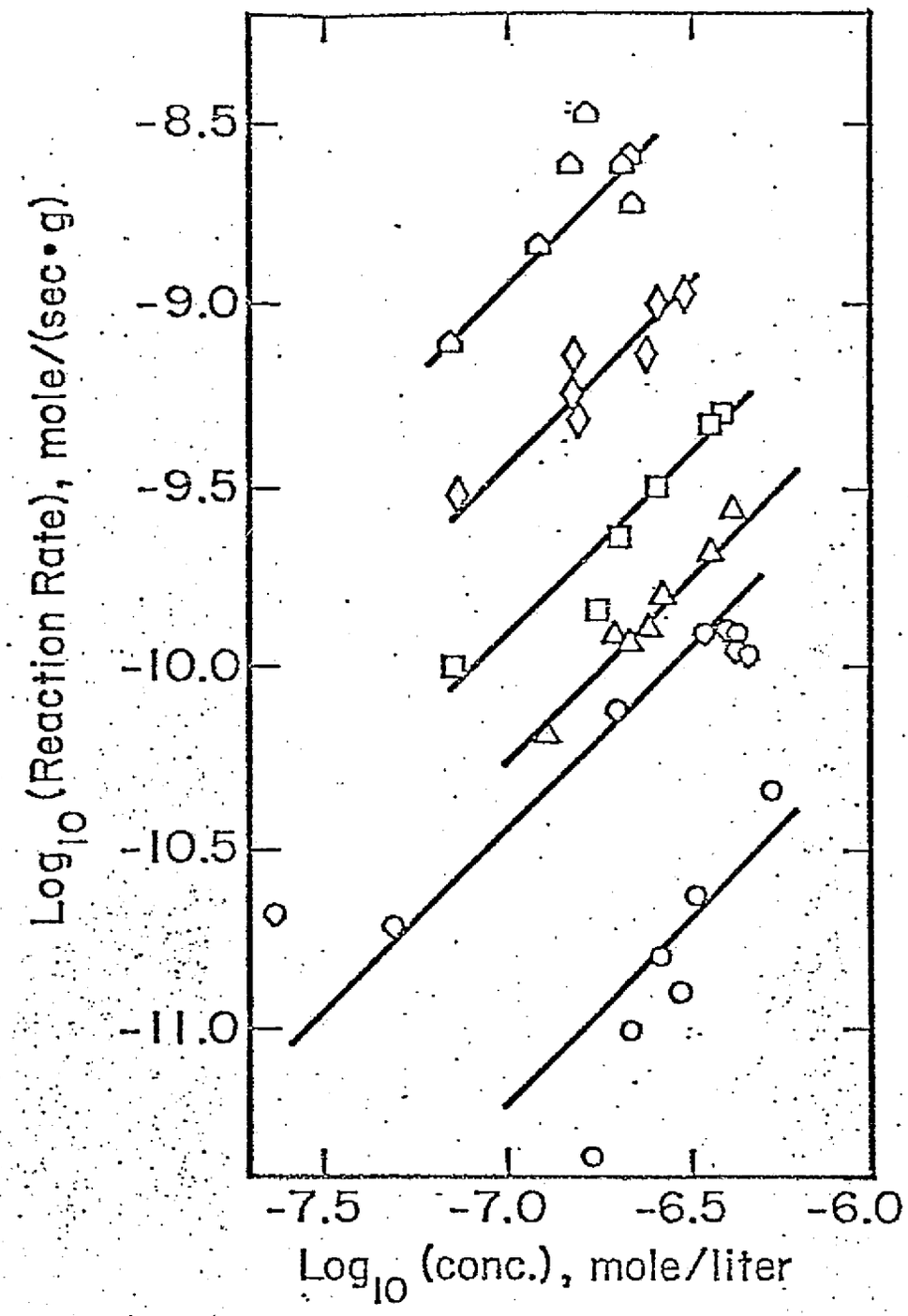

Fig. 3 Steady state reaction order runs, first catalyst load, 1.1 grams, 200-300°C. Two activity levels are represented, ◇ 197°C, pre-exponential k_w is 1.1×10^{12} $cm^3/(sec \cdot g)$ and ○ 198°C, △ 227°C, □ 248°C, ◊ 271°C, ⌓ 301°C, pre-exponential is 2.1×10^{11} $cm^3/(sec \cdot g)$.

concentration in moles/liter. Approximately first order kinetics were observed. This run represents the highest stable oxidation rate coefficient obtained with this catalyst, a pre-exponential of 1.1×10^{12} $cm^3/(sec \cdot g)$. The adsorption saturation procedure used in the remaining runs in this series (200-270°C) caused the catalyst to deactivate appreciably. At 270°C the extrapolated pre-exponential amounted to 0.59×10^{11} $cm^3/(sec \cdot g)$. Oxidation treatment at 380°C for 8-10 hours resulted in only partial recovery of the initial activity. The pre-exponential on the next run (reported below) was 2.1×10^{11} $cm^3/(sec \cdot g)$. To investigate the concentration and temperature dependence of the reaction rate from 200-300°C the procedures for the steady-state reaction order runs and the temperature runs were combined. After pretreating the catalyst with air at 380°C for ∿10 hours, the catalyst temperature was dropped to ∿200°C and the catalyst adsorption was saturated with the selected ethane concentration in the reactor feed gas. The catalyst temperature was then monotonically increased to four higher temperatures. Reaction order runs were done at each of the five different temperatures. After each

run to determine reaction order the catalyst was lowered to ∿200°C and the activity checked. The activity after each reaction run was within the scatter of the data for the initial reaction run at 200°C. Within the scatter in the data activity corrections were not warranted.

No voltage regulator was used for these experiments and hence the reactor temperature varied by as much as 5°C. In the reaction order runs the reaction rates at constant concentration were corrected to the average temperature of all experimental points in that run using 27 kcal/mole for the activation energy.

The reaction order data is represented in Figure 3. A first order line is drawn for each set of data. The overall temperature run is represented in Figure 4. The slope of the line drawn corresponds to 27 kcal/mole, the pre-exponential k_w is 2.1×10^{11} $cm^3/(sec \cdot g)$.

After these experiments, the effect of freon poisoning was investigated with a few freon injections. The poisoning was reversible and this work is described in Appendix 7. Subsequent to the freon poisoning experiments the oxidation of diethyl ketone was studied, poisoning in these experiments was also reversible and is reported in the next section below.

Prior to the hydrogen sulfide poisoning experiments and after the diethyl ketone experiments another temperature run (200-320°C) was done, Figure 5. The slope of the line drawn corresponds to 29 kcal/mole. Extrapolated with

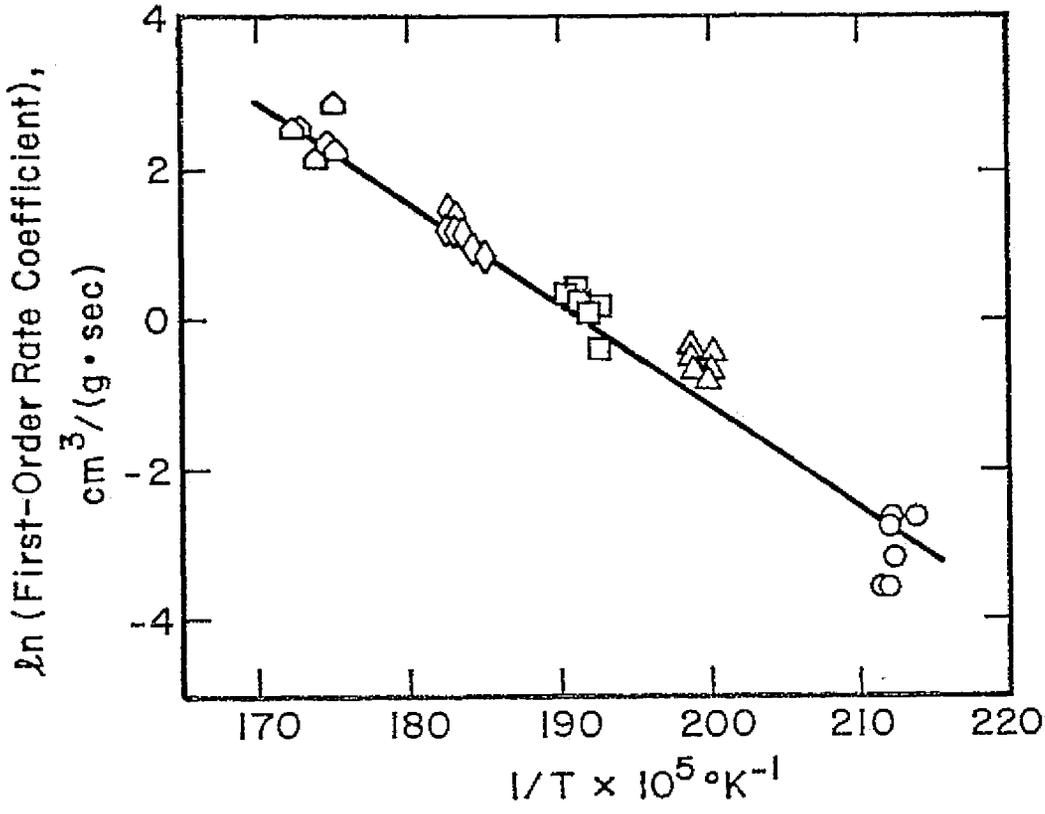

Fig. 4 Arrhenius plot of the lower activity data presented in figure 3. Apparent E_a and pre-exponential are 27 kcal/mole and 2.1×10^{11} $cm^3/(sec \cdot g)$.

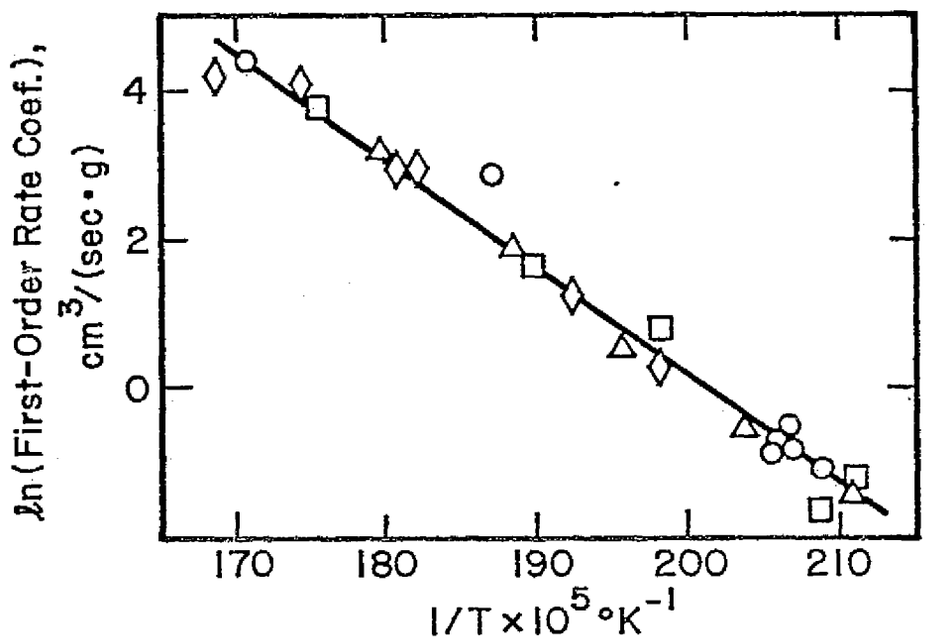

Fig. 5 Arrhenius plot of data taken before the hydrogen sulfide poisoning. E_a from the slope of the line drawn in 29 kcal/mole. Assuming 27 kcal/mole at 254°C yields a pre-exponential k_w of 8.6×10^{11} $cm^3/(sec \cdot g)$. CO chemisorption of 0.85 m^2/g translates this value to a pre-exponential k_s of 1.0×10^8 cm/sec. Four runs over 5 days, O 1st, □ 2nd, Δ 3rd, ◊ 4th.

27 kcal/mole from 254°C the pre-exponential k_w is 8.6×10^{11} $cm^3/(sec \cdot g)$. The CO chemisorption before and after this run gave 0.85 m^2/g and a pre-exponential of 1.0×10^8 cm/sec. The total surface of the catalyst (BET Method) was 118 m^2/g.

The apparent activation energies and pre-exponentials from the data in Figures 3 and 4 are similar to those evaluated from the data of R. Vincent* (210-300°C) using 0.17 grams of the same catalyst, see Figure 6. Although Vincent also observed the production of methane no quantitative methane data was reported hence only the disappearance of ethane was used to calculate the first order rate coefficients. The value of E_a from the slope of the line drawn is 25 kcal/mole, the pre-exponential k_w extrapolated from 242°C with 27 kcal/mole is 3.7×10^{11} $cm^3/(sec \cdot g)$.

On a second catalyst load used in this work, 1.66 grams, a few unsteady-state experiments were carried out to confirm the first order concentration dependence of the reaction rate. Plots of the natural logarithm of the mole fraction of ethane vs. time were linear and are represented in Figure 7.

Although the data fits first order two discrepancies should be noted. (1) The first order rate coefficients

*Unpublished data taken in this laboratory.

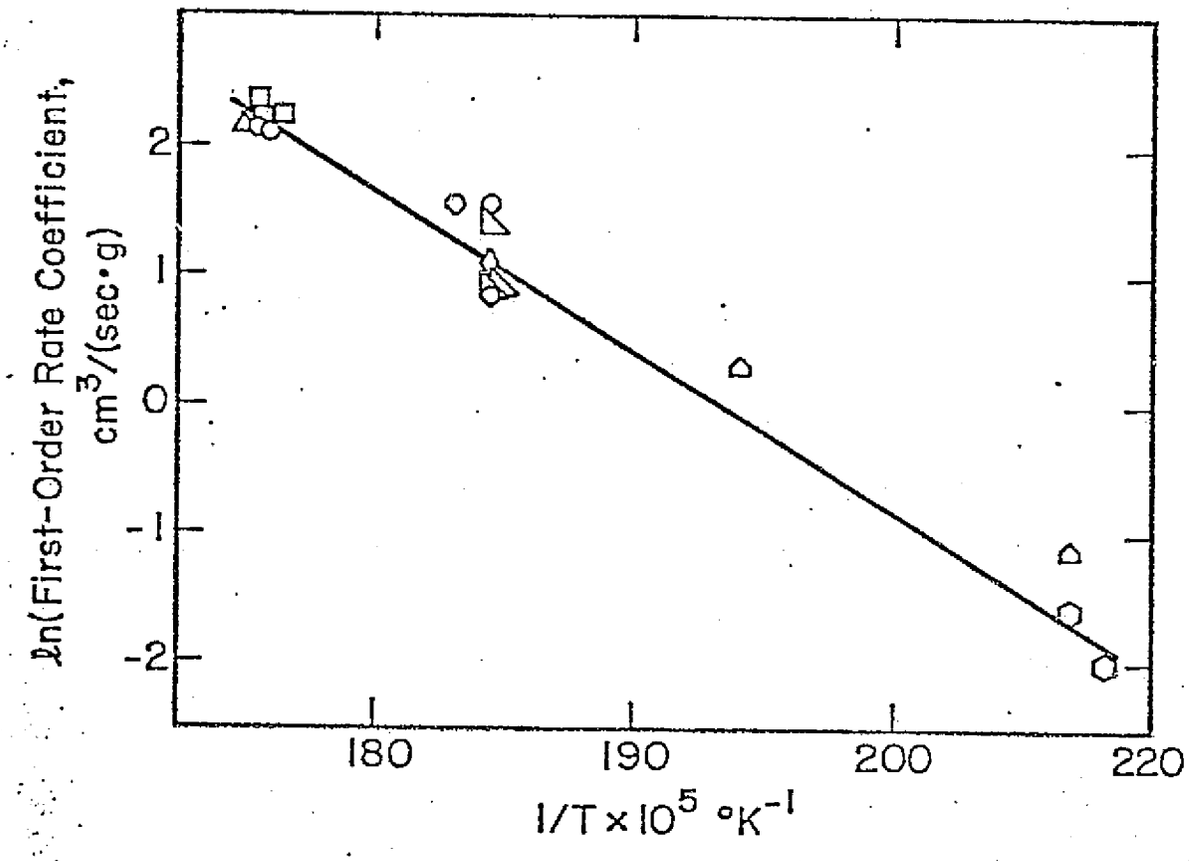

Fig. 6 Arrhenius plot, 210-300°C on 0.17 grams of catalyst. Data of R. Vincent. Rate coefficients are calculated on the first order disappearance of ethane. Apparent E_a from the slope of the line drawn is 25 kcal/mole. Assuming 27 kcal/mole at 242°C yields a pre-exponential k_w of 3.7×10^{11} $cm^3/(sec \cdot g)$. Data in sequential order ⬡ 1/30, ⌂ 1/31, ◺ 2/13, ◇ 2/19, △ 2/20, ○ 2/26, □ 2/27.

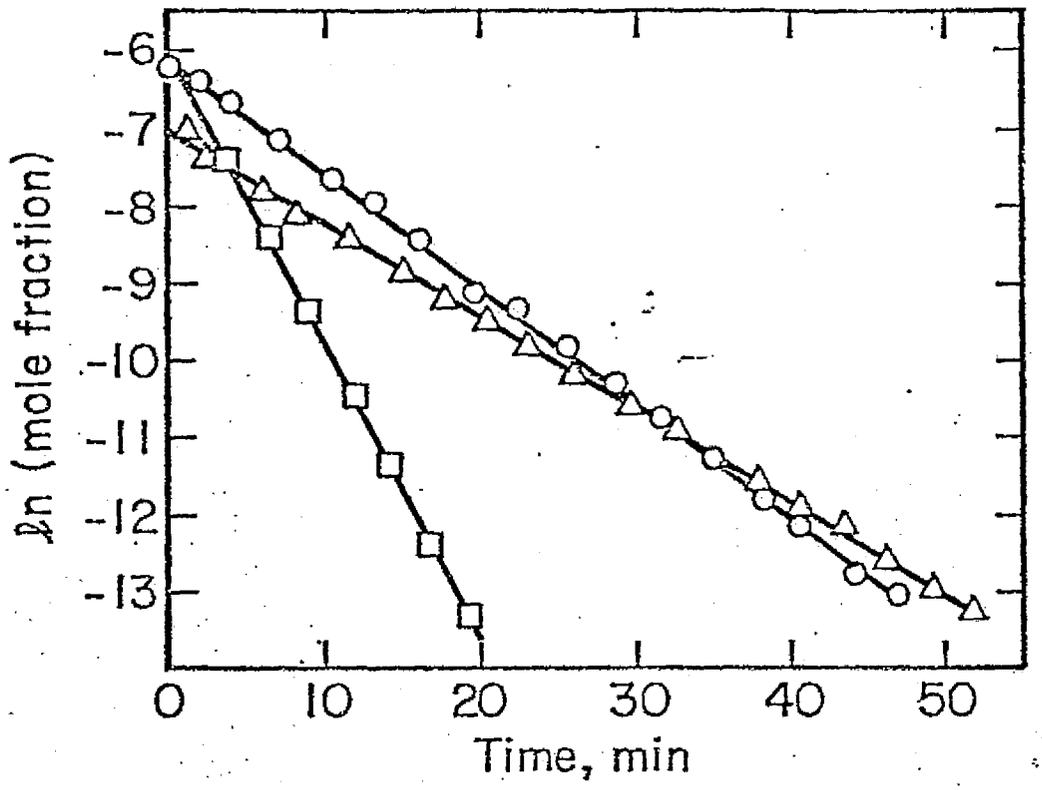

Fig. 7 Unsteady state reaction order runs on the second catalyst load, 1.66 grams, mole fraction ethane versus time. Three different reaction temperatures, Δ 230°C, volumetric flowrate 48.8 cm^3/min., 19.9 μ moles of ethane injected, O 261°C, volumetric flowrate 57.3 cm^3/min., 43.7 μ moles of ethane injected, □ 284°C, volumetric flowrate 125.0 cm^3/min., 43.7 μ moles of ethane injected.

calculated from the slopes of the lines are in every case smaller than the rate coefficients calculated from steady-state measurements immediately prior to each run: at 284°C $k/k_{ss}=\frac{1}{2}$; at 261°C $k/k_{ss}=\frac{2}{5}$; and at 230°C $k/k_{ss}=\frac{2}{3}$. The half order and second order models do not represent the kinetic data. Plots assuming half and second order kinetics are shown in Appendix 4. (2) The initial concentrations from extrapolation to zero time for the 43.7 μ mole injections are about 15% too high. The initial concentration from the 19.9 μ mole injection agrees well with the calculated value if an effective reactor loop temperature of 70°C is used. The temperature of 70°C agrees with the average temperature as measured by thermocouples attached to the outside of the recycle loop. When the time axis of the plots for the 43.7 μ mole injections are expanded there appears to be a slight curvature near zero time in both cases and if the curvature is extended the calculated initial mole fraction is obtained. This phenomenon is more exaggerated for larger injection volumes not reported here.

II. Diethyl Ketone Oxidation Kinetics

Prior to the diethyl ketone, DEK, oxidation runs the catalyst was pretreated with 380°C air for ∿10 hours.

Initially the concentration dependence of the reaction rate was investigated. A temperature of 137°C was chosen because it was near the temperature reported by Rabb (2)

where the maximum rate of DEK desorption occurs. At this temperature injections of DEK were required to establish a measurable steady-state DEK concentration in the reactor effluent.

Quantitative measurement of the initial reaction rate was not possible due to the extremely long times required to attain a steady-state adsorption of DEK on the catalyst. Furthermore, the large amount of physical adsorption on the catalyst combined with the very slow adsorption-desorption rates and concurrent catalyst deactivation made it impossible to measure reaction rates for different concentrations at constant catalyst activity. A large change in the DEK pressure at 137°C resulted in such a large and slow adsorption or desorption rate that by the time the catalyst had come to a steady adsorption the rate coefficient had significantly changed. It was found that if the adsorption on the catalyst was saturated at a constant flowrate the pressure changes caused by the catalyst deactivation were slow enough that the rate of poisoning could be measured. The poisoning phenomenon is represented in Figure 8, the apparent activity having decreased by a factor greater than 2.2.

The concentration dependence of the reaction rate was studied after the catalyst reached a stable activity (Figure 9). First order kinetics were observed. After the reaction order run three temperature runs were done, Figure 10. Whenever the catalyst temeprature was lowered

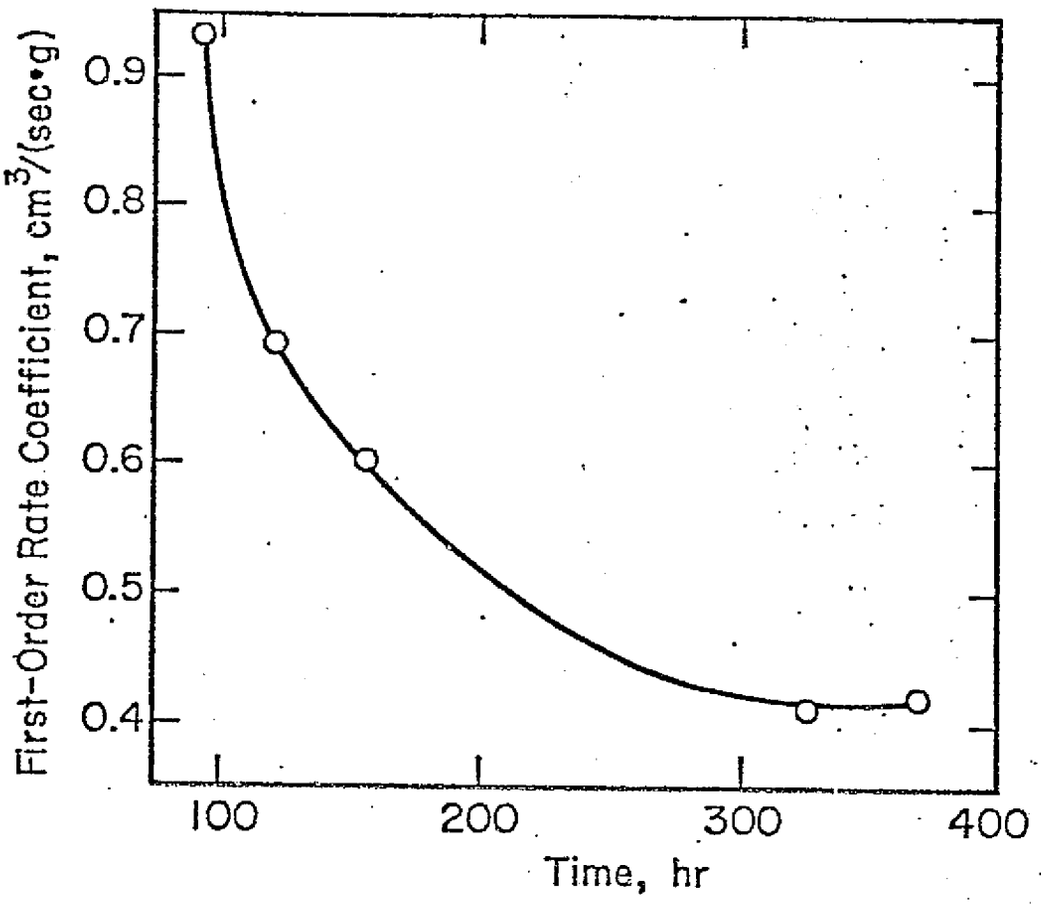

Fig. 8 Self poisoning of diethyl ketone oxidation, first order rate coefficient vs. time. Diethyl ketone input was 30.2 ppm at an average flow of 0.70 cm^3(STP)/sec.

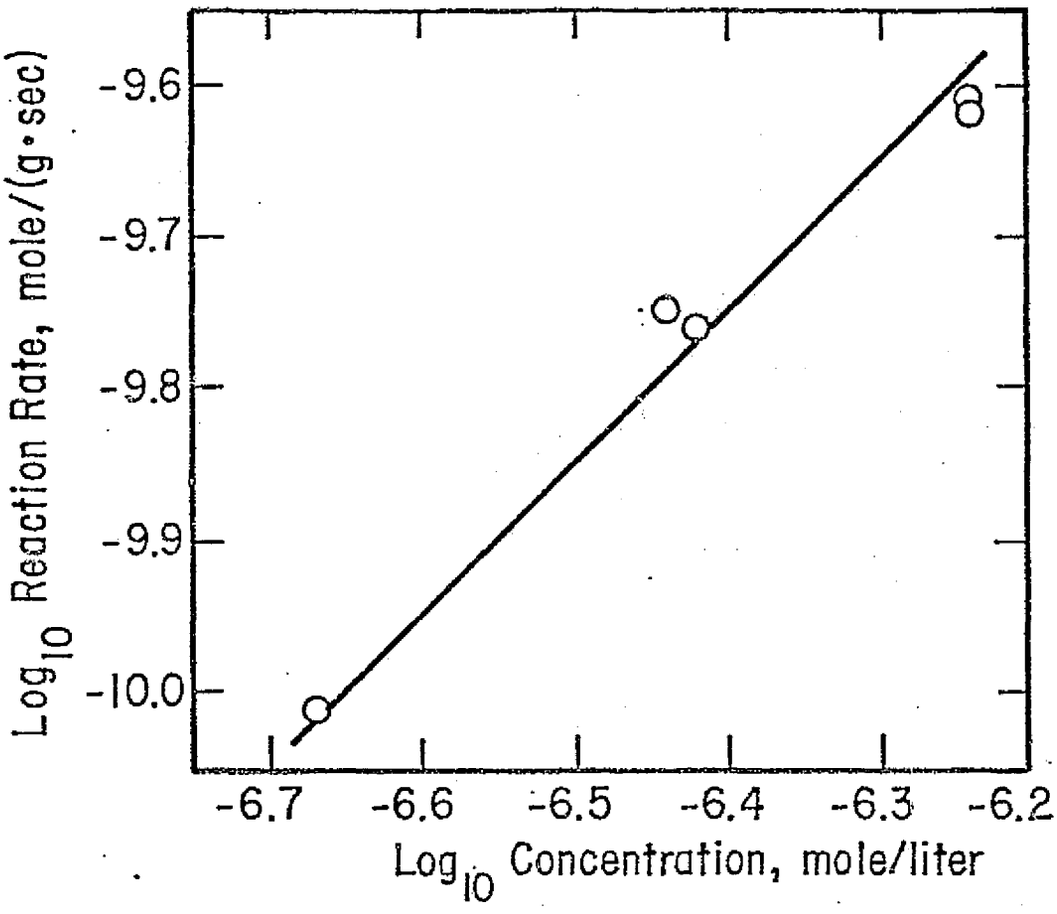

Fig. 9 Diethyl ketone oxidation at 137°C. Reaction rate vs. concentration, after stable activity was reached. First order line is drawn.

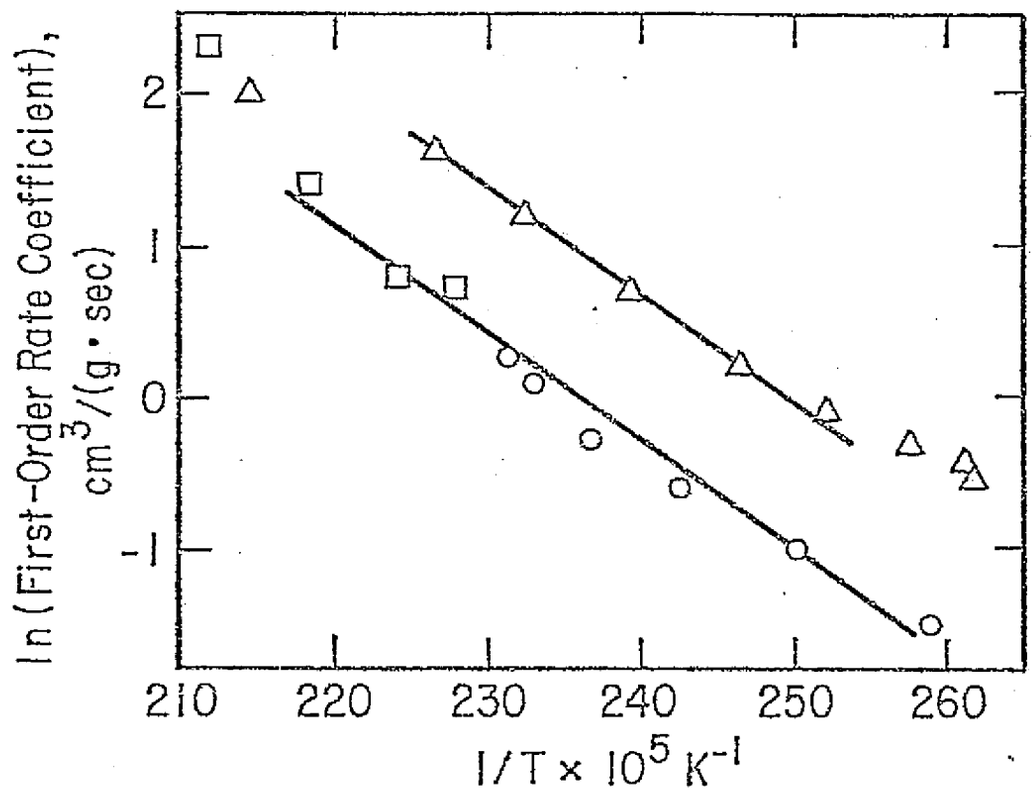

Fig.10 Arrhenius plot for diethyl ketone oxidation. Three runs over 5 days: ○1st and 2nd, □3rd, △ 4th and 5th day. Apparent E_a from slope of line drawn is 14 kcal/mole, pre-exponentials k_w are 1.74×10^7 and 4.47×10^7 $cm^3/(sec \cdot g)$. Subsequent CO chemisorption gave 0.79 m^2/g, this yields a pre-exponential k_s of 5.66×10^3 cm/sec.

injections of DEK were required to re-establish the steady-state. After the second temperature ru~ there was some regeneration of the catalyst activity. The apparent activity on the second run increased by a factor of ∿ 2.6. The slopes of the lines drawn in Figure 7 yield 14 kcal/mole, the corresponding pre-exponentials k_w are 1.74×10^7 and 4.47×10^7 $cm^3/(sec \cdot g)$. Subsequent CO chemisorption gave 0.79 m^2/g and a pre-exponential k_s of 5.66×10^3 cm/sec.

III. Hydrogen Sulfide Poisoning

The complete oxidation and removal of a continuous low level input of H_2S (0.86 ppm), as mentioned in the apparatus and procedure section was observed at ∿ 140°C, residence time of 2.56 minutes. This is far below the temperatures needed for intermediate conversions of ethane at reasonable residence times (∿ 1-10 minutes) for the amount of catalyst used in this work that could be loaded into the reactor (∿ 0-2 grams). It was then decided to introduce the poison by the injection method which presumably would result in transient high H_2S concentrations. Adsorption of and oxidation of H_2S by Al_2O_3, $H_2S + [O]_{ads} \rightarrow H_2O + S_{ads}$, has previously been reported. (23) As a preliminary to the poisoning of the catalyst with H_2S injections, the oxidation behavior of hydrogen sulfide injections using about one gram of the catalyst support was investigated.

The result was that the complete oxidation of an injection of 15.1 μ moles of H_2S was very fast. After ∿ 0.4 residence times at 200°C there was no measurable H_2S concentration. However, the injection method for H_2S introduction represented a method whereby measurable H_2S concentrations could be introduced into the reactor using the relatively slow volumetric flowrates with which concurrent ethane kinetics could be measured. A graphical representation of the oxidation of H_2S injections over the catalyst support is given in Appendix 8.

After these preliminary experiments on H_2S oxidation by the alumina base the recycle tubing was visibly sulfided. Prior to reloading the catalyst used in the previous hydrocarbon oxidation experiments the recycle loop was rigorously cleaned in a series of acid baths by the Lawrence Berkeley Laboratory plating shop.

The catalyst was then loaded back in and pretreated in air at 380°C for ∿ 10 hours. Afterwards the temperature run shown in Figure 5 was done. This plot gives a good representation of the scatter involved in the temperature runs. The pre-exponential k_w of 8.6×10^{11} $cm^3/(sec \cdot g)$ is equivalent (within experimental error) to the highest activity seen on the first reaction order run at 197°C, Figure 1.

Four poisoning experiments were done at 256 ±3°C on this catalyst load. Throughout the poisoning runs the ethane cracking rate coefficient was 2-3% of the oxidation rate coefficient.

The approach taken in these poisoning experiments was to use a series of small hydrogen sulfide injections to decrease incrementally the rate coefficient and then to measure the amount of CO adsorbed by the poisoned catalyst. As stated in the appendix, the sulfur detector saturates at 14 ppm and calibrations above 14 ppm were obtained with H_2S dilutions. The sulfur concentration given in the illustrations below are based upon the H_2S calibrations. From a mass balance on the SO_2 output for a given injection the sulfur calibration for SO_2 is a factor of 2.0-2.5 too high assuming a negligible sulfur sink in the reactor. It is therefore expected that the sulfur concentrations above 14 ppm given in the illustrations below are at least a factor of 2 too high.

The overall poisoning of the catalyst and CO chemisorption is represented in Figure 11. Plotted in Figure 11 are the first order rate coefficients for oxidation and cracking of ethane at 256°C in $cm^3/(sec \cdot g)$ vs. the total amount of H_2S injected in μ moles. Throughout the four series of injections plotted in Figure 11 the reactor temperature was 256 ± 3°C and the rate coefficients plotted were corrected to their values at 256°C using an E_a of 27 kcal/mole. The unsteady-state behavior of the rate coefficients immediately after H_2S injections for 231 to 408 μmoles and for 408 to 592 μmoles H_2S injected are shown in Figures 12 and 13.

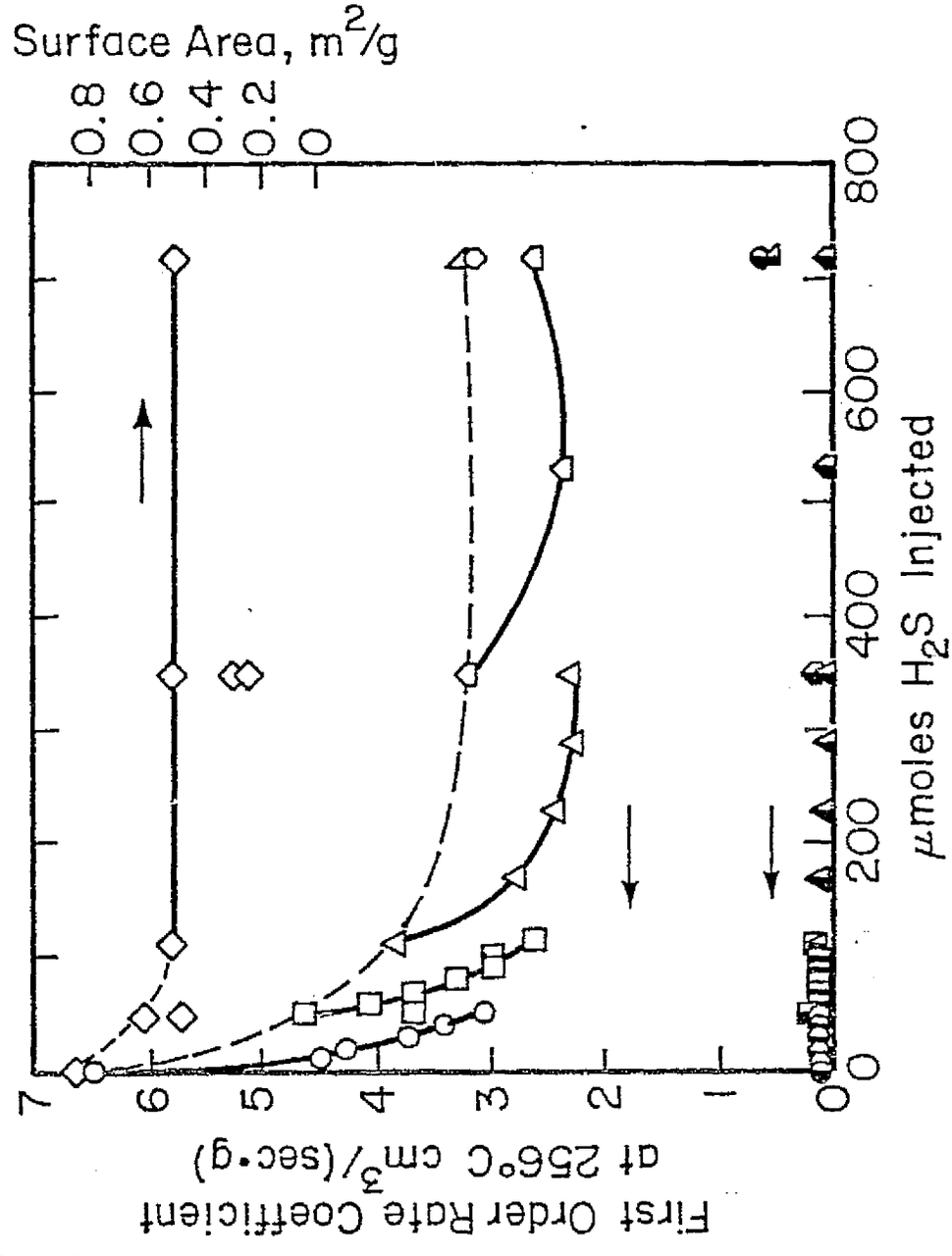

Fig.11 Hydrogen sulfide poisoning of the first catalyst load, 1.1 grams. Open symbols are oxidation rate coefficients, half shaded symbols are cracking coefficients. Four series of injections are represented. First series, 5 injections, ○, of 10.2 μ moles each at a residence time of 2.5 min., 258°C, second series, □ , 6 injections of 10.3 μ moles each at a residence time of 4.9 min., 255°C. Third series, △ , four injections of 59.0 μ moles each at a residence time of 5.0 min., 254°C. Fourth series, ⌂ , 2 injections of 184.1 μ moles each at a residence time of 5.0 min., 254°C. Rate coefficients after the fourth series: ◺ , after outgassing to 380°C, ◇ , after oxygen treatment at ∿ 600°C.

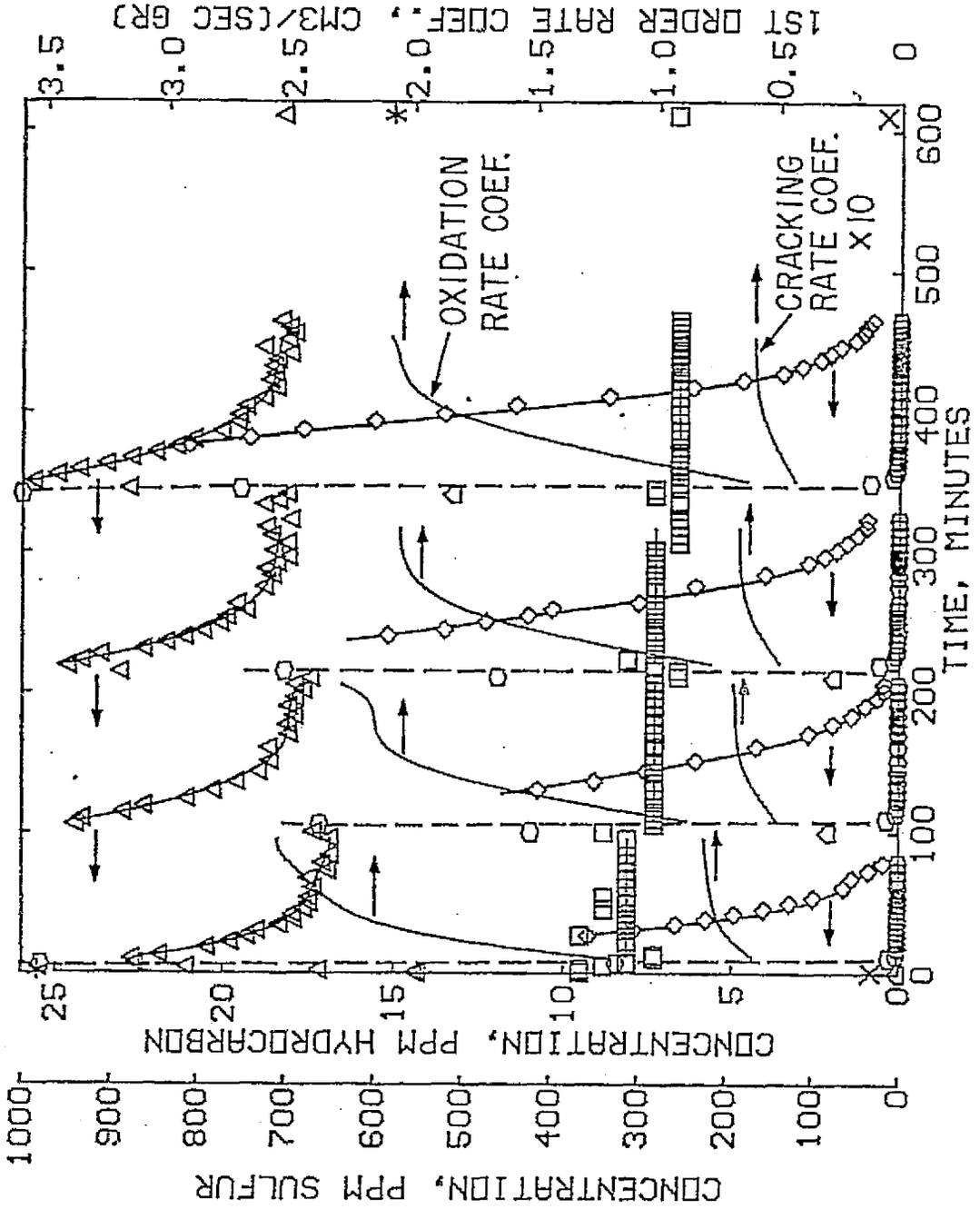

Fig.12 Unsteady state behavior of third poisoning series for 59 μ mole injections. Cumulative sulfur loading corresponds to 113-349 μ moles H_2S on figure 11. Reaction temperature is 254°C, residence time is 5.0 min. Ethane feed level is 30 ppm. Symbols: *, x, initial and final oxidation and cracking rate coefficients, respectively, calculated from steady state data, ○ SO_2, ◊ SO_2 x 500, △ H_2S, □ CH_4 x 10, Δ C_2H_6.

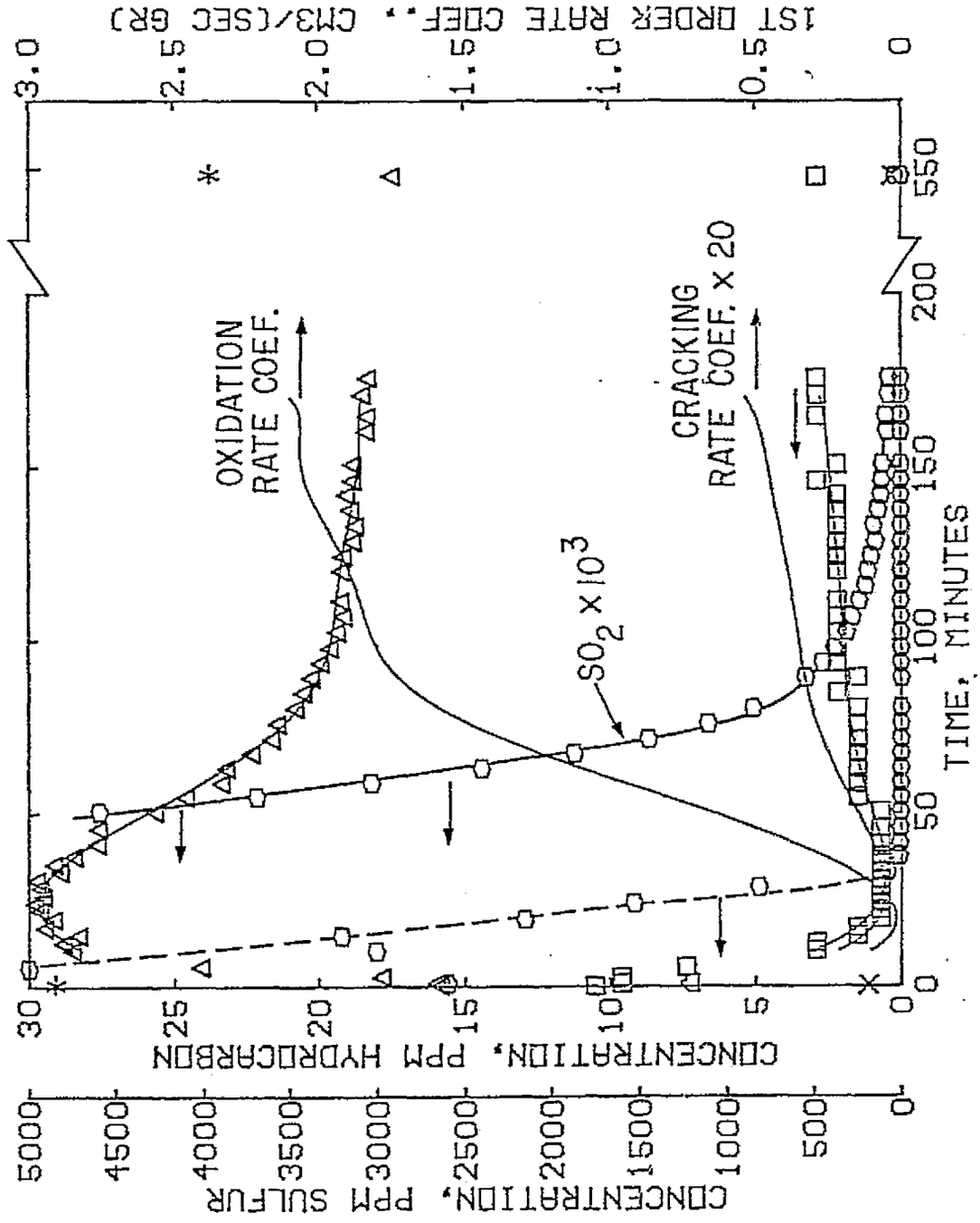

Fig.13 Unsteady state behavior of the first injection on the fourth poisoning series, 184.1 μ mole injection. Cumulative sulfur loading corresponds to 349-533 μ moles. Final rate coefficients are those after a second 184 μ mole injection at 283 minutes, 717 μ moles on figure 11. Reaction temperature is 254.2°C, residence time is 5.0 min., ethane feed level is 30 ppm. Symbols: *, x, initial and final oxidation and cracking rate coefficients, respectively calculated from steady state data, ○ SO_2, △ H_2S, □ CH_4 x 10, △ C_2H_6.

Plotted in Figures 12 and 13 are the concentrations* of ethane and methane in ppm, the corresponding first order oxidation and cracking rate coefficients and the concurrent H_2S and SO_2 concentrations in ppm which are plotted against time in minutes. These figures (also fig. 19 and 20) were computer drawn. The lines drawn through the ethane and methane concentration data were generated from an n^{th} order polynomial curve fit to the time dependent concentrations. The concentration-time derivatives needed to compute the rate coefficients for the plots were evaluated from the fitted polynomial. The salient features of these plots are (1) the H_2S is removed from the gas phase very fast, much less than one residence time, (2) the SO_2 is present in the reactor much longer than would be expected for a simple concentration wash out of a CFSTR** and (3) the rate coefficients are inversely proportional to the SO_2 concentration.

The method used initially to measure the CO chemisorption in these runs was to adsorb CO at low temperature and low pressure and then to measure the desorption at high temperatures. This method proved to be difficult to use

*As mentioned in a previous footnote ppm is not equivalent to concentration but in this work it is used in lieu of mole fraction x 10^6.

**For a simple washout in a CFSTR the concentration should decrease by a factor of e^{-1} every residence time.

for two reasons: (1) the thermal conductivity of CO is very close to the reaction gases relative to the He carrier gas. The integral of the change in the thermal conductivity of the carrier gas was used as a measure of the amount of CO desorption and no provision was made to separate CO from other desorbing gases. A quantitative measure of the desorbing CO then required the catalyst to be well outgassed at a temperature in excess of the CO desorption temperature. (2) the outgassing procedure required for the CO desorption measurements resulted in some restoration of the catalytic activity.

This regeneration phenomena is illustrated by figure 11. The gain in activity is shown by the difference between the ending value of the rate coefficient in one series of injections and the much larger beginning value of the subsequent injection series.

Further discussion of fig. 11 is presented below. By far the largest activity loss $\sim$ 30% occurs with first injection 10.2 μmoles.

Another peculiarity in this first injection is that the concentrations stabilized very fast $\sim$30 minutes whereas $\sim$50 minutes was required for the other injections in that series.

Of some interest is that the activity level after the first H_2S injection of the first and second injection series correspond closely to the initial activity of the second and third runs.

After the first poisoning run the catalyst was outgassed and the CO desorption measurement gave 0.62 m^2/g. An attempt

was made to verify this value with H_2 desorption in an N_2 carrier due to the possibility of other desorbing gases. The method suggested by Boudart (15) was used for obtaining hydrogen surface coverage on Pd. Hydrogen desorption in a N_2 carrier seemed attractive for two reasons: (1) the temperatures needed to desorb hydrogen are less than the reaction temperature. (2) all the reaction gases have thermal conductivities very close to N_2 in comparison with H_2. For three hydrogen adsorptions the average desorbable hydrogen at 200°C amounted to about 4% of the CO adsorption, assuming a ratio of CO/H coverage of 0.73. Due to the extremely low value of H_2 desorption, the CO desorption was again measured, it was found to have decreased from 0.62 to 0.49 m^2/g. The initial oxidation rate coefficient after CO and H_2 adsorbtions was 3.7 $cm^3/(sec \cdot g)$, after $\sim$ 15.5 hours at the reaction temperature of 256°C the rate coefficient had increased to 4.6 $cm^3/(sec \cdot g)$ and was stable at this level for $\sim$ 3 hours. At that point a second series of H_2S injections were begun. After the second run the catalyst was outgassed and the CO adsorption gave $\sim$ 0.52 m^2/g.

In an effort to try to measure CO adsorption after the H_2S injections and before outgassing a method involving adsorption of CO from CO slugs injected into the He carrier gas was tried. Although this method did not give as reproducible results as the CO desorption method the errors were small. Based on CO adsorption after second run the

errors were ∿10% while the errors in the desorption experiments were <5%.

Immediately after the third poisoning the adsorption from CO slugs was used. Five cycles of adsorption - desorption of CO were done, figure 14. Care was taken to heat the bed uniformly to the reaction temperature to desorb the CO. An apparent plateau was reached during the second, third and fourth cycles. The corresponding values of apparent surface area are plotted in figure 11. After the fifth cycle the catalyst temperature was raised to 380°C in flowing He, the SO_2 desorption is shown in figure 15 where the rate of SO_2 desorption in moles/sec is plotted vs reactor temperature. After outgassing the CO adsorption gave 0.51 m^2/g.

For the last poisoning run two relatively large injections of H_2S were used, the first injection resulted in deactivation as expected. The second injection resulted in some regeneration of activity. The same effect was seen at higher temperatures and larger H_2S injections on a second catalyst load which will be mentioned later. After outgassing at 380°C the rate coefficient at 265°C was ∿3 $cm^3/(sec \cdot g)$.

After the H_2S injection runs and outgassing to 380°C the catalyst was heated in flowing air to ∿600°C, the SO_2 concentrations are shown in figure 16. Plotted in figure 16 are the SO_2 desorbtion rate and concurrent reactor temperature in °C vs time in minutes. The

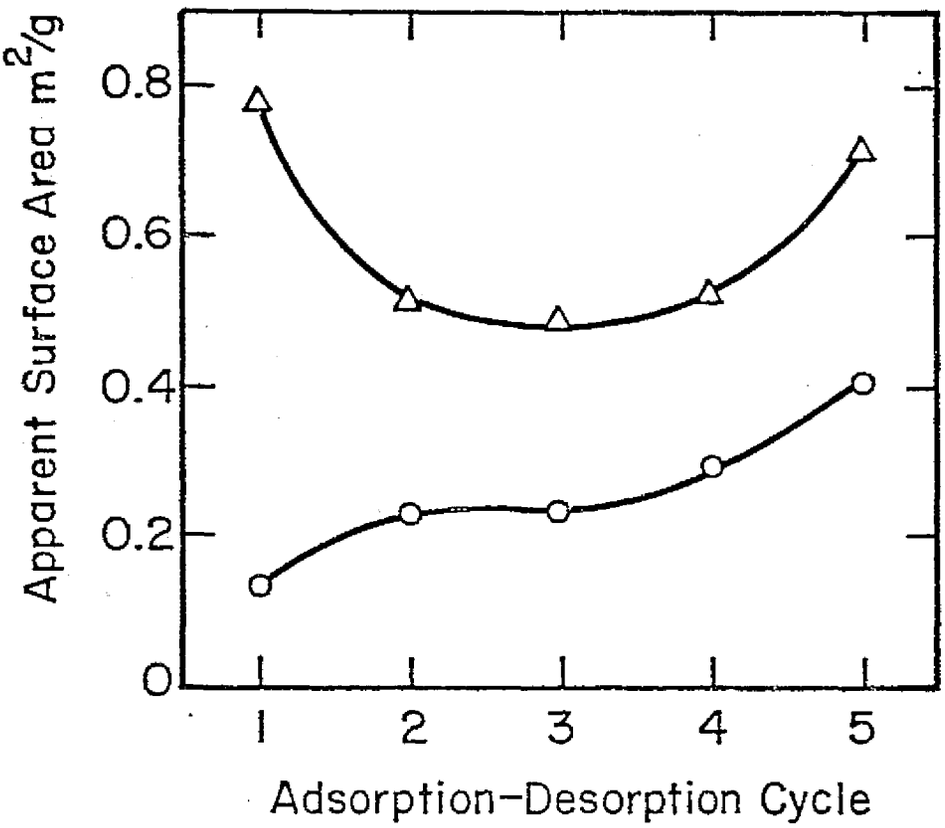

Fig.14 Adsorption - desorption of CO after third poisoning series and before high temperature outgassing. Five cycles of adsorption from CO slugs at 25°C and subsequent desorption at the reaction temperature of 254°C, O, adsorption; Δ , desorption.

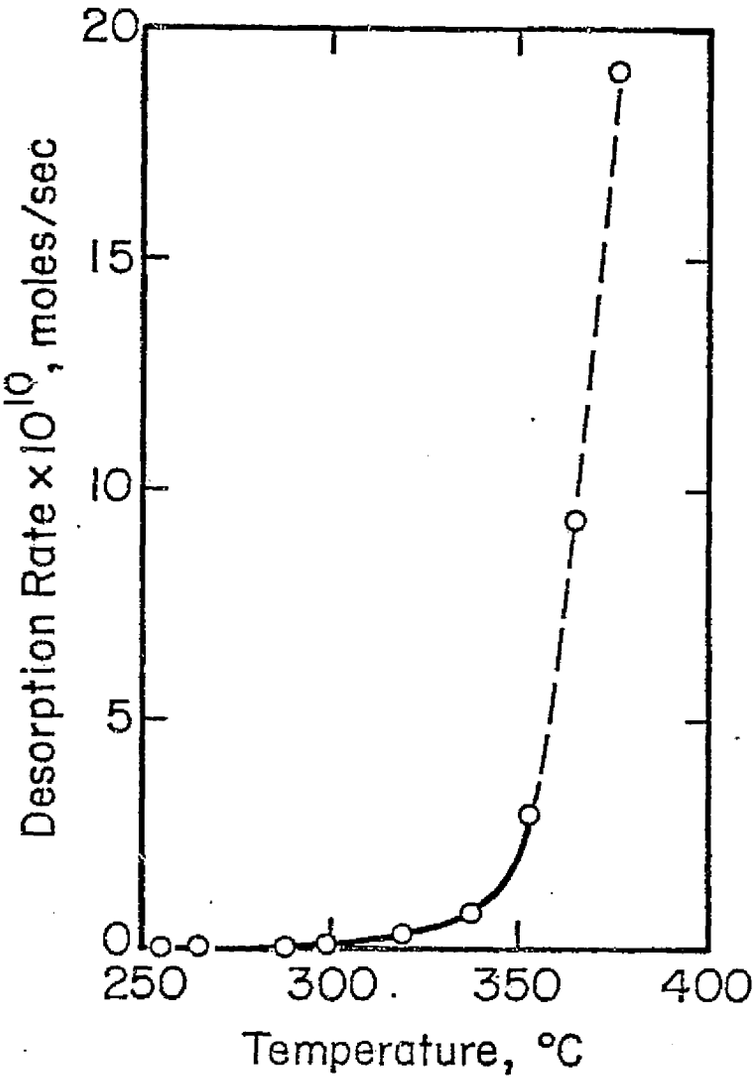

Fig.15 Sulfur dioxide desorption rate in flowing helium 0.40 cm^3/sec. After 5 cycles of CO adsorption - desorption the catalyst temperature was raised to 380°C with a linear heating schedule of 0.11°C/sec. The dashed line represents concentrations above the sulfur dectector saturation point of 14 ppm.

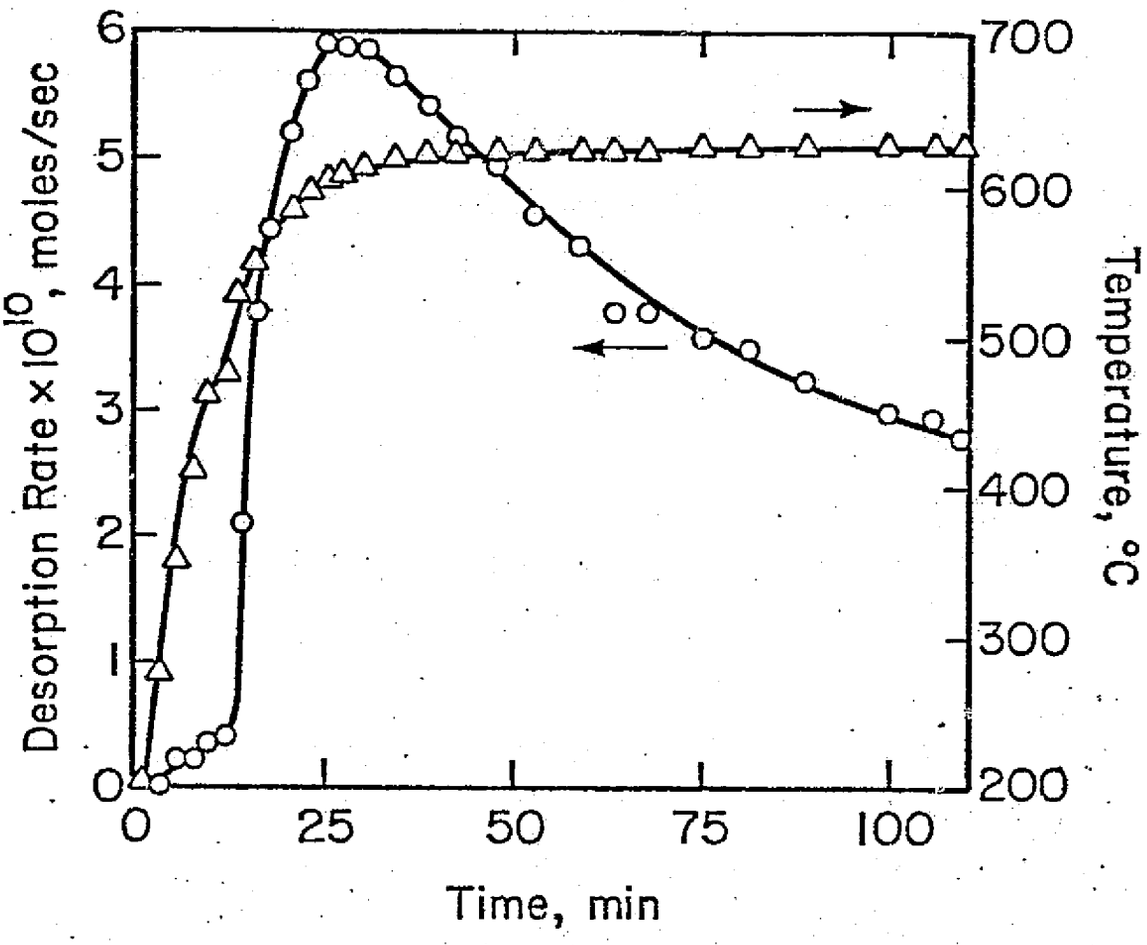

Fig.16 Sulfur dioxide desorption during high temperature oxygen treatment. After the fourth series of hydrogen sulfide injections and subsequent outgassing to 380°C the catalyst temperature was programmed to ∿ 620°C in flowing air, at 2.42 cm^3/sec.

oxidation rate coefficient after this treatment remained at ∿3 $cm^3/(sec \cdot g)$. Carbon monoxide adsorption after the high temperature O_2 treatment gave ∿0.50 m^2/g.

A second catalyst load, 1.66 grams was charged into the reactor to investigate further the H_2S poisoning of this catalyst. The method used to measure CO chemisorption on this catalyst was to outgas at 380°C and measure the adsorption from slugs of CO. Two different temperatures, ∿310°C and ∿250°C were used in three series of hydrogen sulfide injections. Some reaction order runs were initially done, figure 7, these experiments are discussed in the previous section on ethane oxidation kinetics. Next two temperature runs were done 217-331°C. These data along with steady-state data from the reaction order runs was used in the Arrhenius plot shown in figure 17. For comparison the initial temperature runs before the hydrogen sulfide poisoning of the first catalyst load are also plotted in figure 17. Although the Arrhenius plot for the second catalyst is nonlinear overall, the apparent Ea corresponds to roughly 13-14 kcal/mole from 256-331°C. The initial CO chemisorption gave 1.3 m^2/g. The overall poisoning phenomena on this catalyst load is represented in figure 18. Plotted in figure 18 are the first order rate coefficients for the oxidation and cracking of ethane in $cm^3/(sec \cdot g)$ extrapolated to 256°C vs. the total amount of H_2S injected in μ moles. The rate coefficients in

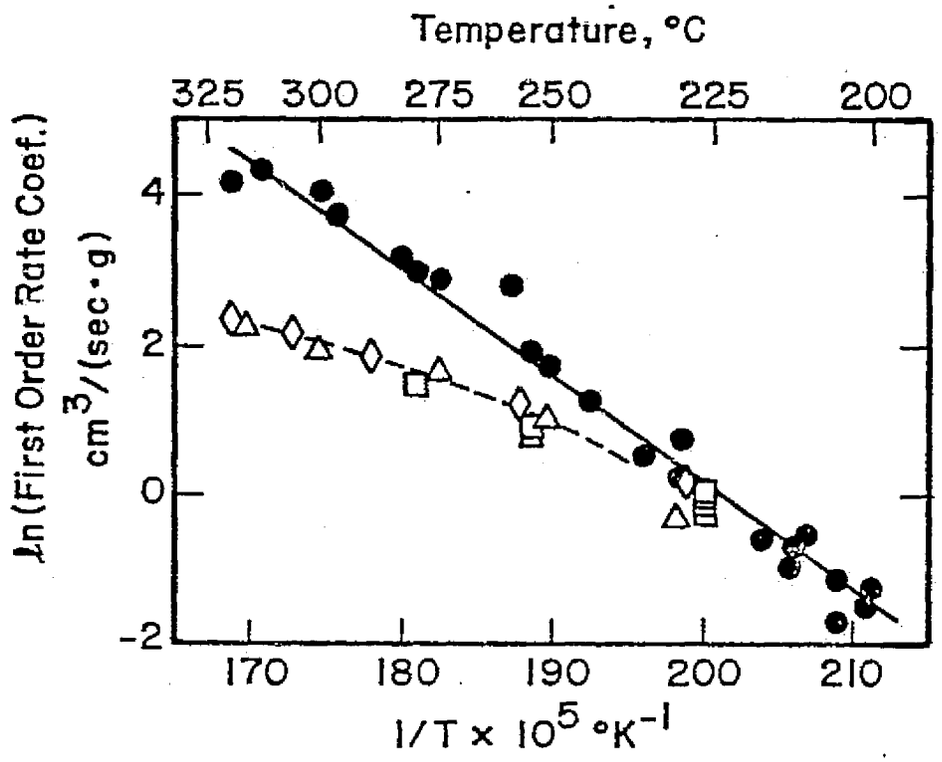

Fig.17 Arrehinus plot for data on catalyst loads one and two, prior to hydrogen sulfide injections. Temperature run on first catalyst load, , data from figure 5. Open symbols are data on the second catalyst load: □ , initial rate coefficients measured along with the unsteady state reactiion order runs; △ , ◊ , two temperature runs on consecutive days after the reaction order runs.

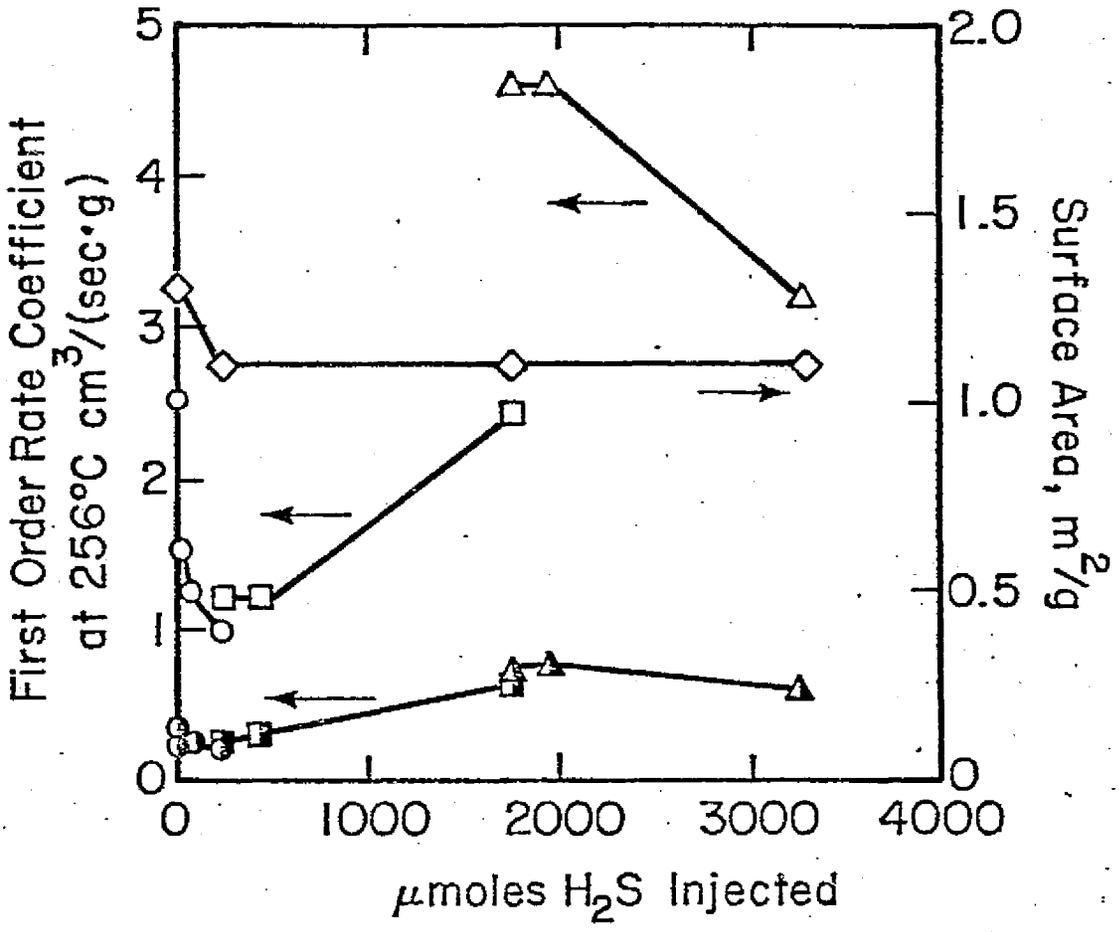

Fig.18 Hydrogen sulfide poisoning of the second catalyst load, 1.66 grams. Open symbols are oxidation rate coefficients, half shaded symbols are cracking coefficients. Three injection series are represented: First series, 2, injections, ○, 58.7 and 184.3 μ moles at a residence time of 5.18 min., 309.1°C; second series, □ , 2 injections 184.3 and 1326 μ moles at a residence time of 5.18 min., 309.9°C; third series, △, ◭ injections, 183.9 and 1322 μ moles at residence times of 8.46 and 2.84 min. and reactor temperatures of 249.5 and 256.0, respectively.

figure 18 above 256°C are corrected to 256°C with 13.5 kcal/mole, those below are corrected with the arbitrary value of 27 kcal/mole. Due to the uncertainity in the Ea for this catalyst load only a qualitive comparison between the rate coefficients extrapolated from ∿310°C on the first two injection series and the rate coefficients extrapolated from 250°C on the third injection series can be made.

The initial oxidation rate coefficient plotted in figure 18, 2.5 $cm^3/(sec \cdot g)$, was taken from the previous temperature run and was extrapolated from 300°C since the initial poisoning runs were at a reaction temperature of ∿310°C. The apparent cracking rate coefficient is ∿14% of this magnitude. After the temperature runs the catalyst was left at room temperature in the reaction gases for ∿41 hours. When the reactor was heated up again the rate coefficient at 256°C extrapolated from 309°C had decayed to 1.5 $cm^3/(sec \cdot g)$, the cracking coefficient remained at 14% of the oxidation coefficient. These rate coefficient values are plotted in figure 18. Reaction rates measured at two different temperatures 309.2 and 282.8°C immediately before the first poisoning gave an apparent Ea of 13.9 kcal/mole.

The first series of injections at 309°C decreased the oxidation rate coefficient while the cracking coefficient increased slightly. The surface area decreased from 1.3 to 1.1 m^2/g, throughout the remainder of the experiments the CO chemisorption stayed at this level. The two

injections in the second poisoning run at 310°C had different effects. The first, 184.3 μ moles, which was the same amount as the last injection on the first run didn't effect the oxidation rate coefficient. The second injection, 1326 μ moles, resulted in reactivation to about the level of activity measured in the temperature runs at this temperature. The unsteady state behavior after this injection is shown in figure 19. The two injections in the third and last run at 249°C also had varing effects. The first injection having the same amount as the first injection on the second run, 184.3 μ moles, similiarly did not effect the oxidation rate coefficient. The second injection of the third run having the same amount of H_2S as the second injection of the second run 1326 μ moles resulted in deactivation. The non-steady state behavior on the first injection of the 3rd run is shown in figure 20.

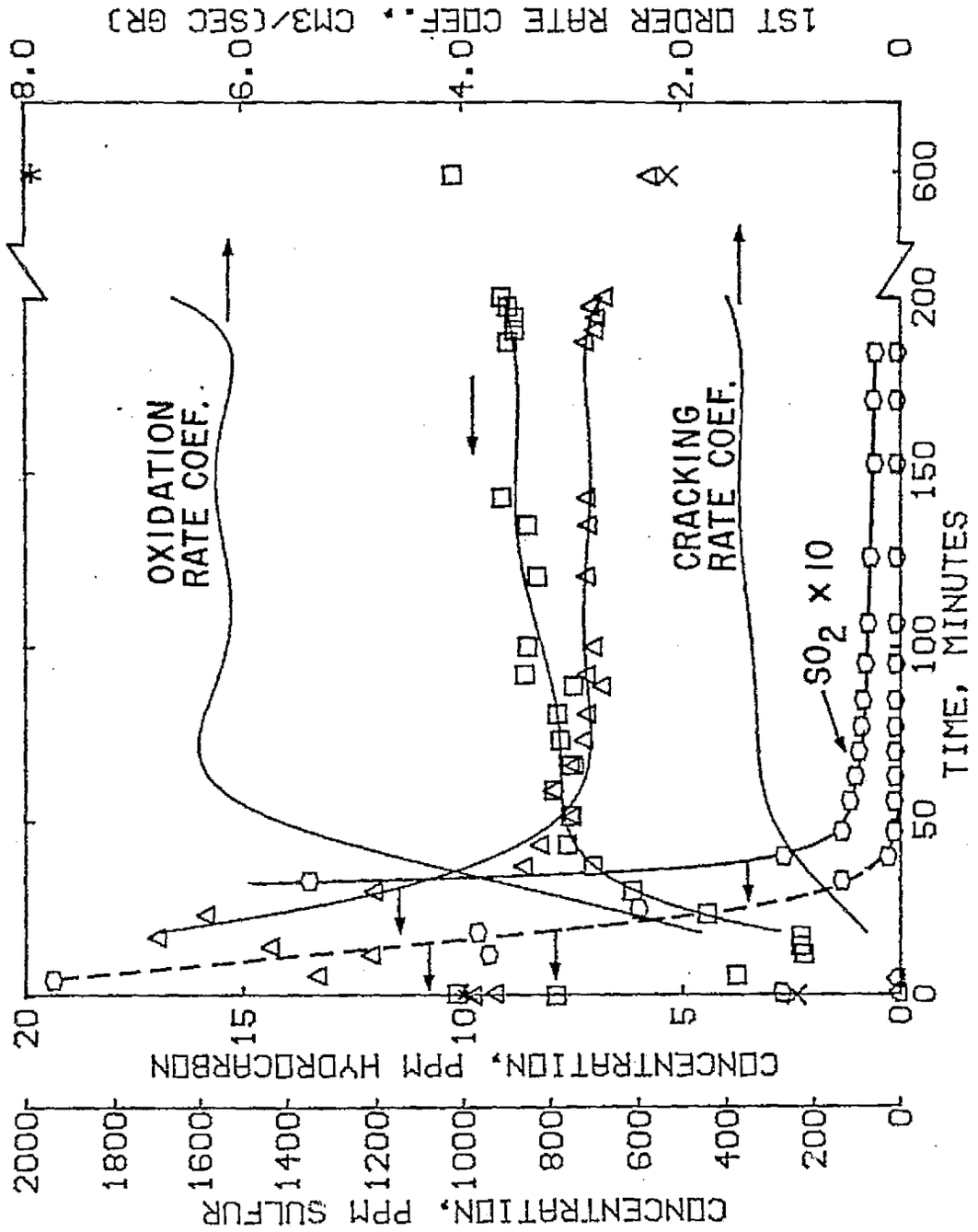

Fig.19 Unsteady state behavior, second catalyst load, after 1326 μ mole hydrogen sulfide injection. Second injection of third series, 427.4-1753.4 μ moles on figure 18. Reaction temperature is 309.9°C, residence time is 5.18 min., ethane feed level is 30 ppm. Symbols: *, x, initial and final oxidation and cracking rate coefficients, respectively, Calculated from steady state data, ⬡ SO_2, △ H_2S, □ CH_4, △ C_2H_6.

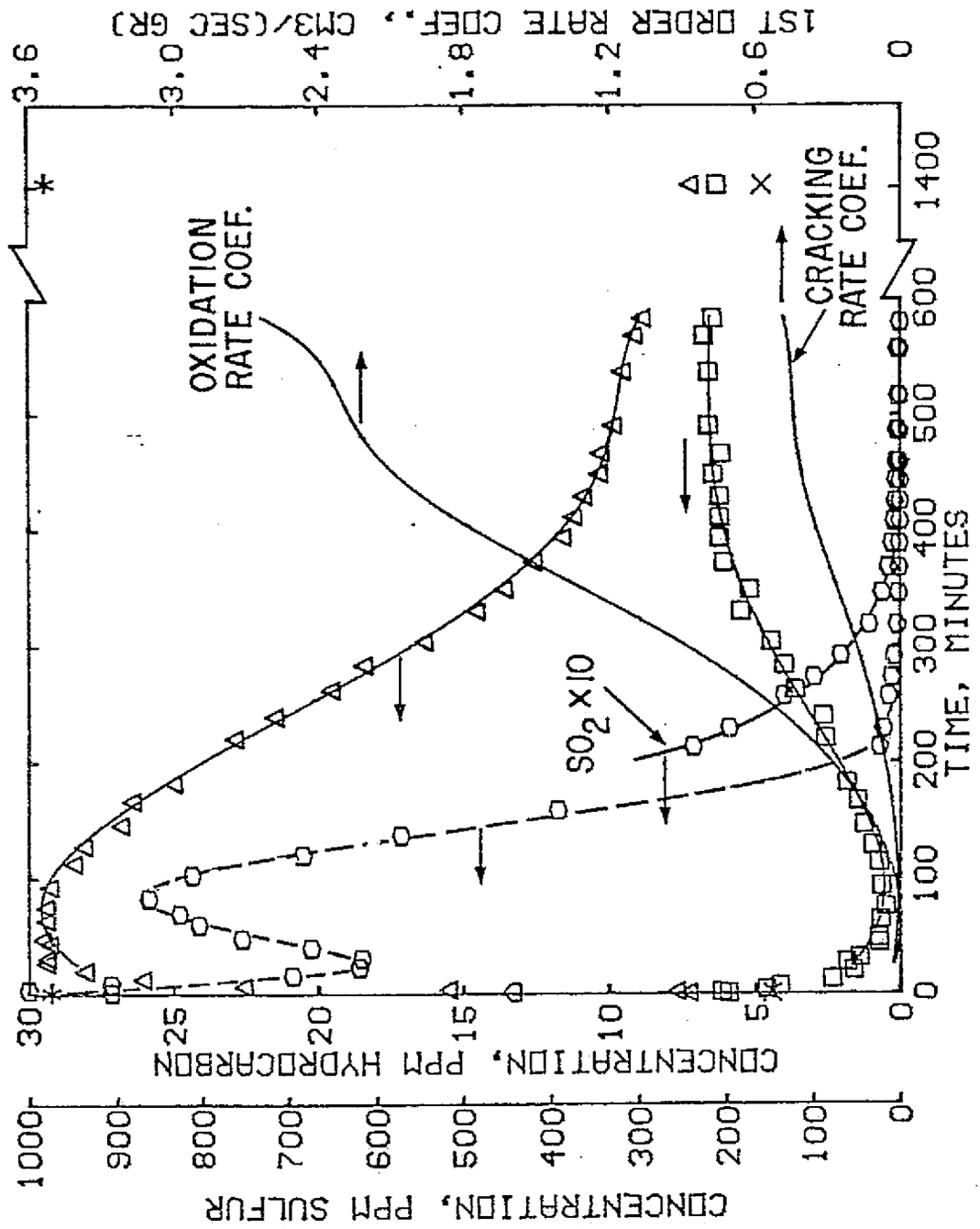

Fig.20 Unsteady state behavior, second catalyst load after 184 μ mole hydrogen sulfide injection. First injection of third series, 1753-1937 μ moles on figure 18. Reaction temperature is 249.5°C, residence time is 8.46 min., ethane feed level is 30 ppm. Symbols: *, x, initial and final oxidation and cracking rate coefficients respectively, calculated from steady state data, ○ SO_2, △ H_2S, □ CH_4, △ C_2H_6.

Discussion

I. Intrinsic Kinetics

1. Ethane Oxidation

Under the reaction conditions used in this work, $\sim 10^{-2}$ torr C_2H_6, $\sim 10^2$ torr O_2, $\sim$ 200-300°C, C_2H_6 oxidation follows first order kinetics with an apparent E_a of 27 kcal/mole. The highest stable pre-exponential k_s measured was 1.0×10^8 cm/sec. A previous work in this laboratory (2) using an integral reactor with a 0.5 wt % Pd Englehard catalyst had reported first order kinetics and an E_a range 21-33 kcal/mole. Temperatures of 90-185°C were used with the same ethane and oxygen pressures as in this work. The widest range of temperatures used in any E_a determination in Rabbs work (2) was $\sim$ 25°C. Considering the scatter in the data in this work and in Rabbs work temperature ranges much larger than 25°C should be used to determine an E_a. Low E_a values over a small temperature range are attributable to ethane adsorption-desorption effects. Changing the catalyst temperature results in net ethane adsorption or desorption at a rate of the same magnitude as the reaction rate based on the disappearance ethane. Lowering the catalyst temperature can result in a significant but slow net adsorption rate and thus can lead to low apparent E_a. Raising the temperature causes net ethane desorption, leading to a suprious low reaction

rate based on ethane disappearance and a low calculated E_a. These adsorption - desorption effects are minimized when the temperature range used to determine the E_a is large giving rise to very large changes in the oxidation reaction rate which are large compared to the adsorption desorption rates. Of the two catalyst loads used by Rabb the pre-exponentials computed* assuming an effective E_a of 27 kcal/mole at 162°C are 9.3×10^8 and 3.7×10^8 cm/sec. In both computations a CO chemisorption of 17 μ mole/g which translates to ∿ 1.2 m^2/g Pd has been assumed. It is of some interest that Rabb's CO chemisorption on the fresh catalyst translates to ∿ 1.3 m^2/g which is the same surface measured initially on the second catalyst load used in this work. This result is unexpected since the support surface areas are of comparable magnitude and the Englhard catalyst has a surface impregnation (0.42 of the pellet volume), whereas this catalyst has a deeper impregnation (0.78 of the outer pellet volume) in this work.

*Rabb's reported reaction rates are based on gross volume of catalyst bed, the catalytic rate coefficient is given by k_s [cm/sec] = [k_v V/S] catalyst bed volume, V has been back calculated from the formula given in his thesis appendix, assuming that his reported bed heights of 0.7-1.5 in. correspond to the catalyst loads of 3.9 and 7.8 grams respectively. The Pd surface area of each catalyst load, S, was calculated assuming 17 μ moles of CO adsorbed per gram of catalyst.

The Pd loading was the same for both catalysts so one might have expected a greater Pd surface area in the catalyst used in this work.

There is very little data in the literature on ethane oxidation by noble metals. Wise (8) using the catalytic ignition method with a Pt wire has reported first order kinetics, an E_a of 27.3 kcal/mole and a pre-exponential of 2.8×10^{10} cm/sec. Pressures of $\sim 10^2$ torr O_2 and $\sim$ 10 torr ethane were used and the transition ignition temperatures which are used in the Arrehius plot were in the range 440-480°C.

2. Diethyl Ketone Oxidation

First order kinetics were observed at 137°C. The apparent E_a calculated from first order rate coefficients in the range 110-190°C is $\sim$14 kcal/mole. The highest stable pre-exponential was 5.7×10^3 cm/sec, based on a surface area of 0.79 m^2/g measured after the DEK runs.

Nonlinear self poisoning of the reaction was observed at 137°C, the poisoning was reversible. After the temperature was increased to $\sim$190°C on the second temperature run, figure 10, there was some apparent regeneration. This was confirmed by the apparent pre-exponential on the third temperature run. Self poisoning of ethane oxidation at temperatures below 190°C has been reported by Rabb.

Wise (8), using the catalytic ignition method has

reported first order kinetics, an E_a of 14.7 kcal/mole and a pre-exponential of 9.5×10^8 for the oxidation of DEK on a Pt wire.

The temperature range was not reported, pressures were $\sim 10^2$ torr oxygen and ~ 10 torr DEK. Although the activities of Pd and Pt are not expected to be the same, they are often of the same magnitude for hydrocarbon reactions. That the pre-exponentials differ by a factor of 10^{-5} is not reasonable. This result casts some doubt on the relatively high value of Wise's reported Pt pre-exponential for ethane oxidation.

3. Comparison of Ethane and Diethyl Ketone Oxidation Rates

Since the temperature regions used to obtain intermediate conversions of the two hydrocarbons did not overlap in this work and the kinetics of ethane oxidation were more extensively studied, for comparison of the oxidation rates a temperature of 175°C is chosen. This is well within the temperature region of the DEK experiments and yet requires little extropolation of the kinetics obtained in the 200-300°C region for ethane oxidation. The pre-exponentials and E_a used in this comparison are 5.7×10^3 cm/sec and 14 kcal/mole for diethyl ketone and 1.0×10^8 cm/sec and 27 kcal/mole for ethane. The concentration of hydrocarbon used is

equivalent to 10 ppm (7.6×10^{-3} torr) at 175°C and one atmosphere total pressure. At these conditions the DEK turnover number (molecules/sec cm^2) is 1.4×10^{11} and the ethane turnover number is 1.1×10^{9}. Using the Hertz-Knudsen equation (22) to calculate the impingment rate for each hydrocarbon, at this temperature, the reaction probability for DEK is 1.0×10^{-7} and the ethane reaction probability is 4.8×10^{-10}.

4. Mechanism and Predicted Pre-Exponentials of Hydrocarbon Oxidation on Noble Metals

The sticking coefficients of hydrocarbons on noble metals are much less than that of oxygen and the oxygen pressure used in this work was $\sim 10^4$ times larger than those of the hydrocarbons hence it is reasonable to conclude that the clean Pd surface is covered with a near monolayer of adsorbed oxygen. With this in mind there appear to be two plausible simple oxidation mechanisms which will exhibit first order kinetics. (1) Surface-gas reaction between gaseous hydrocarbon and adsorbed oxygen. The form of the rate equation is:

$R = k_{sg}[H\text{-}C]_{gas}\ \theta_{oxygen}$, and since $\theta_{oxygen} \simeq 1.0$, $R = k_{sg}[H\text{-}C]_{gas}$.

(2) Bimolecular surface reaction between adsorbed oxygen and adsorbed hydrocarbon. The form of the rate equation is:

$R = k_s\ \theta_{H\text{-}C}\ \theta_{oxygen}$, since $\theta_{oxygen} \simeq 1.0$ then $R = k_s\ \theta_{H\text{-}C}$.

Assuming Langmuir adsorption of the hydrocarbon and since $\theta_{oxygen} \simeq 1.0$, $\theta_{H-C} \simeq 0$ then $\theta_{H-C} = K_L [H-C]_{gas}$, which leads to $R = k_s K_L [H-C]_{gas}$.

The magnitudes of the pre-exponentials of the predicted first order rate coefficients, k_{sg} and $[k_s K_L]$ can be estimated from transition state theory. They are, in fact, indistinguishable within that formalism and predicted to be between unity and 10^7 cm/sec. Though the calculated pre-exponential for ethane oxidation is 10^8 cm/sec, a factor of 10 too large, the correct value may be well within the expected range because of the experimental uncertainty in E_a. The pre-exponential for diethyl ketone is well within the expected range.

II Hydrogen Sulfide Poisoning

1. First Catalyst Load

Hydrogen sulfide poisoning of the ethane oxidation reaction exhibited both reversible and irreversible poisoning. The irreversible poisoning is characterized by a fast initial deactivation 30% with a relatively small hydrogen sulfide input, 51.0 μ moles. During a series of injections it was not possible to separate the reversible from the irreversible poisoning effects, since the catalyst was outgassed after a series of injections a measure of the irreversible poisoning was only available

after the cumulative effect of the entire injection series. The close correspondence of the activity after the first injection 10.2 μ moles and the irreversible poisoning after the first injection series 51 μ moles suggests that ∿30% of the initial activity is irreversibly lost with the first hydrogen sulfide injection.

There are two noteworthy similarities between the reversible and irreversible poisoning phenomena. (1) The nonlinear behavior of the rate coefficient vs. the amount of hydrogen sulfide injected. The nonlinear irreversible poisoning is represented by the dotted line, figure 11. As mentioned in the results section this curve is drawn through the oxidation rate coefficients after the catalyst had been outgassed and thus by irreversible poisoning it is meant that the poisoning is not reversible with respect to outgassing. The nonlinear reversible poisoning can be identified on the third injection series from the asymptotic behavior of the oxidation rate coefficient at a level well below the irreversible poisoning curve. (2) There appears to be a base level of the oxidation rate coefficient for reversible and irreversible poisoning as shown by the asymptotic behavior in both cases. For irreversible poisoning it is 3.2 $cm^3/(sec \cdot g)$, for reversible poisoning it is 2.2 $cm^3/(sec \cdot g)$.

Rabb also found that the CO surface area measurement decreased with a decreasing rate coefficient. However, he

found that an overall decrease in his rate coefficient of 75% caused by sulfur poisoning and high temperature treatment in oxygen resulted in a 50% decrease in the CO chemisorption. The differences may be attributable to the different poisoning temperatures used or to differences in the CO chemisorption preparation procedures.

There is some evidence that the reversible poisoning is caused by adsorption of sulfur dioxide on the catalyst. Temperature programmed desorption of sulfur dioxide after a hydrogen sulfide injection and the sulfur dioxide wash out after a hydrogen sulfide injection demonstrated strong retention of sulfur dioxide by the catalyst. The recovery of the rate coefficient at small sulfur dioxide pressures after hydrogen sulfide injections and the further restoration after high temperature outgassing suggest reversible poisoning by sulfur dioxide.

It is thought that the CO chemisorption itself did not result in reactivation for two reasons: (1) Bonzel and Ku (24) reported no direct interaction of adsorbed sulfur (deposited by H_2S gas) and CO on Pt (110) although adsorption of sulfur did cause the desorption energy of CO to decrease slightly. (2) Repeated activity measurement and subsequent CO adsorption cycles resulted in the same CO adsorption before poisoning.

Sulfur dioxide may also be responsible for the irreversible poisoning phenomena. No separate experiments

using sulfur dioxide alone were done.

Wheeler (25) has shown that with a sufficiently large diffusion modulus a small amount of pore mouth poisoning results in severe mass transfer limitations, accordingly the intrinsic kinetics will not be observed after the first introduction of poisoning. Petersen's time dependent poisoning model (26) has shown that the nonlinear time dependent poisoning as seen by Rabb (2) can also be explained by increased diffusion resistance caused by progressive pore mouth poisoning if the diffusion modulus is large.

Evidence of pore mouth poisoning of H-C oxidation by sulfur has been reported on auto exhaust catalysts (G.M. propreitary Cu-Cr on 1/8 inch γ alumina pellets.) (27) A fuel of $\sim$300 ppm sulfur content resulted in sulfur deposits of 6-10 mils deep.

Calculations contained in the appendix on diffusion limitations assuming Wheeler's model (25) have shown that increased diffusion resistance caused by pore mouth poisoning did not effect the reaction rate at 256°C on the first catalyst load.

It should be mentioned that the prediction of intrinsic diffusion limitations on this catalyst preparation lie between those seen on the two catalyst loads used. These calculations are contained in appendix 9 on diffusion limitations.

From the data taken it is not possible to say whether or not the activity loss is caused by progressive pore mouth poisoning. Wheeler's model (25) predicts pore mouth poisoning will cause transition of the intrinsic E_a to the diffusional E_a (∿1-2 kcal/ mole) at large intrinsic diffusion modulus. The temperatures needed to increase the diffusion modulus enough to demonstrate an appreciable deviation from the intrinsic E_a were not used after the poisoning. Furthermore since the intrinsic diffusion limitation of this catalyst load were not encountered throughout the temperature range used deviation of the apparent E_a would be difficult to interpret.

2. The Second Catalyst Load

The kinetic behavior of the second catalyst load was markedly different from the first load. Although first order kinetics were observed the Arrhenius plot was non-linear. Poisoning of the second catalyst load was not characterized by the continuous poisoning phenomena exhibited by the first load. This may be attributable in part to the higher temperatures used on the first and second hydrogen sulfide injection series. The degree of poisoning and loss of surface area was small and the poisoning was reversible.

The nonlinear Arrhenius plot is characteristic of a

large diffusion resistance. Whether the diffusion resistance represents pore mouth poisoning or intrinsic mass transfer limitations or a combination is difficult to tell from the reaction rate data taken.

There is some evidence of the catalyst being poisoned by residual pressure of sulfur species in the reactor left from the poisoning experiments on the first catalyst load. If the catalyst were already poisoned prior to hydrogen sulfide injections it would explain the reversible poisoning result and the minimal loss in surface area after the hydrogen sulfide was injected. Assuming Wheeler's pore mouth poisoning model (25), if the nonlinear Arrehinus plot was an artifact of intrinsic diffusion limitations then because of the large intrinsic diffusion modulus at the poisoning temperatures used a very small amount of poison should cause a very large increase in the diffusion resistance and accordingly a very large decrease in the apparent rate coefficient. No large decrease was observed with the first introduction of hydrogen sulfide.

To calculate an intrinsic activity of this catalyst load the kinetics observed before poisoning must be assumed to be intrinsic kinetics. With this assumption the intrinsic activity can be estimated using the Thiele model, since the Arrhenius plot is approximately linear (13-14 kcal/mole) from $1/T \times 10^5 = 169\text{-}189$. Calculations in Appendix 9 on diffusion limitations show that

assuming the onset of the approximate halving of the intrinsic E_a to be at $1/T \times 10^5 = 189°K^{-1}$ an apparent intrinsic pre-exponential can be calculated, 2.9×10^{12} $cm^3/(sec \cdot g)$. The pre-exponential prior to poisoning of the first catalyst load was about 8.6×10^{11} $cm^3/(sec \cdot g)$. The ratio of these pre-exponentials is $\sim$3.4 whereas the second catalysts surface area is only about 1.5 times as great.

There is however some justification for assuming the intrinsic activity may be higher since the surface area per gram corresponds to that of the fresh catalyst used in Rabb's work and his pre-exponentials k_w measured on two catalyst loads were 1.1×10^{13} and 4.4×10^{12} $cm^3/(sec \cdot g)$.

If the second catalyst does represent intrinsic kinetics the relative activities of the two catalyst loads points to a very much different pore structure or catalytically active metal distribution. In this regard it should be mentioned the catalyst preparation procedures used in loads 1 and 2 differed in one significant area. When the second catalyst was charged into the reactor the exhaust from an oxygen gas torch used to seal the catalyst into the reacter loop caused the catalyst to turn jet black. This did not occur with the first catalyst load. Subsequent oxygen treatment $\sim$20 hrs. in air at 400°C resulted in removal of the

sooty outside appearance of the pellets.

Some comparison can be made between the hydrogen sulfide poisoning at both catalyst loads. (1) The recovery of the rate coefficients after hydrogen sulfide injection is inversely proportional to the sulfur dioxide pressure. (2) Restoration of some activity after high temperature outgassing. (3) Some surface area loss with poisoning (4) Large injection of hydrogen sulfide caused some regeneration. The interpretation of this last point is that the transitory heating of the catalyst by the highly exothermic combustion of hydrogen sulfide combined with the water vapor created by combustion in effect steamed off catalytic poisons. Steam injection is a well known procedure used to regenerate reforming catalysts.

3. Comparison of Hydrogen Sulfide Poisoning Observed in This Work with Other Work in this Laboratory (2)

In comparison* with other work done in this laboratory (2) this catalyst preparation at the temperature 256°C

*This comparison is only meant to be a qualitative one since an integral bed poisoned by a continuous poison input is expected to exhibit much different poisoning phenomena from a catalyst in an equivalent CFSTR poisoned by high transients of poison concentration. It would be expected though that for the same dosing the CFSTR would exhibit larger activity losses since the catalyst pellets are uniformly accessible and much higher poison concentrations are used. For instance a 10.2 μmole hydrogen sulfide injection should result in an immediate concentration spike in the reactor of 466 ppm.

is very much less susceptible to hydrogen sulfide poisoning than the catalyst Rabb used at ∿175°C. Rabb reported, using a catalyst already partially deactivated from ethyl mercaptan poisoning that a loss of 53% of the catalyst activity occurred at ∿ 175°C with ∿36.7 (μmoles H_2S/gram catalyst) and that this loss was irreversible with respect to high temperature oxidation treatments.

However at the temperature used on the first catalyst load in this work, ∿ 256°C, it took more than 180 (μmoles H_2S/gram catalyst) to reach a plateau of 51% loss of the initial activity; this loss was irreversible with respect to outgassing at 380°C.

One last point is worth mentioning with respect to hydrogen sulfide poisoning of the catalyst. Although significant irreversible activity losses occurred the catalyst does retain a substantial amount of the initial activity and only the pre-exponentials are affected. Hence for noble metals assuming an effective E_a range for hydrocarbons of those seen in this work, ∿ 14-27 kcal/mole at 250°C a loss of 50% activity can be recovered by increasing the temperature of the active bed by ∿ 10-20°C.

4. Comparison of Freon and Hydrogen Sulfide Poisoning of the First Catalyst Load.

A complete report of Freon* poisoning of the first catalyst load, which is discussed below, appears in Appendix 7.

Poisoning of ethane oxidation was investigated on the first catalyst load at ∿256°C by hydrogen sulfide and to a smaller extent by Freon compounds at ∿247°C. In both cases the observed decrease in the first order rate coefficient with the amount of poison injected was nonlinear and asymptotic. Freon poisoning was much more severe than hydrogen sulfide poisoning. For instance at 247°C, residence time 10.3 minutes, more than 95% of the catalytic activity of the first catalyst load, 1.1 grams, was lost after ∿200 μmoles of Genetron 142-B was injected whereas at ∿256°C and residence times of 2.5-5.0 minutes, the maximum activity loss from hydrogen sulfide injection amounted to 65% at ∿300 μmoles**.

*By Freons it is meant halogenated refrigerants. Two were used in this work: Freon 22 and its C_2 methylated analogue, Gentron 142-B.

**The conditions under which these poisoning experiments were done are not the same, the temperatures varied by ∿10°C and the residence times were substantially different. However the comparison is a fair one since the difference in the poisoning temperatures is small and the severity of the poison dosing is not strongly dependent on the residence time. The injected poisons were removed from the gas phase very rapidly, within a few minutes, thus the true residence time of the unoxidized poison is dependent upon its chemical structure and to a much lesser extent upon the residence time based on the volumetric flowrate purging the reactor.

In comparision the Freon injections and hydrogen sulfide injections resulted in, qualitatively, much the same transient decay and slow recovery of the oxidation rate coefficient with time. In the case of hydrogen sulfide there was evidence that strong retention of the oxidation product SO_2 resulted in reversible poisoning. The halogenic acids that are produced in Freon oxidation could not be detected with the analytical train used in this work. However, a reasonable inference from the slow recovery of the rate coefficients after the poison injections is that the poisoning of the catalyst is dependent no only on the nature of the injected poison but upon the catalyst's retention of oxidation products resulting from combustion of the poison. Thus the time dependent recovery after a poison injection may be attributed to slow outgassing at the reaction temperature.

There are two noteworthy differences between hydrogen sulfide poisoning and Freon poisoning. (1) Freon poisoning is reversible* by oxidation treatments at 380°C whereas poisoning by hydrogen sulfide is only partially reversible. (2) As previously mentioned, Freon poisoning is much more severe than hydrogen sulfide poisoning.

The explanation is that Freons are much more stable compounds than hydrogen sulfide and thus have much more

*Reversible poisoning by halogenated hydrocarbons of methane oxidation on Pd has previously been reported, see reference 7, C.F. Cullis, et al., in J. Cat.

accessibility to the unpoisoned part of the catalyst. In contrast, hydrogen sulfide is very unstable, it is oxidized in air and by γ Al_2O_3 before it can reach the unpoisoned surface. However the sulfur species once formed on the Pd surface is not as easily removed as the residue deposited by Freons.

References

1. Butt, J.B., "Catalyst Deactivation", Advan. Chem. Ser. 1972, 109 (Chem. React. Eng., Inst. Symp. 1st), 259-496.

2. Rabb, D.T., M.S. Thesis, U.C. Berkeley, Department of Chemical Engineering, 1973.

3. Anderson, R.B., K.C. Stein, J.J. Feenan, and L.J.E. Hofer, I. and E.C., 53, No. 10, pp. 809-812 (1961).

4. Johns, R.H., P.L. Garwig, M. Markels, Technical Report AFFDL-TR-65-46, (1965).

5. Cullis, C.F., D.E. Keene, and D.L. Trimm, Trans Faraday Soc., 67, Pt. 3, 864-76, (1971).

6. Wheeler, A., A.J. Robell, J. of Catalysis, 13, pp. 299-305 (1969).

   Thomas, F.S., J.K. Musick, J.E. Johnson, I. and E. and C., Research Results Service (1970).

7. Cullis, C.F., D.E. Keene and D.L. Trimm, J. of Catalysis, 19, 378-385 (1970).

   Olcott, T.M., Nas 1-9242, (1972).

8. Hiam, L., H. Wise and S. Chaikin, J. of Catalysis, 9-10, 272-276 (1968).

   Schwartz, A., L.L. Holbrook, and H. Wise, J. of Catalysis, 21, 199-207 (1971).

9. Bird, B.R., W.E. Steward, and E.N. Lightfoot, "Transport Phenomena", p.46, John Wiley and Sons, (1960).

10. Dow Corning Corporation, Silicons from Dow Corning, Circular #05-235.

11. Gillespie, B. and J.J. Carberry, I. and E.C. Fundamentals, 5, 164-171, (1966).

12. Sternberg, J.C., W.S. Gallaway, and D.T.L. Jones, "Gas Chromatography, Third International Symposium Analysis Instrumentation Division of the Instrument Society of America, June 13-16, 1961", pp.248-265, N.Brenner, J.E. Callen, and M.P. Weiss, editors, Academic Press, New York, (1962).

13. Stevens, R.K., J.D. Mulik, A.E. O'Keefe, and K.J. Krost, Analytical Chemistry, 43, 827-831, (1971).
Stevens, R.K., A.E. O'Keefe, and G.C. Ortman, Environmental Science and Technology, 3, 652-655, (1969).

14. Aben, P.C., J. of Catalysis, 10, 221-229, (1968).

15. Boudart, M. and H.S. Hwang, J. of Catalysis, 39, 44-52 (1975).
Conrad, H., G. Ertl and E.E. Latta, Surface Science, 41, 435-446 (1974).

16. Harkness, A.C., F.E. Murray and L. Girard, Atmospheric Environment, 2, 303-320, (1968).

17. Nelsen, F.M., and F.T. Eggertsen, Analytical Chemistry, 30, 1387-1390, (1958).

18. Gruber, H.L., Analytical Chemistry, 34, 1828-1831, (1962).

19. Adamson, A.W., "Physical Chemistry of Surfaces", p. 586, Interscience Publishers, New York, (1967).

20. Conrad, H., G. Ertl, J. Koch and E.E. Latta, Surface Science, 43, 462-480, (1974).

21. Scholten, J.J.F. and A. Van Montfoort, J. of Catalysis, 1, 85-92, (1962).

22. Hirschelder, J.O., C.F. Curtiss and R.B. Bird, "Molecular Theory of Gases and Liquids", John Wiley and Sons, New York, (1954).

23. Liu, C.L., T.T. Chuang, and I.G. Dalla Lana, J. of Catalysis, 26, 474-476 (1972).

24. Bonzel, H.P., and R. Ku, J. Chem. Phys. 59, 1641-1651, (1973).

25. Wheeler, A., "Catalysis II", P.H. Emmett, Ed. Chapter 2, pp. 105-164, Reinhold, New York, N.Y., (1955).

26. Petersen, E.E., "Chemical Reaction Analysis", Prentice Hall, Englewood Cliffs, N.J., (1965).

27. Hunter, J.E., Research Laboratories General Motors Corp., Society of Automotive Engineers Publication #720122.

28. Satterfield, C.N. and T.K. Sherwood, "The Role of Diffusion in Catalysis", Addison-Wesley Publishing Co., Reading, Mass., (1963).

29. Aris, R., Chem. Eng. Sci., 6, 262, (1957).

30. Weisz, P.B. and C.D. Prater, "Advances in Catalysis and Related Subjects, Vol. VI", W.G. Frankenburg et al, Eds., pp. 143-196, Academic Press, New York, N.Y., (1954).

31. Damköhler, G.Z., Phys. Chem., A193, 16 (1943).

32. Prater, C.D., Chem. Eng. Sci., 8, 284, (1958).

Appendix 1.

Tracer Experiments

To investigate the mixing phenomena and measure the effective volume of the recycle loop tracer experiments using helium and air at room temperature and pressure were performed. The gas mixtures were analyzed by taking a small bleed off the recycle loop effluent and putting it through a calibrated thermal conductivity cell. The cell was calibrated at the bleed flowrate for each run. Care was taken to minimize the amount of tubing which transported the loop effluent to the cell and since the cell has a small internal volume any segregated flow in the small amount of tubing in the effluent and T.C. cell is not thought to have affected the concentrations in the effluent.

The experimental procedure involved introducing a flow of helium into the air filled recycle loop with the catalyst bed bypass valve open. In a well stirred vessel the logarithm of the volumetric fraction of air left in the recycle loop should be directly proportional to the amount of time after the helium was introduced.

The results of five runs at varior volumetric flowrates are represented in figure 21. The equation plotted is

$$-\ln(\text{fraction air}) = (\text{residence time})^{-1}(\text{time})$$

knowing the volumetric flowrate the effective volume of the recycle loop can be calculated from the slope of the

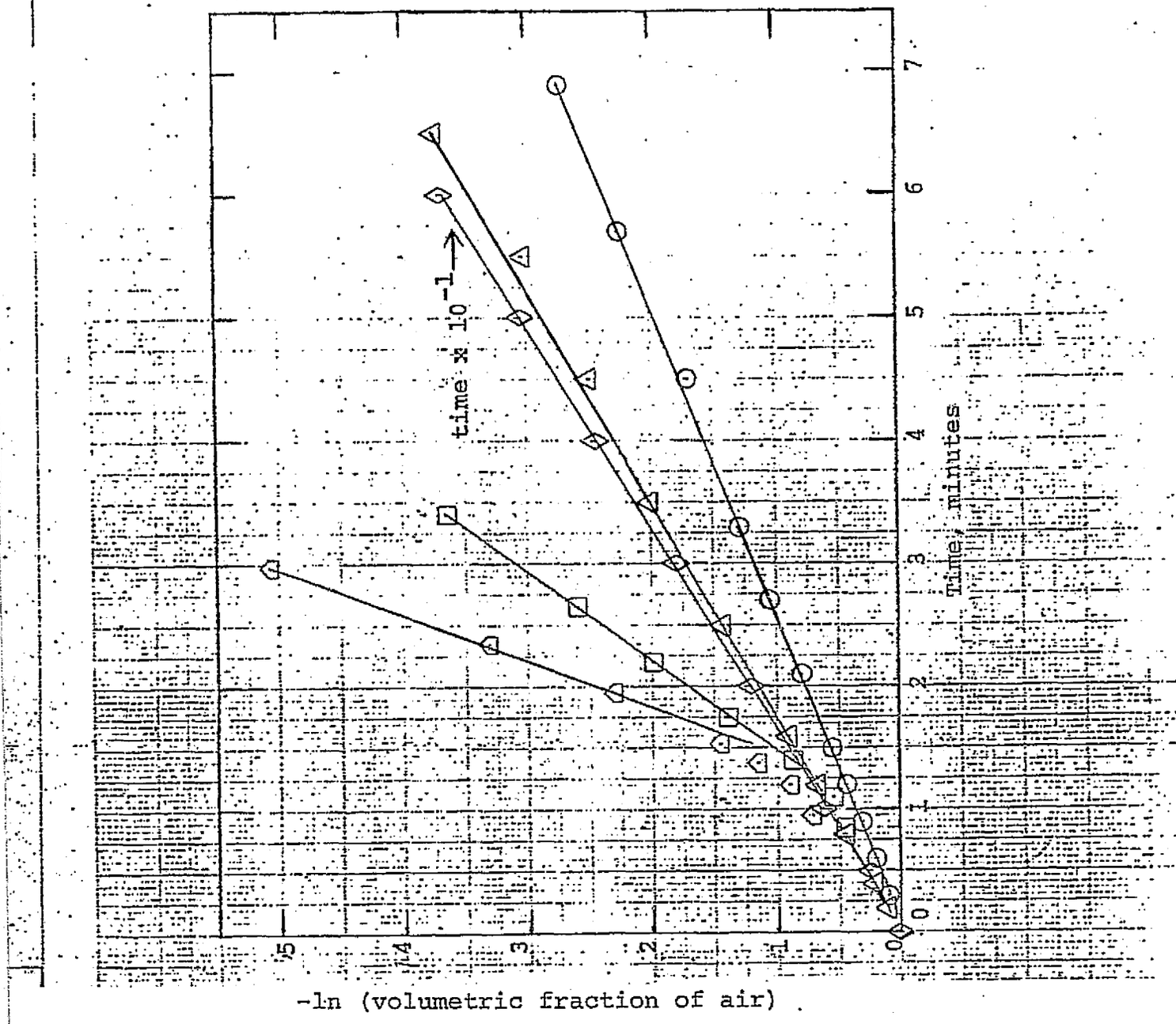

Figure 21 Tracer experiments. At t=o a flow of helium was introduced into the air filled recycle loop with catalyst bed bypass valve open. Slopes of the lines drawn should be equal to inverse residence time. The calculated recycle loop volume, (cm^3)/volumetric flow, (cm^3/min) are: ◇ 38.1/619, ○ 253.6/633, △ 361.4/630, □ 1019/782 ⌂ 2035/926.

-ln [ ] v.s. time line, volume = volumetric flowrate ÷ slope. The runs at 253.6 and 361.4 cm^3/min. were reproducible, no attempt was made to reproduce the other runs.

The calculated effective recycle loop volume was ~ 630 cm^3, nonlinearities and deviations of the calculated recycle loop volume at high flowrates, 1019 and 2035 cm^3/min., are attributable to imperfect mixing.

When compared with the calculated helium breakthrough assuming a reactor loop volume of that seen in the tracer experiments with flowrates of 38.1 to 361.4 cm^3/min., the experimental breakthrough at high flowrates was much too slow.

This phenomena is what one might expect since increasing the flow feeding the recycle loop at constant pumping rate should result in a smaller recirculation ratio and increasingly less active flow regions in the loop. Presumably it is the slow mixing of the incoming gas with the less active regions that results in the phenomena exhibited at high flowrates.

The effect of restricting the flow bypassing the catalyst bed by closing the bypass valve was not investigated.

Appendix 2.

Thermal Conductivity Cell Response

Concentrations in binary gas mixtures were measured in the surface area determinations and tracer experiments by a thermal conductivity cell. The cell used was a hotwire* type with a small internal volume (250 μ l), Gow Mac model 10-301. The cell and bridge completion resistors were insulated with a thick layer of glass wool thus cell temperature was determined by the heating of the cell housing and insulation by the filaments. Cell amperages of 100 mA for Air-He, N_2-He and N_2-H_2 mixtures and 200 mA for CO-He mixtures were used.

The cell was calibrated by injecting sample loops of a known concentration into the constant flow feeding one side of the cell with the other side (reference filament) of the cell at constant concentration and flowrate, thus a square wave cell output was obtained. It was found that the cell output and linearity at a constant amperage and reference cell flow both increased as the cell flow was decreased. As recommended by Gow Mac flows of 5-15 cm^3/min. were used, generally $\sim$6 cm^3/min.

*This cell was originally equipped with dual helix rhenium-tungsten filaments (Gow Mac #W2x). These filaments were inadvertantly exposed to air at high amperage and burnt out. They were replaced with single helix rhenium-tungsten filaments (Gow Max #Wx). Although the Wx filaments were less sensitive they gave a sufficiently high output and the calibrations in figs. 22 and 23 are for the Wx filaments.

Two typical cell calibrations for binary gas mixtures, cell output (mV) vs volumetric fraction of one component, are presented in figures 22 and 23. Plotted in figure 22 is a calibration for air-He mixtures used for a tracer experiment. The range of concentrations used in this calibration was 0-100% air, the overall non-linear cell response is typical of thermal conductivity detectors. However, as shown in figure 23, a calibration for He-CO mixtures over a small range ($\sim$ 0-10^{-2} volumetric fraction CO), the cell output is effectively linear.

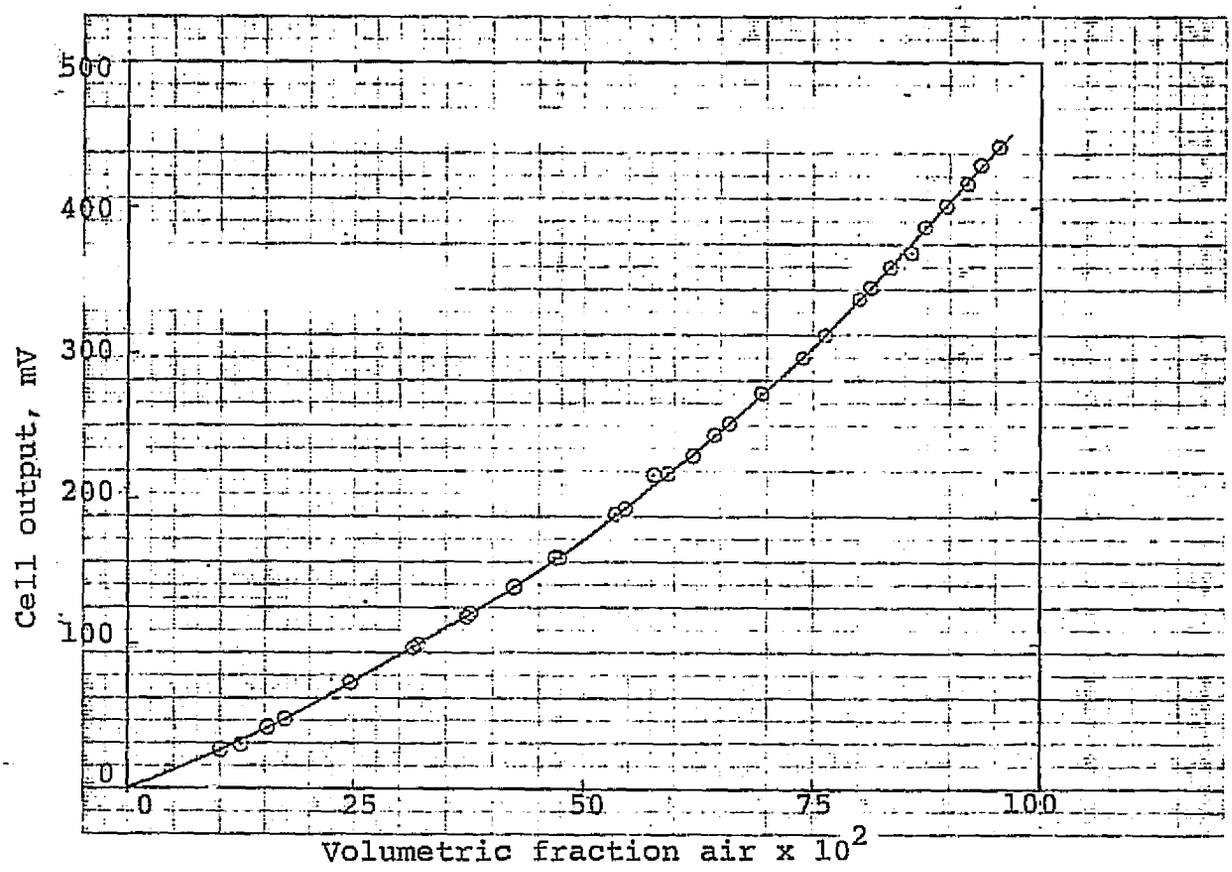

Figure 22 Thermal conductivity cell calibration for air-He mixtures. Cell amperage 100 mA; cell flow rate 6 cm^3/min.

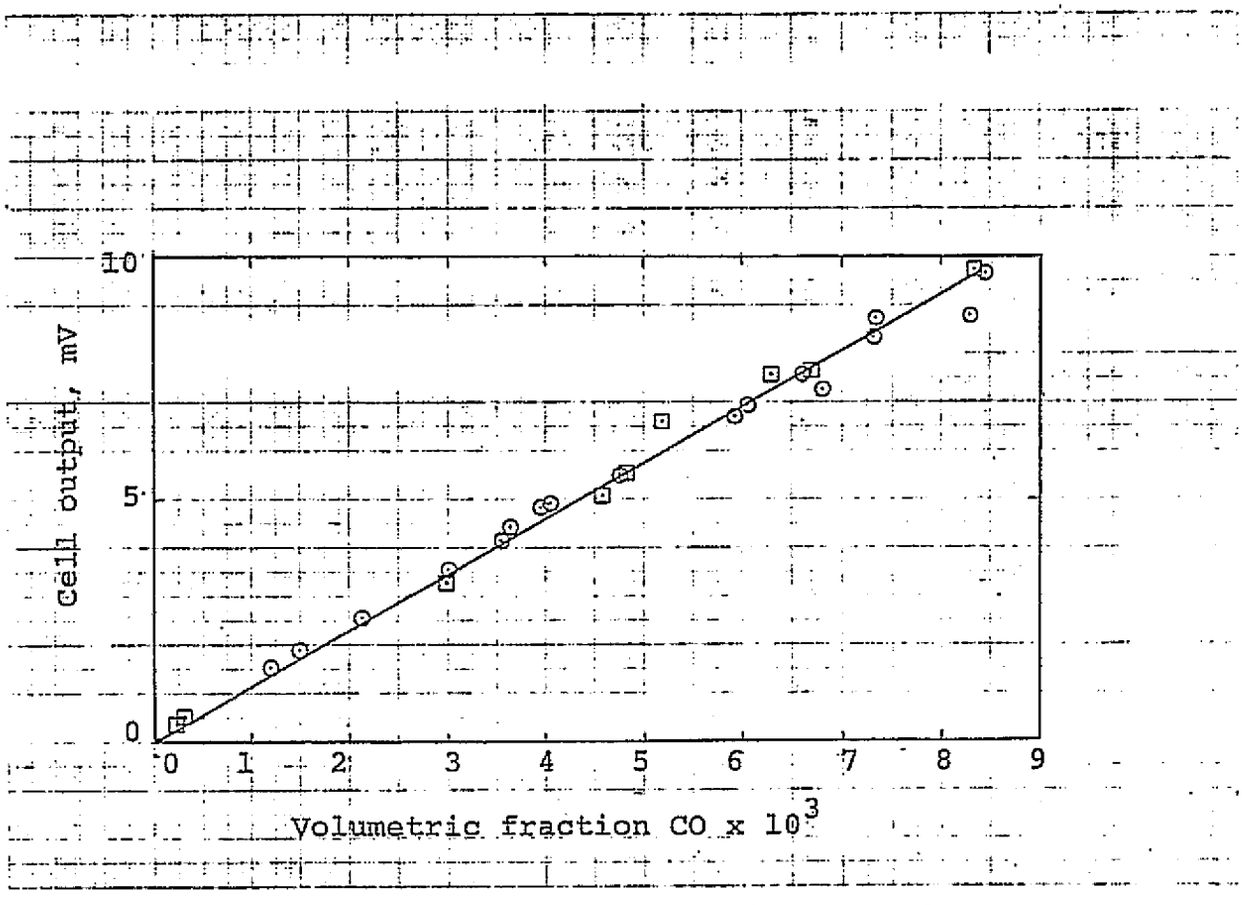

Figure 23 Thermal conductivity cell calibration for CO He mixtures. Cell amperage 200 mA; cell flow rate 6 cm^3/min. Two calibrations are represented. The first, O, was done when new filaments were installed; another calibration, □, 4 months later showed no deterioration in cell performance.

Appendix 3.

Flame photometric detector response

Concentrations of sulfurous gases were detected by a Tracor, FPD, flame photometric detector, model 274010-00. The operating conditions used in this work were those recommended by Rabb* and a detailed description of these conditions are given in his thesis (2).

The operating principal of this detector is that the photoemission of sulfur species in a hydrogen flame is proportional to their concentration. Reported calibrations by Varian Instruments** for the FPD used in this work are that the detector output, I, which is directly proportional to the photoemission, depends on the concentration to some small power, n; $I \propto C^n$ where n is generally about 2 and ranges from 1.8-2.2. Stevens (13) using a similar FPD has reported powers of 1.939 for hydrogen sulfide and 1.950 for sulfur dioxide and virtually the same detector sensitivity for both compounds. The concentration region where this power function holds is reported to be ∿10 ppb-10ppm. Around 1-10 ppm the instrument output is

*Since both hydrogen sulfide and sulfur dioxide were simultaneously being detected, the low column temperature, 80°C, recommended for hydrogen sulfide was used.

**Personal communication with workers at Varian Instruments, Sunnyvale and Walnut Creek, California, 1975.

attenuated and begins to continously decrease beyond 20-30 ppm. Stevens (13) has reported this saturation phenomenon begins at ∿ 2 ppm.

The reason most widely offered for the detector response characteristics is that the detector measures the luminescence of an S_2 species in the hydrogen flame, hence one would expect the S_2 concentration and therefore the detector output to be proportional to the square of the sulfur concentration. The reported discrepancies, powers other than 2, are attributed to imperfect mixing in the flame combustion chamber. The attenuated detector output at high concentrations is much less effectively explained. The reasons offered, however, involve photo-molecular interaction and not the saturation of the photomultiplier tube or electrometer.

In an effort to investigate the concentration dependence of the FPD used in this work a small flow of hydrogen sulfide gas was diluted in two stages with high flows of helium. The resulting FPD calibration is shown in figure 24. Plotted in figure 24 is the $\log_{10}$ coordinates of the detector output vs the hydrogen sulfide concentration as calculated from the two stage dilution of hydrogen sulfide gas. A line with a slope of 2 fits the data from ∿ 0-14 ppm, beyond 14 ppm the plot is non-linear.

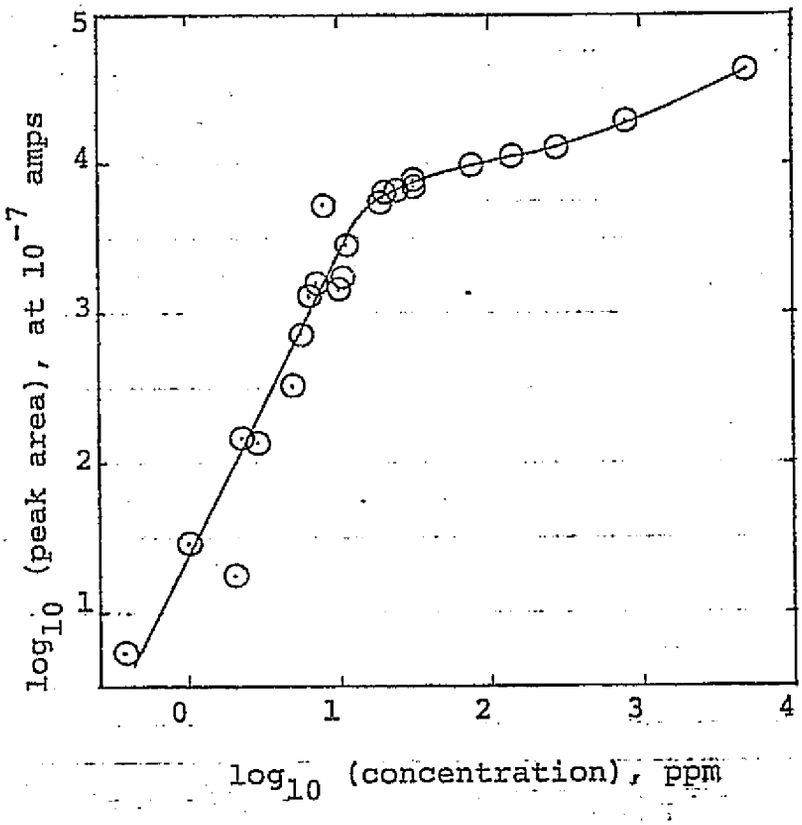

Figure 24 Hydrogen sulfide calibration of flame photometric dectector. The $\log_{10}$ coordinates of peak area (at an electrometer setting of 10^{-7} amps) is plotted vs. concentration.

This saturation point ∿14 ppm is at a somewhat larger concentration than that reported by Varian, 1-10 ppm. However, the different FPD operating conditions used in this work would be expected to extend the concentration limit where $I \propto C^n$. The H_2-O_2 flows used in this work should result in a flame 3.2 times larger than the H_2-O_2 flows recommended by Varian and dilution of the H_2-O_2 flows by inert gases in this work was a factor of 3 larger than the dilution by the flows recommended by Varian.

A good deal of time was expended in preliminary efforts to calibrate the FPD with premixed ppm of hydrogen sulfide and sulfur dioxide in nitrogen. These gases were mixed and analyzed by Matheson Gas and stored in steel tanks. Based on calibrations in figure 24 this analysis was inaccurate at the time the gas mixtures were used in this work.

Calibrations using the gases in these tanks, assuming the same detector sensitivity for hydrogen sulfide and sulfur dioxide are presented in figure 25. Plotted in figure 25 are the $\log_{10}$ coordinates of the detector output and the corresponding sulfur concentrations. For both gases the calibration shows that the detector output depends on the square of the sulfur concentration.

It should be mentioned that the calibrations plotted in figure 25 were complicated by severe losses of the sulfur compounds in the stainless steel tubing transporting the

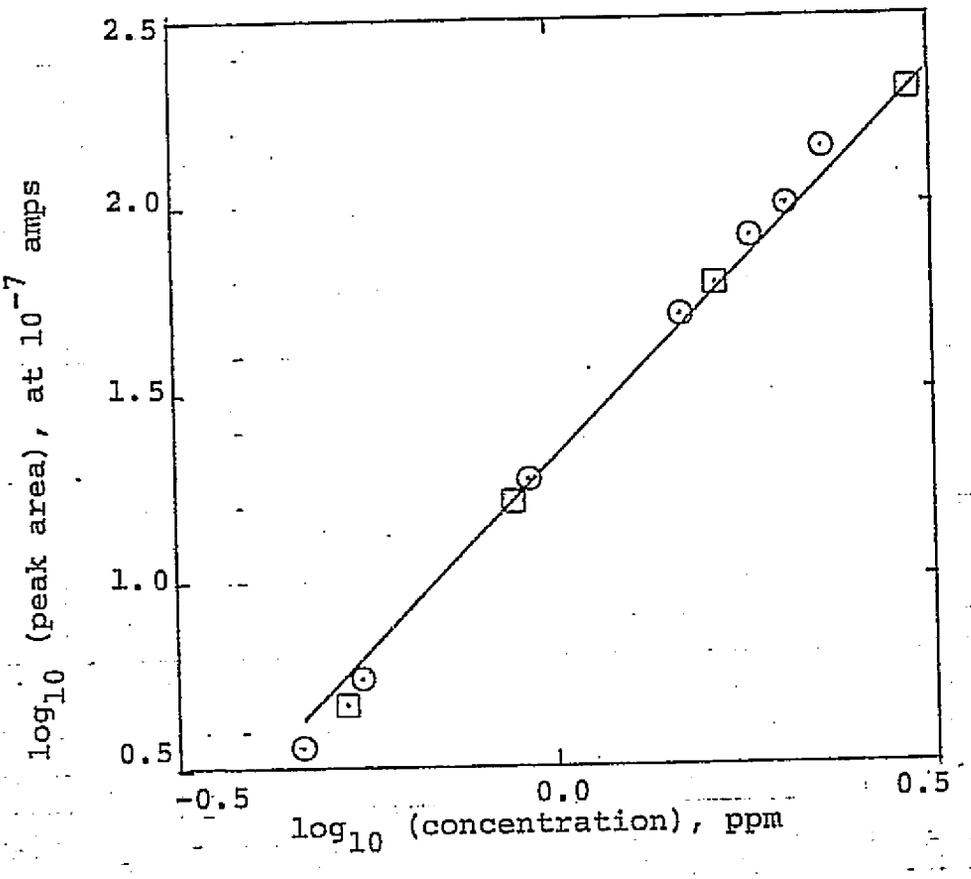

Figure 25 Flame photometric detector calibration. Sulfur dioxide □ ; hydrogen sulfide ○ . The $\log_{10}$ coordinates of peak area (at an electrometer setting of 10^{-7} amps) is plotted vs. concentration.

sulfurous gas flows.* It was found, however, that the removal of sulfur compounds followed approximately first order kinetics (see Appendix 6). Accordingly, the interrelation of the concentration reaching the detector, C, the tank concentration, C_o, and the volumetric flowrate, f, is $\ln(C_o/C) \propto 1/f$, hence, $C_o/C \rightarrow 1.0$ as $f \rightarrow \infty$ and at a constant f the ratio C_o/C is constant. With this in mind, the procedure adopted for calibrating the detector was to mix flows of sulfurous gases with inert gas streams and maintain a constant high flowrate through the tubing transporting the sulfurous gas mixtures. This is predicted to result in a small and constant percentage error in the calculated amount of sulfur reaching the detector based on dilution of the sulfur containing gases.

---

*This effect was minimized in the reactor effluent tubing since most of that tubing was made of teflon.

Appendix 4.

Equations Used in Calculations

The symbols and relations used in the calculations below are defined here.

Symbols

N = number of moles

X = mole fraction

T = temperature, °K

V = volume of recycle loop, cm^3

P = total pressure, atm

p = partial pressure, atm

C = concentration, moles/cm^3

f = volumetric flowrate, cm^3/sec.

t = time, sec.

R = gas constant, (atm cm^3)/(mole °K)

k = experimentally observed first order rate coefficient, cm^3/sec.

s = catalyst surface area, cm^2

w = catalyst weight, grams

Subscripts

e = recycle loop effluent

f = recycle loop feed

r = reactor

rl = reactor loop

ox = oxidation

cr = cracking

Superscripts

eth = ethane

meth = methane

Relations Assumed

$k = k_w \cdot w = k_s \cdot S$

$PV = NRT$

$P_i = PX_i$

The conservation equations for ethane and methane in the reactor recycle loop are:

(1) $$\frac{dN_{rl}^{eth}}{dt} = (fC^{eth})_f - (fC^{eth})_e - k_{ox}C_r^{eth} - (\text{rate of cracking})$$

(2) $$\frac{dN_{rl}^{meth}}{dt} = -(fC^{meth})_e + 2(\text{rate of cracking})$$

Equation (2) above assumes no methane feed, stoichometric cracking and negligible methane oxidation; rate of cracking = 1/2 rate of methane production. Using the following relations the rate coefficient in equation (1) can be solved for

$$(\text{rate of cracking}) = \frac{1}{2}\left[\frac{dN_{rl}^{meth}}{dt} + (fC^{meth})_e\right]$$

$P_e = P_f = P_r = P_{rl}$; $X_e = X_r = X_{rl}$

$$C_i = \frac{PX_i}{RT_i}\ ;\ N_i = \frac{PVX_i}{RT_i}$$

C-2

From a mole balance since $\Delta N \approx o$ in the reactor loop (ppm of reactant)

$$\left(\frac{f}{T}\right)_f = \left(\frac{f}{T}\right)_e$$

$$k_{ox} = \frac{\left(\frac{f}{T}\right)_f T_r \left[X_f^{eth} - X_e^{eth} - \frac{1}{2}X_e^{meth}\right]}{X_e^{eth}} - \frac{\left[V\frac{T_r}{T_{rl}}\right]\left[\frac{dX_e^{eth}}{dt} + \frac{1}{2}\frac{dX_e^{meth}}{dt}\right]}{X_e^{eth}}$$

Under conditions approximating steady state the second term drops out.

Similaiarly an ethane cracking rate coefficient can be calculated. For assumed first order ethane cracking,* no methane feed, where the rate of cracking in equation (2) is $k_{cr}\, C_r^{eth}$

$$k_{cr} = \frac{V\frac{T_r}{T_{rl}}\frac{dX_e^{meth}}{dt} + \left(\frac{f}{T}\right)_f T_r X_e^{meth}}{2X_e^{eth}}$$

The rate coefficients, k_{ox} and k_{cr}, represent the relative ethane disappearance rates for oxidation and cracking. It can easily be shown that their sum $(k_{cr} + k_{ox})$

*Log plots of the rate of methane production vs ethane concentration have shown this to be a good approximation.

is equivalent to the overall first order rate coefficient for disappearance of ethane.

Experimentally the quantities X^{meth} and X^{eth} are directly proportional to the area of their FID gas chromatograph peaks. For the same peak area, $2X^{meth} = X^{eth}$, since the FID dectector is linear with carbon number when detecting low carbon number parrafins. (12)

Equations for Non-Steady State Reaction Order Runs

The experimental procedure involved introducing a large ethane concentration into the reactor loop by injecting a known amount of ethane into a constant air flow feeding the recycle loop. Since those injections were small in volume (~ 0.49-1.1 cm^3) and the volumetric flowrates were large (~ 0.81-2.1 cm^3/sec) all injection volumes were introduced into the reactor in ~1.1 sec or less. The short injection times and the instaneous mixing in the reactor should yield an initial ethane mole fraction in the reactor loop given by

$$X = \left(\frac{V}{T}\right)_{injection} \cdot \left(\frac{T}{V}\right)_{reactor\ loop}$$

An estimate of the effective temperature in the reactor loop 70°C for the temperature range used in the reactor was obtained from the volume averaged surface temperatures of the reactor loop.

It will be shown that the analysis of the data assuming half and second order kinetics requires that the steady reaction rate be known at the conditions of the

reaction order run. However the kinetic analysis of the reaction order for the disappearance of ethane is simplified if there is no constant ethane feed to the reactor. The conservation equation governing this system is

$\frac{dN_{r\,1}}{dt} = -kC_r^n - (fC)_e$. In this equation $C \equiv C^{eth}$ and the rate coefficient k is the overall disappearance coefficient, $(k_{ox} + k_{cr})$. Using the relations and substitutions mentioned in the beginning of this appendix the solutions to the conservation equation for $n = \frac{1}{2}, 1, 2$ in the form $y = mx + b$ where $X \equiv X^{eth}$ and $f \equiv (f)_f$ are:

$n = 1$

$$\ln X_e = -\left(\frac{kT_f}{fT_r} + 1\right)\left(\frac{T_{r1}}{T_f}\frac{f}{V}\right)t + \ln X_{e,i}$$

$n = \frac{1}{2}$

$$\ln\left[X_e^{1/2} + \frac{kT_f}{f}\left(\frac{R}{T_r P}\right)^{1/2}\right] = \left[-\frac{1}{2}\frac{T_{r1}}{T_f}\frac{f}{V}\right]t + \ln\left[X_{e,i}^{1/2} + \frac{kT_f}{f}\left(\frac{R}{T_r P}\right)^{1/2}\right]$$

$n = 2$

$$\ln\left[\frac{1}{X_e} + \frac{kPT_f}{fRT_r^2}\right] = \left[\frac{T_{r1}}{T_f}\frac{f}{V}\right]t + \ln\left[\frac{1}{X_{e,i}} + \frac{kPT_f}{fRT_r^2}\right]$$

the dimensionless constant containing the rate coefficient that makes up part of the arguement of the logarithm in the half and second order solutions is a function of the steady state inlet and outlet of the reactor loop ethane mole fraction at the same flowrate and reaction temperature of the non-steady state reaction order run.

The $\frac{1}{2}$ order dimensionless constant

$$\frac{kT_f}{f}\left(\frac{R}{T_r P}\right)^{1/2} = \left(\frac{X_f - X_e}{X_e^{1/2}}\right)_{\text{steady state}}$$

the 2nd order dimensionless constant

$$\left(\frac{kPT_f}{fRT_r^2}\right) = \left(\frac{X_f - X_e}{X_e^2}\right)_{\text{steady state}}$$

Although the 1st order dimensionless constant is not needed in the reaction order analysis since it does not appear in the argument of the logrithm, it also follows the general pattern

$$\left(\frac{k}{f}\frac{T_f}{T_r}\right) = \left(\frac{X_f - X_e}{X_e}\right)_{\text{steady state}}$$

The dimensionless constants in the above solutions to the conservation equation are a measure of the ratio of ethane removal by reaction to ethane removal by volumetric displacement.

An inspection of the above solutions shows that as the dimensionless constant approaches zero the solutions

for all cases converge to the solution for the mole fraction decay in a well stirred vessel. Thus the data will fit any assumed reaction order if the constant is small.

As shown in figure seven the data fits the first order analysis very well however, the rate coefficients computed from the slope of lines are always significantly smaller than those computed from the steady state reaction measurements.

Plots of all three sets of data assuming half and second order kinetics are non-linear and non-linear plots are still obtained if the half and second order rate coefficients are decreased or increased by a factor of the ratio of the observed first order rate coefficients computed from non-steady state and steady state data. An example is given in figure 26. Plotted in figure 26 are the half and second order assumptions in the form $y = mx + b$ where $y \equiv \ln[\ ]$ and $x \equiv$ time. Non-linear plots are obtained in all cases.

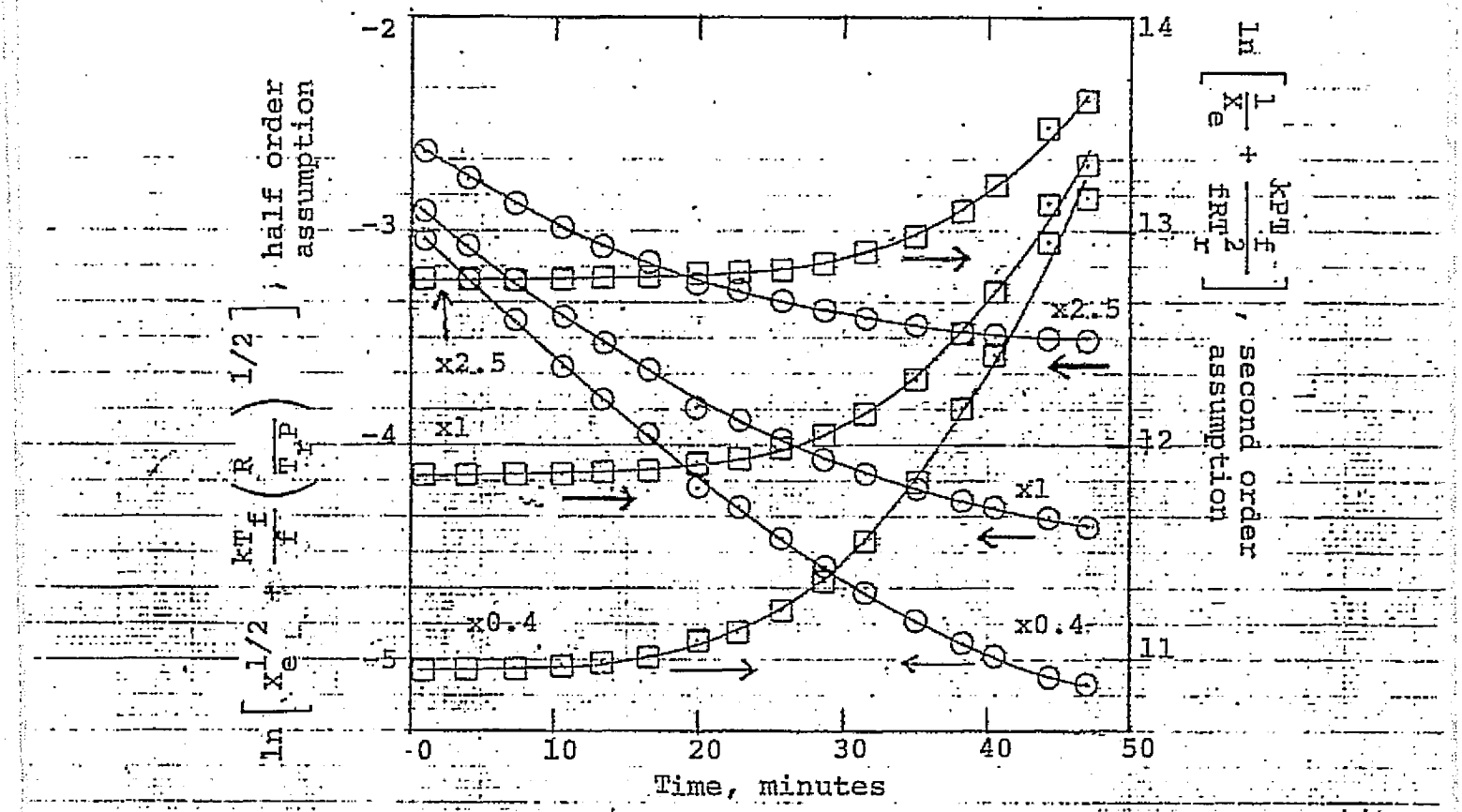

Figure 26 Nonsteady state reaction order run, second catalyst load. Reaction temperature, 260.9°C, residence time, 11.0 minutes. Half and second order assumptions are plotted in the form $y = mx+b$ where $y \equiv \ln [\ ]$, $x \equiv t$. Annotations in the plot refer to the factor by which the n^{th} order rate coefficients have been multiplied. First order assumption is plotted in figure seven.

Appendix 5.

Adsorption of Ethane on the Catalyst

Using a feed of 21 ppm ethane in air at 200°C strong adsorption and retention of ethane by the first catalyst load, 1.1 grams, was observed. Ethane adsorption is represented in two breakthrough curves figures 27 and 28. Time in hours is plotted against reactor effluent concentration in ppm.

Neither set of data was taken with the intention of quantitatively measuring ethane adsorption; flowrates were briefly varied on each run and the temperature was varied on the first run, figure 27. The assumptions used to back calculate the amount of ethane adsorbed when the flowrate rate and catalyst temperature were varied during these runs are included at the end of this appendix. Figure 27 represents the adsorption after the initial catalyst pretreatment. After a steady state was reached the catalyst was oxidized and reduced again and subsequently a second breakthrough curve was recorded, figure 28. The breakthroughs are described below. First adsorption breakthrough, figure 27, took ~ 88 hours to reach a steady state using an average molar feedrate per gram of catalyst of 1.12×10^{-10} moles/(sec·g). The adsorbed ethane amounted to 3.93 moles/gram and concurrently 1.14 moles/gram of catalyst of ethane was cracked and not adsorbed during the adsorption period. Second adsorption breakthrough,

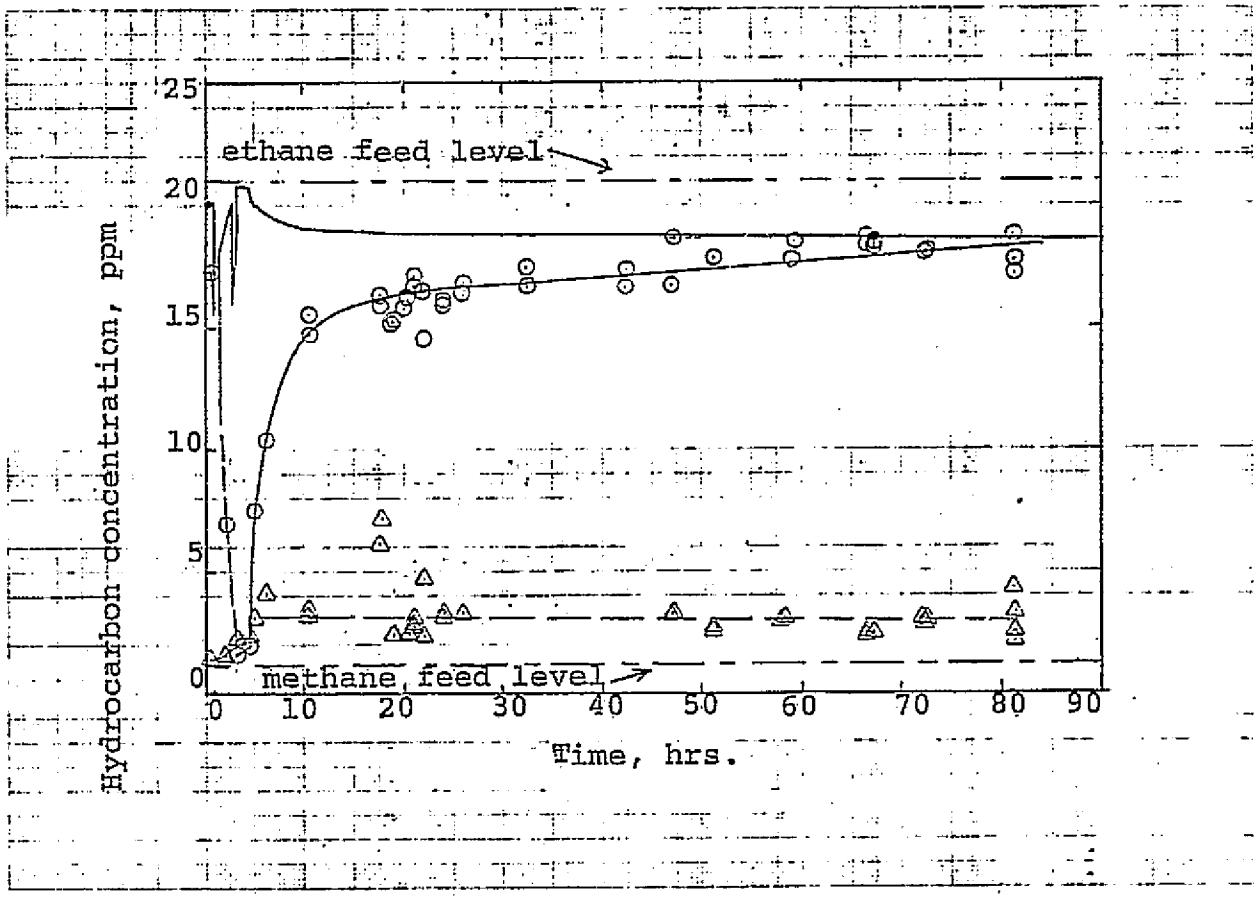

Figure 27 First ethane breakthrough on the first catalyst load, 1.1 grams. Methane △; ethane ○. The upper solid line is the calculated concentration of ethane fed to the reactor which was not oxidized. The integrated area between the two solid lines, weighted by the concurrent flow rate, minus 1/2 the amount cracked is the amount adsorbed. The results were: 3.93 μ moles/gram ethane adsorbed and 1.14 cracked.

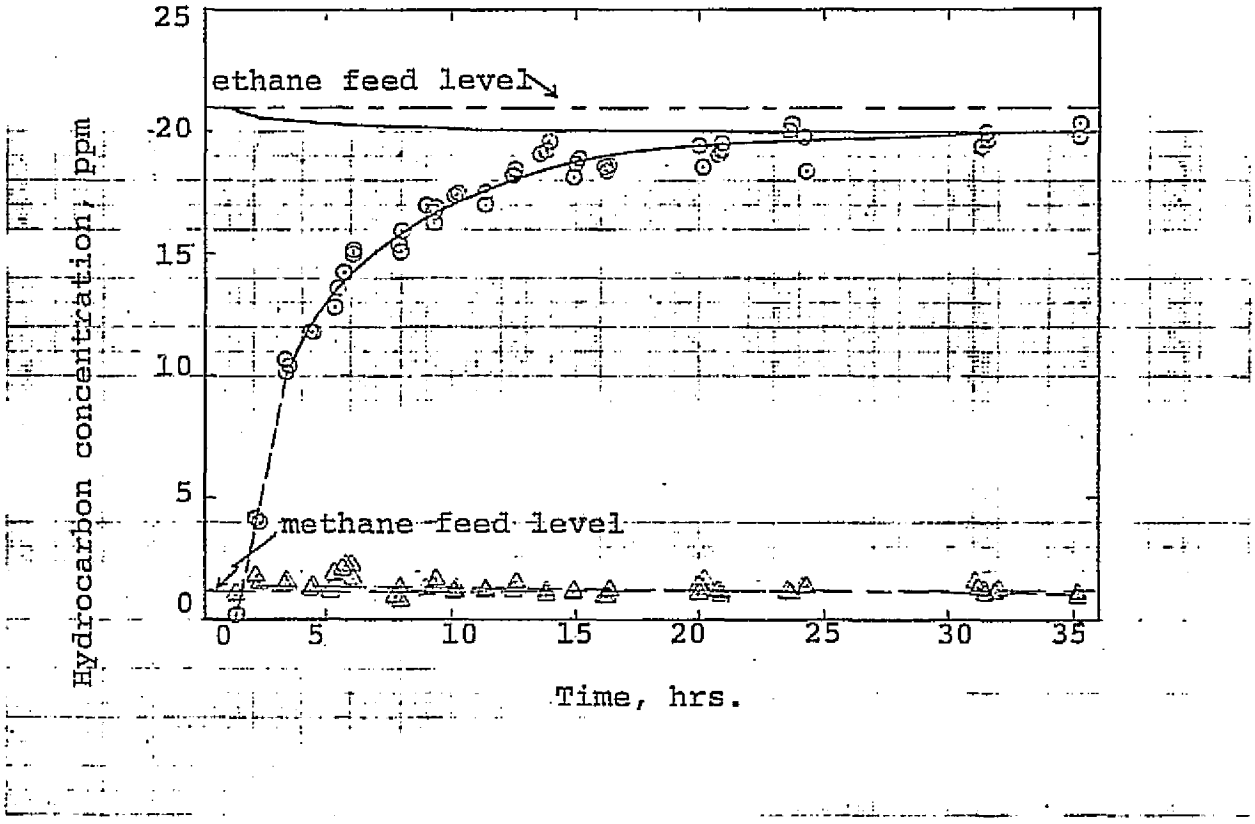

Figure 28 Second ethane breakthrough on the first catalyst load, 1.1 grams. Methane Δ ; ethane O . The upper solid line is the calculated concentration of ethane fed to the reactor which was not oxidized. The integrated area between the two solid lines, weighted by the concurrent flow rate, is the amount adsorbed; a negligible amount of cracking was observed. The adsorbed ethane amounted to 12.20 μ moles/gram.

figure 28, took ~ 33 hours to reach a steady state using an average molar feed rate per gram of 7.75×10^{-10} moles/(sec·g). The adsorbed ethane amounted to 12.20 μmoles/gram and a negligible amount of cracking was observed. The differences in the amount adsorbed between these two runs, 3.93 μmoles on the 1st breakthrough and 12.20 μmoles on the 2nd breakthrough, may be attributable to the greater amount of ethane oxidation in the first adsorption run which would result in larger H_2O and CO_2 pressures. The catalyst base is known to strongly adsorb these gases at 200°C and the oxidation of one ethane molecule results in production of five other adsorbable molecules, $C_2H_6 + 7/2\ O_2 \rightarrow 2CO_2 + 3H_2O$. The time dependent adsorption phenomena is similiar to that seen by Rabb (2) whose used an integral bed. He used an ethane feed level of 20 ppm and a temperature below the ethane conversion temperature for the flowrate used, <180°C. He obtained 7.1 μmoles/gram of ethane adsorbed using a molar feed rate per gram of 4.99×10^{-10} moles/(sec·g). A C-shaped breakthrough curve was observed in which the curve asymtotically approached a slightly sloping plateau after ~ 6 hours. An adsorption time of 6 hours resulted in ~84% saturation and 28 hours was required for a complete breakthrough.

This qualitatively compares with the second adsorption breakthrough recorded in this work figure 28. Here a 68%

breakthrough was obtained in 6 hours using an average molar feed rate per gram of 6.16×10^{-10} moles/(sec g) and a complete breakthrough was obtained in ~33 hours using an overall average molar feed rate per gram of 7.75×10^{-10} moles/(sec g).

After the second adsorption breakthrough the air-ethane mixture was purged out and the catalyst was heated in flowing He (60 cm^3/min.) to ~385°C. The ethane desorption is represented in figure 29 where the ethane desorption rate in (moles/sec) and the reactor temperature in °C is plotted against time in minutes. At 18.3 minutes the recycle pump was turned off and at 29.3 minutes the catalyst bed bypass valve was closed. The ethane wash out is represented by the dotted line with a negative slope near zero time. The desorption maximum occurs at about 310°C and the total amount of ethane desorbed was 0.41 μmoles/gram. This is 3.4% of the amount adsorbed.

It should be mentioned that the ethane adsorbtion seen in this and in Rabb's work (2), 3.93-12.20 μmoles/gram, correspond to small coverages. The catalyst surface area in both works was ∿ 120m^2/g and assuming 10^{15} (surface sites/cm^2) with a coordination # of 8 (surface sites/ethane molecule), the value of 12.2 μmoles/gram translates to ~5% of a monolayer.

In the above adsorption calculations it is assumed no appreciable change in the rate coefficient occurred

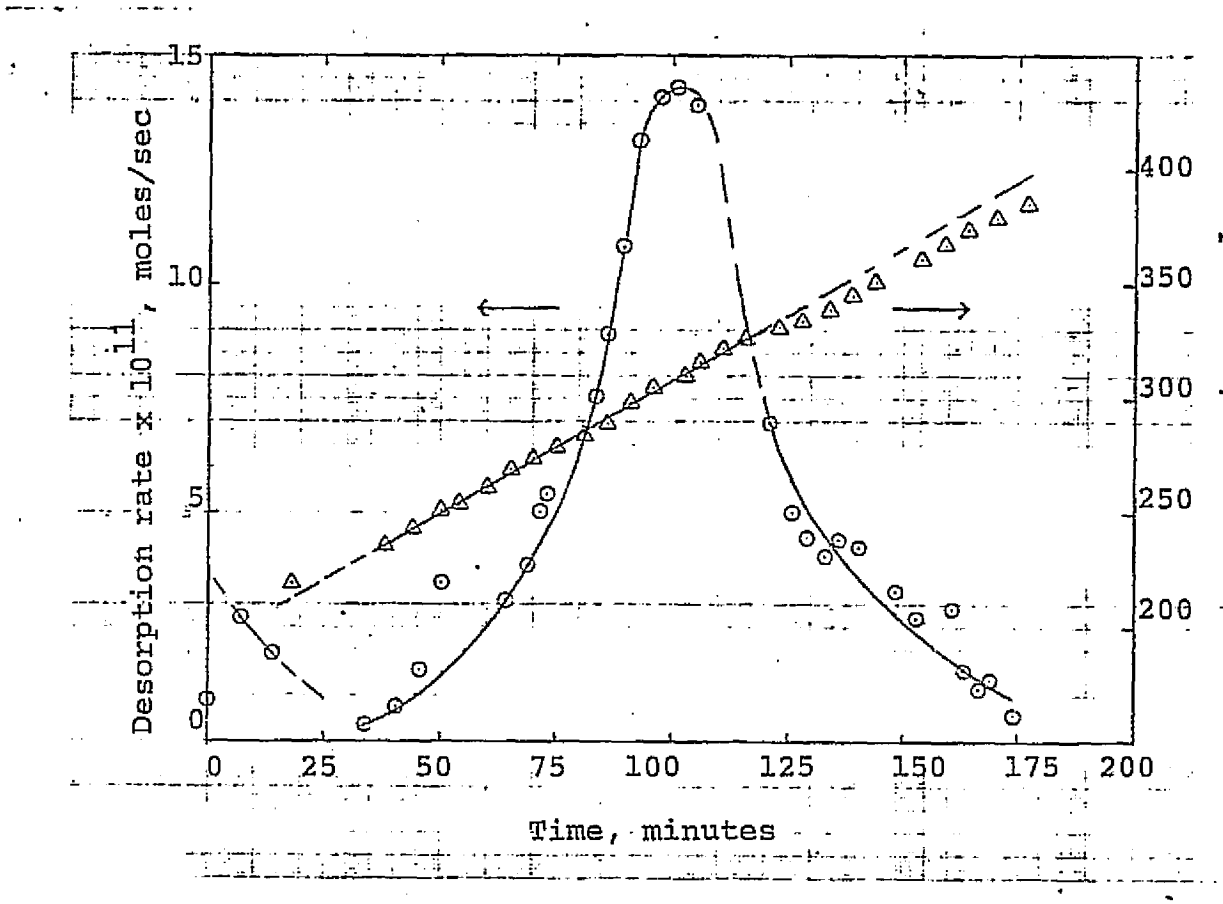

Figure 29 Temperature programmed ethane desorption. Ethane concentration O ; bed temperature △ . After the second breakthrough was recorded, figure 28, the air was purged out and the catalyst temperature was raised to 385°C in flowing helium. The desorbed ethane amounted to 0.41 μ moles/ gram.

during the breakthrough. The amount of ethane oxidized is then back calculated knowing the rate coefficient at the end of the run where the adsorption is saturated using steady state first order kinetics with an E_a of 27 kcal/mole. This amount is subtracted from the inlet ppm (21 ppm) to extrapolate back the steady state ppm concentration not oxidized. The area between the ethane effluent ppm and the ppm not oxidized minus one-half the area of the methane production is then the amount of ethane adsorbed.

Appendix 6

Hydrogen Sulfide Oxidation and Removal by the Apparatus

Low Level Hydrogen Sulfide Oxidation

Catalyst poisoning is easiest to monitor and control using a low level continous input of catalytic poison. However, due to the reported ease of hydrogen sulfide oxidation (16) it was felt that the ability of the apparatus itself to oxidize hydrogen sulfide should be investigated as a preliminalry step.

The catalyst was removed, the quartz packing was left in place. A flow of 0.86 ppm hydrogen sulfide was directed into the recycle loop at a residence time of 2.56 minutes and the temperature was raised. Although a breakthrough was never attained at low temperature this was not deemed necessary to investigate the qualative oxidative removal of hydrogen sulfide. The results are shown in figure 30. All the hydrogen sulfide is being removed or oxidized at $\sim 140°C$.

Low Level Hydrogen Sulfide Removal by Reactor Feed Tubing

In an attempt to calibrate the sulfur detector it was found that the concentration of hydrogen sulfide detectable varied with flowrate through the feed tubing. A representation of the concentration dependence on the flowrate is shown in figure 31. Irreversible removal of hydrogen sulfide at the ppm level by stainless steel tubing

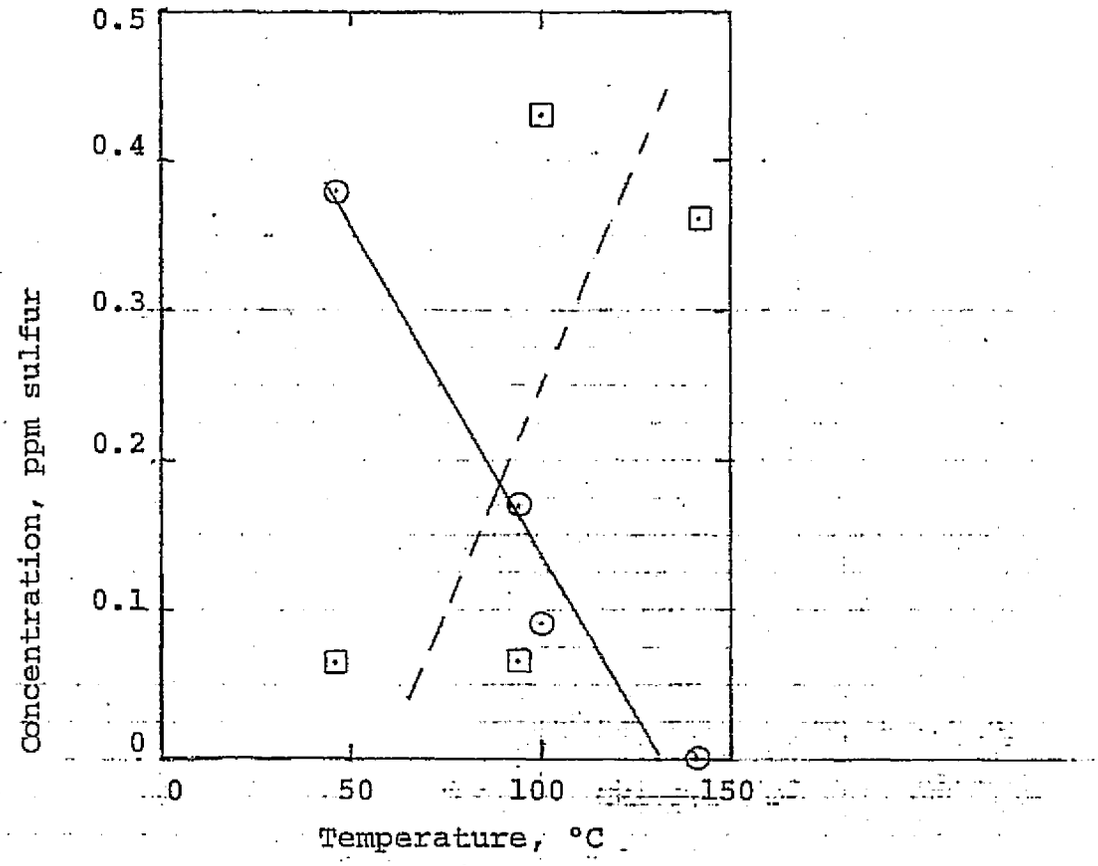

Figure 30 Hydrogen sulfide oxidation and removal in the reactor with no catalyst. Residence time, 2.56 minutes, feed pressures $\sim 10^{2}$ torr oxygen and $\sim 10^{-3}$ torr hydrogen sulfide, 0.86 ppm. Hydrogen sulfide ○ ; sulfur dioxide □ .

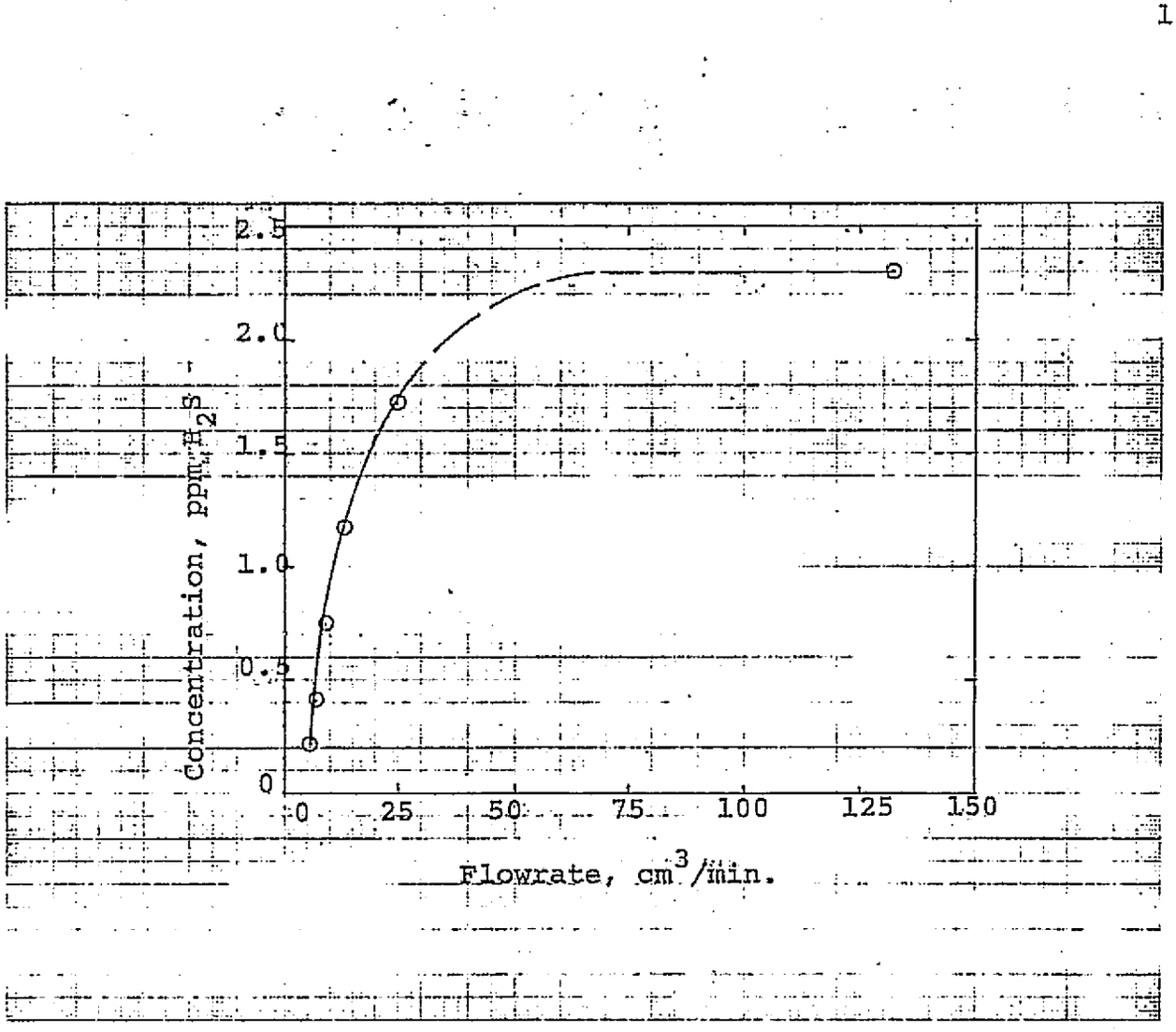

Figure 31. Hydrogen sulfide removal in reactor feed tubing. Inlet concentration ∿2.3 ppm.

has previously been reported. (13) Since this the removal probably involves strong adsorption of hydrogen sulfide one might expect the process to be first order. When the concentration detectable vs flowrate data of figure 30 is plotted ln(conc.) vs flowrate^{-1}, (fig. 32), a fairly linear plot is obtained, indicating first order removal of hydrogen sulfide. The non-linearity is attributable to dispersed rather than plug flow in the small tubing. The calculated Reynolds number* for the flowrates used indicates the flow is in the laminar regime.

---

*see page 47, ref. 9

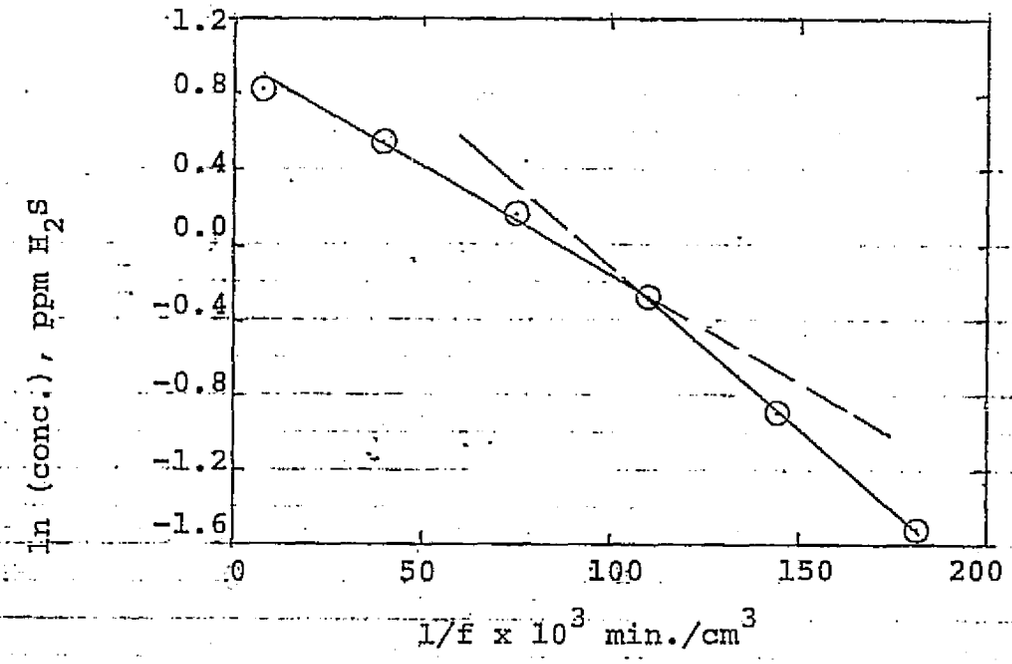

Figure 32 First order plot of hydrogen sulfide removal in reactor feed tubing. Data of figure 31 is plotted.

Appendix 7.

Poisoning of the ethane oxidation reaction by halogenated hydrocarbons.

After the initial kinetic experiments on the first catalyst load and before the hydrogen sulfide poisoning of the catalyst the poisoning by halogenated hydrocarbons was studied. Two chemically similar refrigerants were used, Freon 22 ($HCClF_2$) and Gentron 142-B (CH_3CClF_2). Freon 22 was chosen because its basic halogenated carbon structure $-CClF_2$ reoccurs in many C_2 refrigerants, among them Gentron 142-B and the Freons 113, 114 and 115.

The catalyst surface area was not measured in these experiments hence the reported rate coefficients are based on catalyst weight and are given in units of $cm^3/(sec \cdot g)$.

Some of the gas chromatograph column temperatures used in the studies detailed below did not allow separation of methane and ethane*. The reported first order rate coefficient under these conditions is based upon the first order disappearance of total hydrocarbons. This rate coefficient is roughly 80% of the oxidation rate coefficient.

*High G.C. column temperatures were used for two reasons: (1) high temperatures were needed to elute Gentron 142-B from the Poropak Q column; (2) an intermittant problem with the gas chromatograph was that the FID electrometer's floating output was too far down scale of the recorder zero, increasing the column temperature and thus increasing the background gases in the FID by column outgassing brought the FID output within the recorder zero.

Before the catalyst was poisoned the oxidation rate coefficients were measured over a small temperature range. This data is represented in figure 33 where the rate coefficients, represented by circles, are plotted in an Arrhenius plot along with rate coefficients (triangles) measured after the catalyst was poisoned with Freon 22 and Gentron 142-B. The slope of the line drawn through the rate coefficients measured before the poisoning corresponds to 24 kcal/mole. Extrapolating the rate coefficient at 245.7°C on this run, using 27 kcal/mole as an effective E_a yields a pre-exponential of 4.1×10^{11} $cm^3/(sec \cdot g)$.

As with the hydrogen sulfide poisoning experiments, Freon 22 and Gentron 142-B were introduced into the reactor by injecting small sample loops of known concentration into the gas flow feeding the recycle loop. The general procedure used to poison the catalyst was to use series of small poison injections, each at the same residence time, to incrementally decrease the catalytic activity. After each series the catalyst was left at the reactor operating conditions until the next series. After the effects of each poison were investigated the catalyst was oxidized in air at 380°C for ~ 8 hours.

Poisoning of ethane oxidation by Freon 22.

Catalyst poisoning was first investigated using Freon 22. The overall poisoning of the catalyst by Freon 22 is

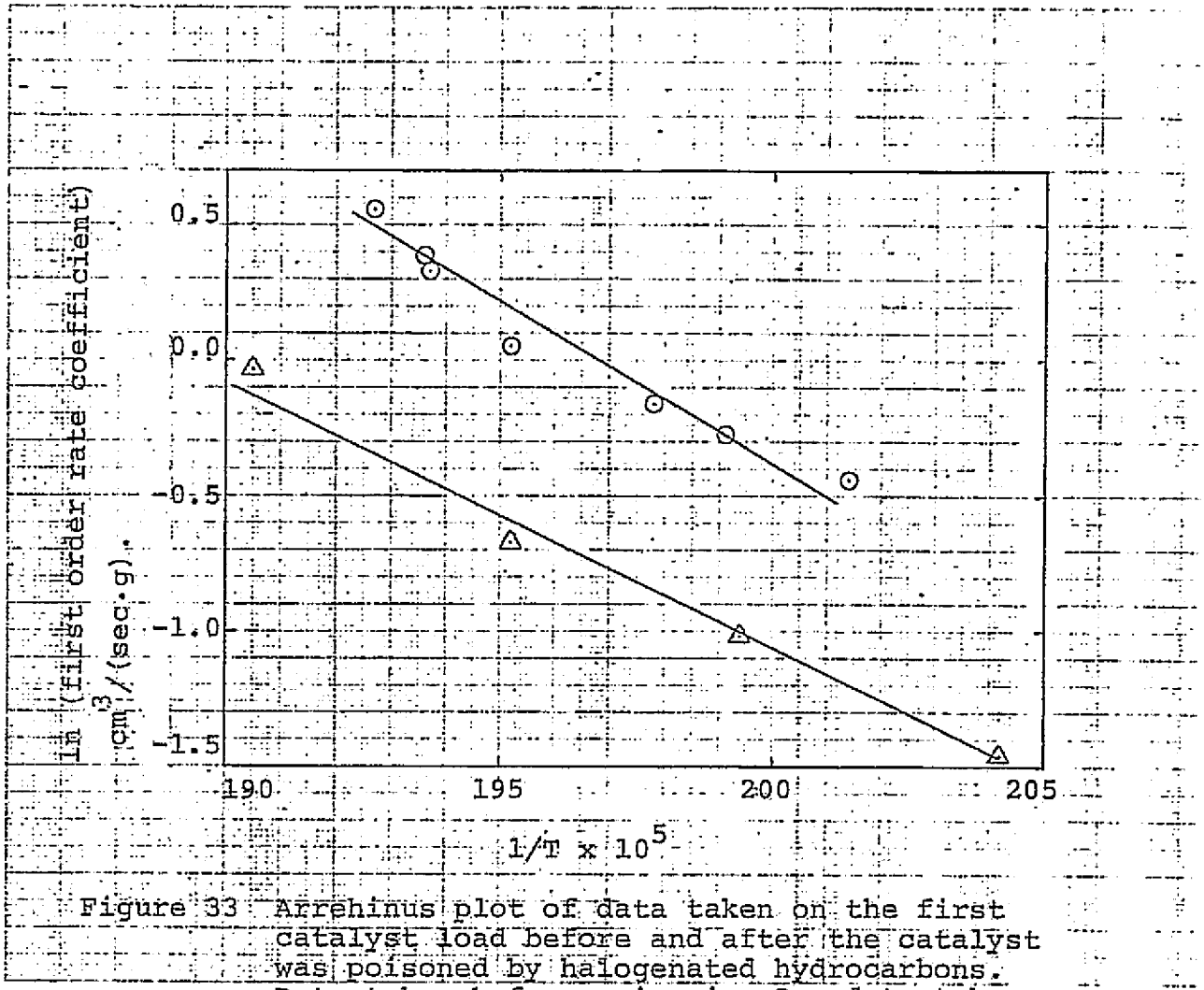

Figure 33 Arrehinus plot of data taken on the first catalyst load before and after the catalyst was poisoned by halogenated hydrocarbons. Data taken before poisoning ○ ; data taken after poisoning △ . The slopes of the lines drawn yield E_a of 24 kcal/mole for the data taken before poisoning and 21 kcal/mole for the data taken after poisoning. Assuming 27 kcal/mole as an effective E_a for the data taken before poisoning the calculated pre-exponential extrapolated from data at 245.7°C is 4.1×10^{11} $cm^3/(sec \cdot g)$. Using the same assumption at 251.7°C for the data taken after poisoning yeilds a pre-exponential of 1.7×10^{11} $cm^3/(sec \cdot g)$.

represented in figure 34. Plotted in figure 34 are the first order rate coefficients for cracking and oxidation of ethane evaluated at 247°C vs the amount of Freon 22 injected. Two sequences of poison injections are represented.

The noteworthy features of this plot are: (1) The decrease in the oxidation rate coefficient with the amount of Freon 22 injected is nonlinear and assymptotic. (2) There is some very slow recovery of the oxidation rate coefficient long after the poison injection. This point is illustrated on figure 34 by the difference between the ending value of the rate coefficient of one injection series and the much larger value at the beginning of the next injection series, an appreciable amount of time having elapsed between the two sequential series of poison injections. Specifically on figure 34 at 18.4 μmoles, 17.9 hours after the last injection the rate coefficient increased from 0.81 to 1.3 $cm^3/(sec \cdot g)$. Again 11.4 hours after the second poisoning series, at 32 μmoles (fig. 34) the rate coefficient recovered from 0.70 to 0.83 $cm^3/(sec \cdot g)$. (3) After catalyst oxidation treatment in air at 380°C the catalyst activity increased. The exact amount of increase is not known because the rate coefficient after the oxidation treatment is based on total hydrocarbon conversion but the oxidation rate coefficient is estimated to have at least increased to 1.56 $cm^3/(sec \cdot g)$ over the previously mentioned value of 0.83 measured 11.4 hours after the last Freon 22 injection.

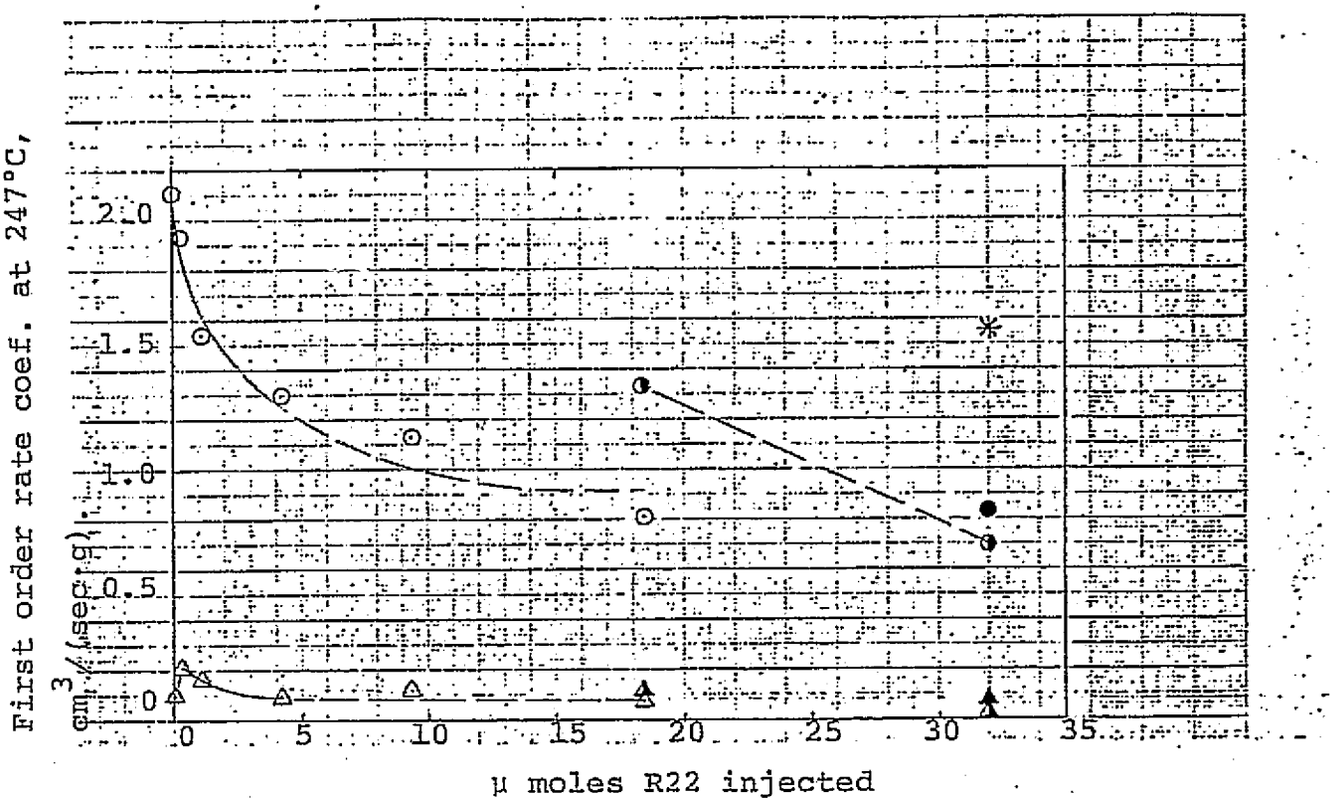

Figure 34 Freon 22 poisoning of the first catalyst load. First order rate coefficient at 247°C for oxidation (circles) and cracking (triangles) of ethane are plotted. Two Freon 22 injection series are represented, residence time was 10.71 minutes, temperature range was 243.8-250.8°C. First series, open symbols, 5 injections, 0-18.4 μ moles. Second series, half shaded symbols, 1 injection, 18.4-32.0 μ moles. Completely shaded symbols at 32.0 μ moles represent data taken long after (11.4 hr.) the last Freon 22 injection. After the catalyst temperature was raised to 380°C for 8 hr. the first order rate coefficient based on conversion of total hydrocarbons (asterick on plot) was measured.

The immediate response to a Freon 22 injection is illustrated in figure 35. Plotted in figure 35 are the ethane and methane concentrations vs the amount of time after the Freon 22 injection. This injection corresponds to 18.4-32.0 μmoles of Freon 22 injected, figure 34. The noteworthy features of this plot were that no Freon 22 was detectable after about 6 minutes (see figure 35 caption) and the reactor ethane concentration stabilized in roughly 50 minutes or after about 5 residence times.

Poisoning of ethane oxidation by Gentron 142-B.

After the Freon 22 poisoning and after the catalyst was oxidized in air at 380°C for ~ 8 hours the poisoning by Gentron 142-B was investigated. The overall poisoning of the catalyst by Gentron 142-B is represented in figure 36. Plotted in figure 36 are the rate coefficients computed from the total hydrocarbon conversion vs the amount of Gentron 142-B injected. Where the methane-ethane gas chromatograph peaks could be resolved the ethane oxidation and cracking coefficients are also plotted.

Three series of injections are represented. The same general features are evident in this figure as in figure 34 representing the Freon 22 poisoning. The poisoning is nonlinear and assymptotic. There is some slow recovery of the rate coefficient long after the poison injection. This point is illustrated by the difference between the last

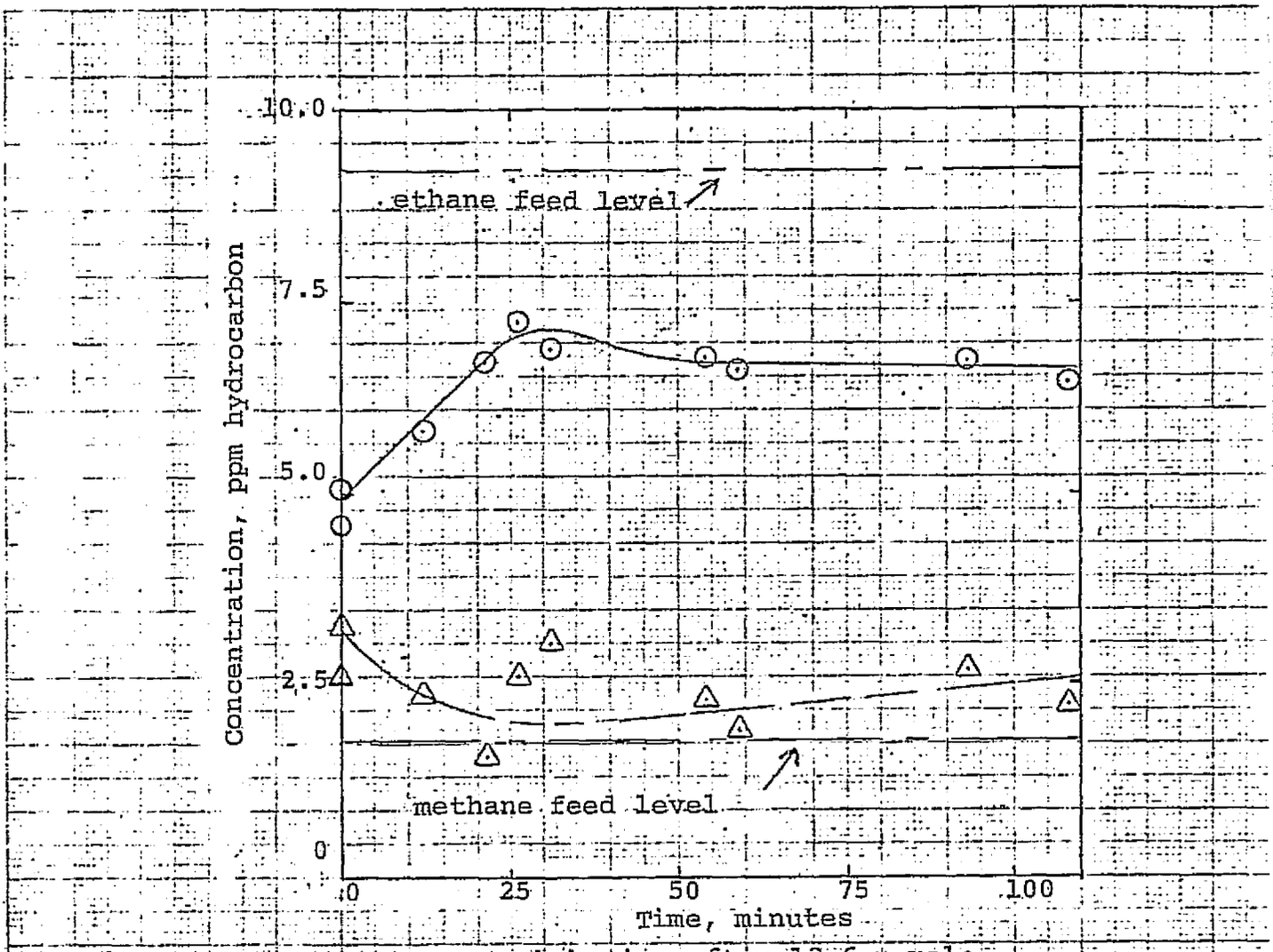

Figure 35 Unsteady state behavior after 13.6 μ mole Freon 22 injection. Methane concentration, △ ; ethane concentration ○ . Residence time, 10.71 minutes; temperature range, 245.3-243.8°C. At 6.25 minutes on the plot a Freon 22 G.C. peak was measured; it corresponded to a concentration in excess of 240 ppm assuming the same effective FID carbon number seen for chloroform, 0.68. (12)

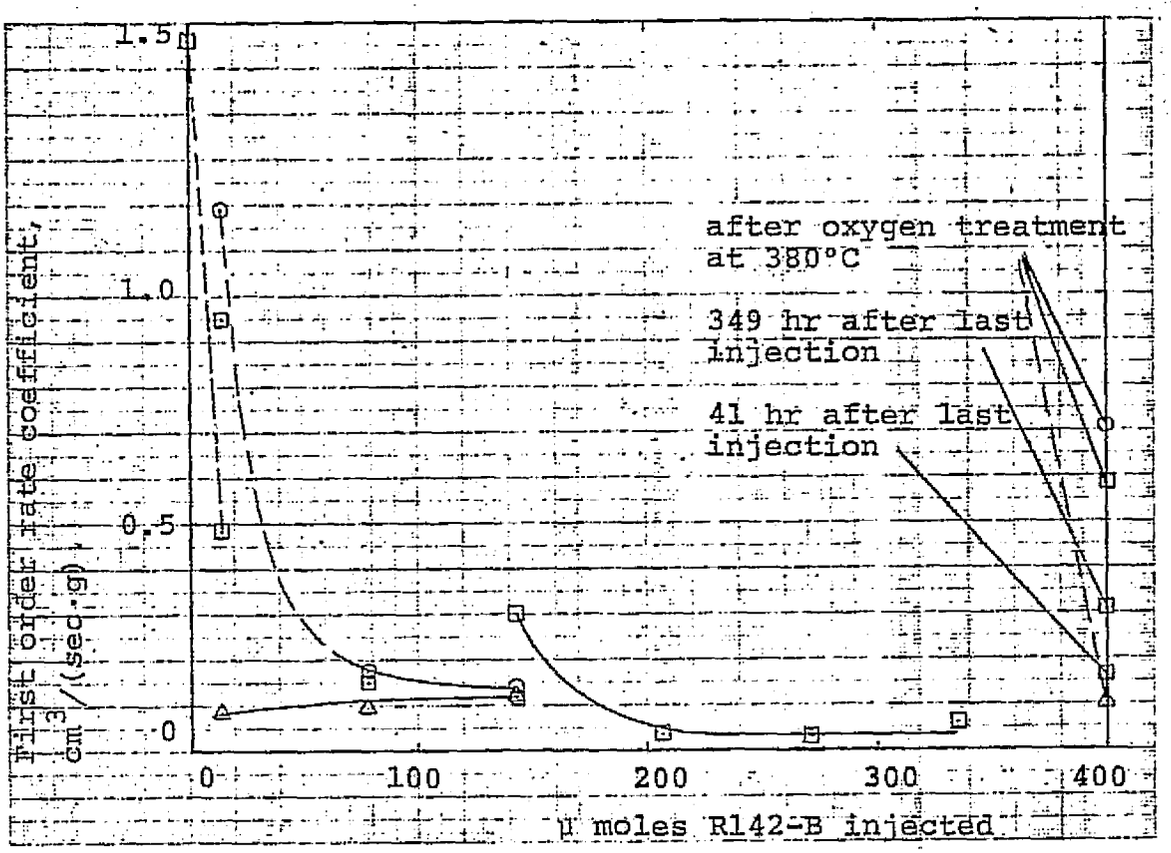

Figure 36 Gentron 142B poisoning of the first catalyst load. First order rate coefficients, at 247°C, based on total hydrocarbon conversion (squares) are plotted. First order rate coefficients for oxidation (circles) and cracking (triangles) of ethane are also plotted when the G.C. operating conditions allowed separation of methane and ethane peaks. Residence time was 10.22 ± 0.09 minutes, temperature range was 240.0-249.9°C. Three injection series are represented. First series, 1 injection, 0-14.4 μ moles. Second series, 2 injections, 64.2 μ moles each, 14.4-142.8 μ moles. Third series, 4 injections, 64.2 μ moles each, 142.8-399.6 μ moles. The rate coefficient immediately after the last injection on the third series, at 399.6 μ moles was not measured. Three rate coefficient measurements, taken at times long after the last injection are represented at 399.6 μ moles (see plot annotations).

recorded rate coefficient of each injection series and the first rate coefficient of the next series. After oxidation in air at 380°C for ~8 hours the catalyst activity again increased.

The immediate response to an injection of Gentron 142-B is shown in figure 37. In figure 37 data from two injections, 62.4 μmoles each, done at slightly different temperatures, are represented. Concentrations of ethane and methane are plotted vs the amount of time after the injection. These injections correspond to 14.4-78.6 μmoles and 78.6-142.8 μmoles Gentron 142-B injected (figure 36). Qualitative data taken after these injections exhibited much the same behavior as seen in the hydrogen sulfide and Freon 22 injections--fast removal of the poison from the gas phase and an initial fast apparent catalyst deactivation. However they differed in one important aspect, exceeding large amounts of methane, > 50 ppm, appeared in the gas phase after an injection. Presumably this is from the cracking of the Gentron 142-B or from the adsorptive displacement of adsorbed methane by Gentron 142-B.

After the catalyst had been oxidized at 380°C in air for ~ 8 hours, subsequent to the Gentron 142-B experiments, some data was taken at various catalyst temperatures. This data is shown in figure 33 plotted in the Arrhenius form along with the previously mentioned data taken before the catalyst poisoning experiments. The slope of the line drawn through this data (triangles) yields a value of 21 kcal/mole,

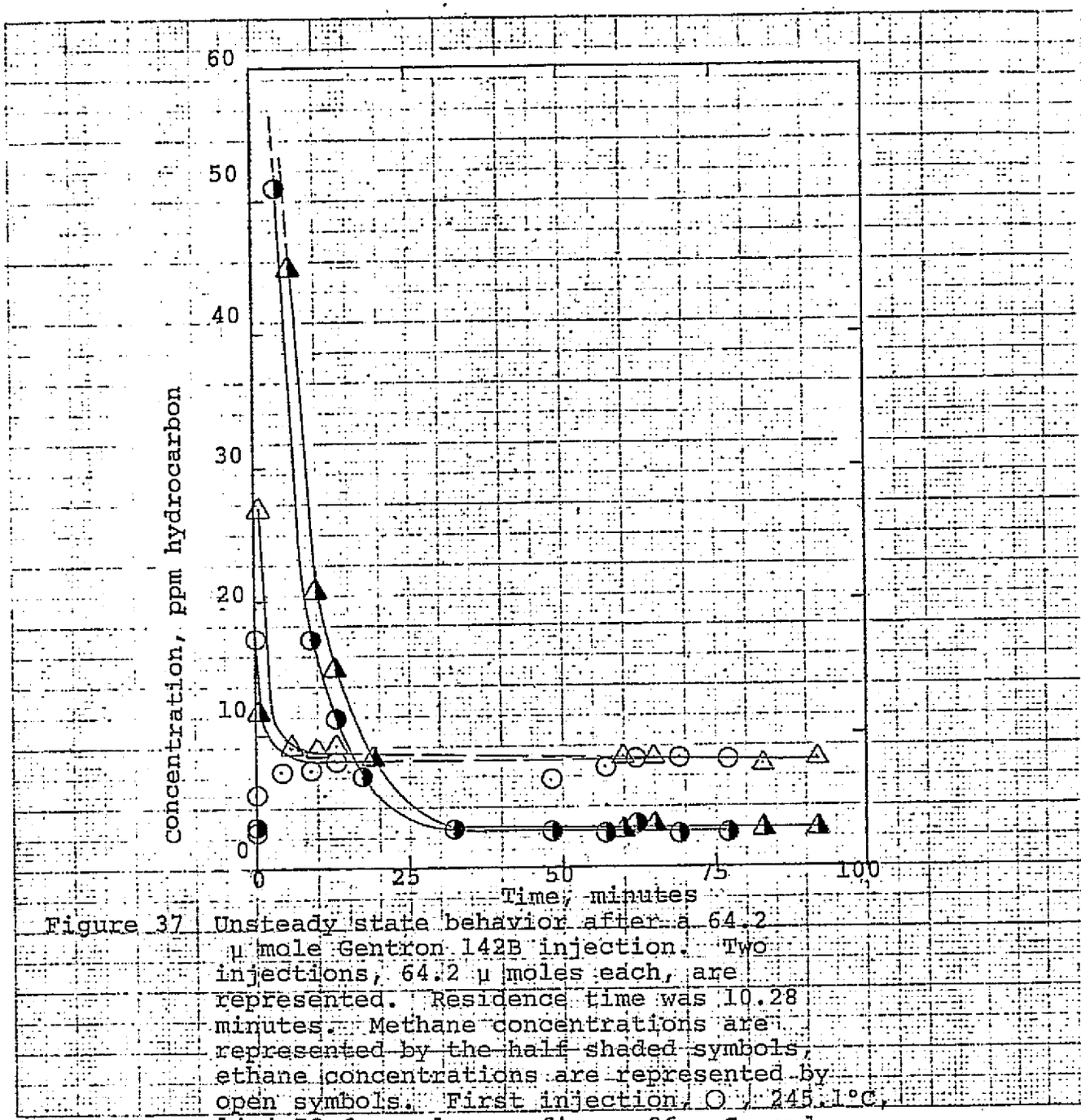

Figure 37 Unsteady state behavior after a 64.2 μ mole Gentron 142B injection. Two injections, 64.2 μ moles each, are represented. Residence time was 10.28 minutes. Methane concentrations are represented by the half shaded symbols, ethane concentrations are represented by open symbols. First injection, ○ , 245.1°C, 14.4-78.6 μ moles on figure 36. Second injection, △ , 247.5°C, 78.6-142.8 μ moles on figure 36. No Gentron 142B was detected.

the pre-exponential extrapolated with 27 kcal/mole from 251.7°C is 1.7×10^{11} $cm^3(sec \cdot g)$. This corresponds to a 59% loss in activity due to the Freon poisoning*.

*After these experiments the catalyst was again oxygen treated at high temperature and the diethyl ketone kinetics were measured. Subsequently, the catalyst was removed, and the preliminary sulfur experiments were done (see Appendix 6,8). Later the catalyst was reloaded for the hydrogen sulfide poisoning experiments. Data taken prior to the hydrogen sulfide poisoning experiments gave a pre-exponential of 8.6×10^{11} $cm^3(sec \cdot g)$, almost double the value of the pre-exponential measured prior to the Freon poisoning experiments. Evidently oxidation treatments after the last one mentioned here resulted in full restoration of the catalytic activity.

Appendix 8.

Oxidation and removal of ethane and hydrogen sulfide by the catalyst support.

Ethane removal.

Ethane removal was investigated over the temperature range 423-513°C using 1.11 gram of the catalyst support, 1/8 inch γ Al_2O_3 pellets. With the gas chromatograph operating procedure used during these runs it was not possible to detect methane.

Data from an experiment to determine the reaction order is represented in figure 38 where the $\log_{10}$ coordinates of the reaction rate and ethane reactor concentration are plotted. In this experimental run the reactor temperature varied (497.7-508.7°C). The reaction rates are corrected to 502°C in figure 38 using an E_a of 25 kcal/mole. The closest integral reaction order the data fits is first order.

The Arrhenius plot of the first order rate coefficients, 423-513°C, is given in figure 39. Two lines can be fitted to the data. The corresponding calculated E_a and pre-exponentials are: 45 kcal/mole and a pre-exponential, k_w, of 9.0×10^{13} $cm^3/(sec \cdot g)$ or k_s of 7.5×10^7 cm/sec assuming an active surface area of 120 m^2/g; and 20 kcal/mole with a pre-exponential of 3.0×10^6 $cm^3/(sec \cdot g)$ or 2.5 cm/sec assuming an active surface area of 120 m^2/g.

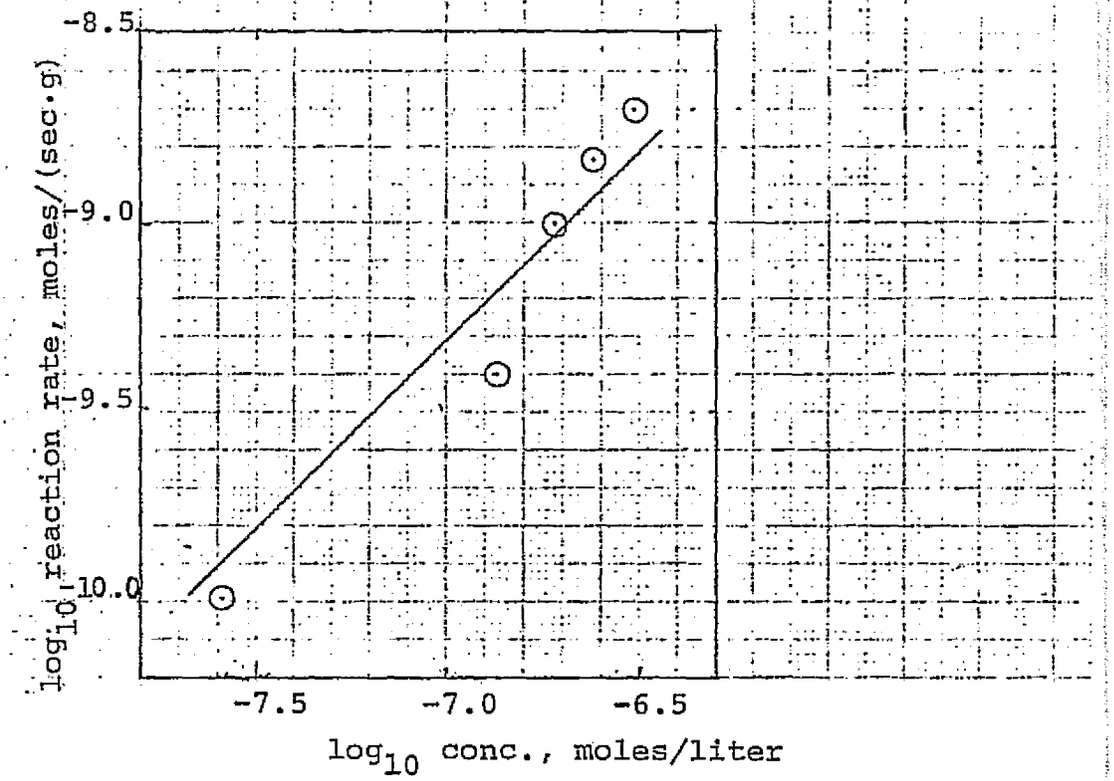

Figure 38 Log plot of concentration vs reaction rate for ethane removal over the catalyst support at 502°C. First order line is drawn.

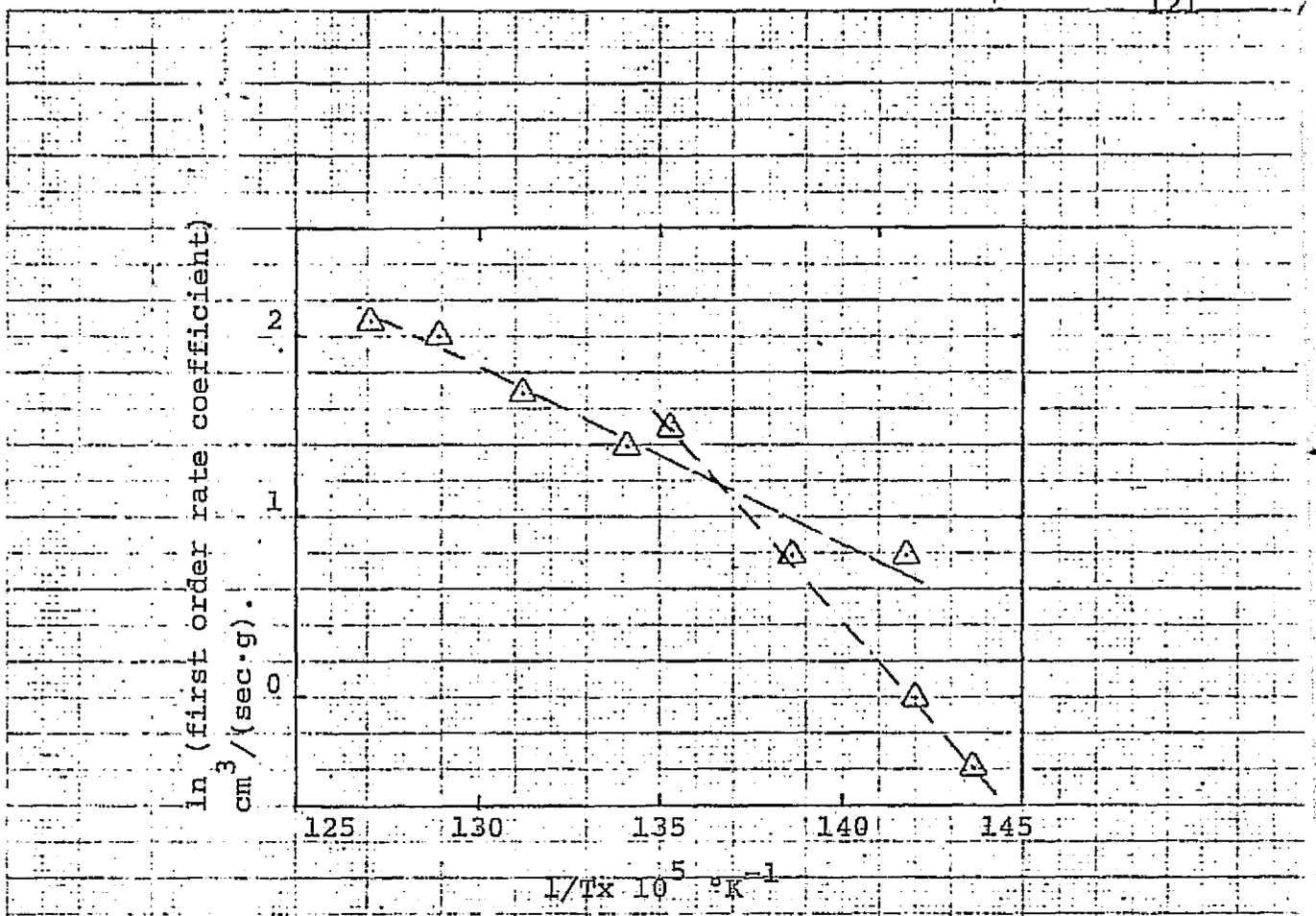

Figure 39 Arrehinus plot of data for the removal of ethane over the catalyst support, 423-513°C. The lines drawn correspond to: 45 kcal/mole with a pre-exponential k_w of 9.0×10^{13} $cm^3/(sec \cdot g)$ or a k_s of 7.5×10^7 cm/sec.; and 20 kcal/mole with a pre-exponential k_w of 3.0×10^6 $cm^3/(sec \cdot g)$ or a k_s of 2.5 cm/sec.

Hydrogen sulfide oxidation.

Oxidation of a hydrogen sulfide injection, 15.1 μmoles, is represented in figure 40. Plotted in figure 40 are the hydrogen sulfide and sulfur dioxide concentrations vs the amount of time after the hydrogen sulfide injection. The data represented in this plot is actually a composite of data taken after 5 hydrogen sulfide injections each at the same residence time, 2.81 minutes, and reactor temperature, ~ 211°C. It was necessary to construct the plot with 5 sets of data because the hydrogen sulfide was removed from the gas phase very quickly and only one gas chromatograph sample could be taken after each injection that contained a measureable amount of hydrogen sulfide.

The important result of this experiment is that hydrogen sulfide injection is oxidized very quickly; much less than one residence time is required for its complete removal. Oxidation of hydrogen sulfide by γ Al_2O_3 has previously been reported (23). It should be mentioned here that the sulfur detector saturates at roughly 14 ppm, concentrations in figure 40 above this level may be high by a factor of 2-2.5.

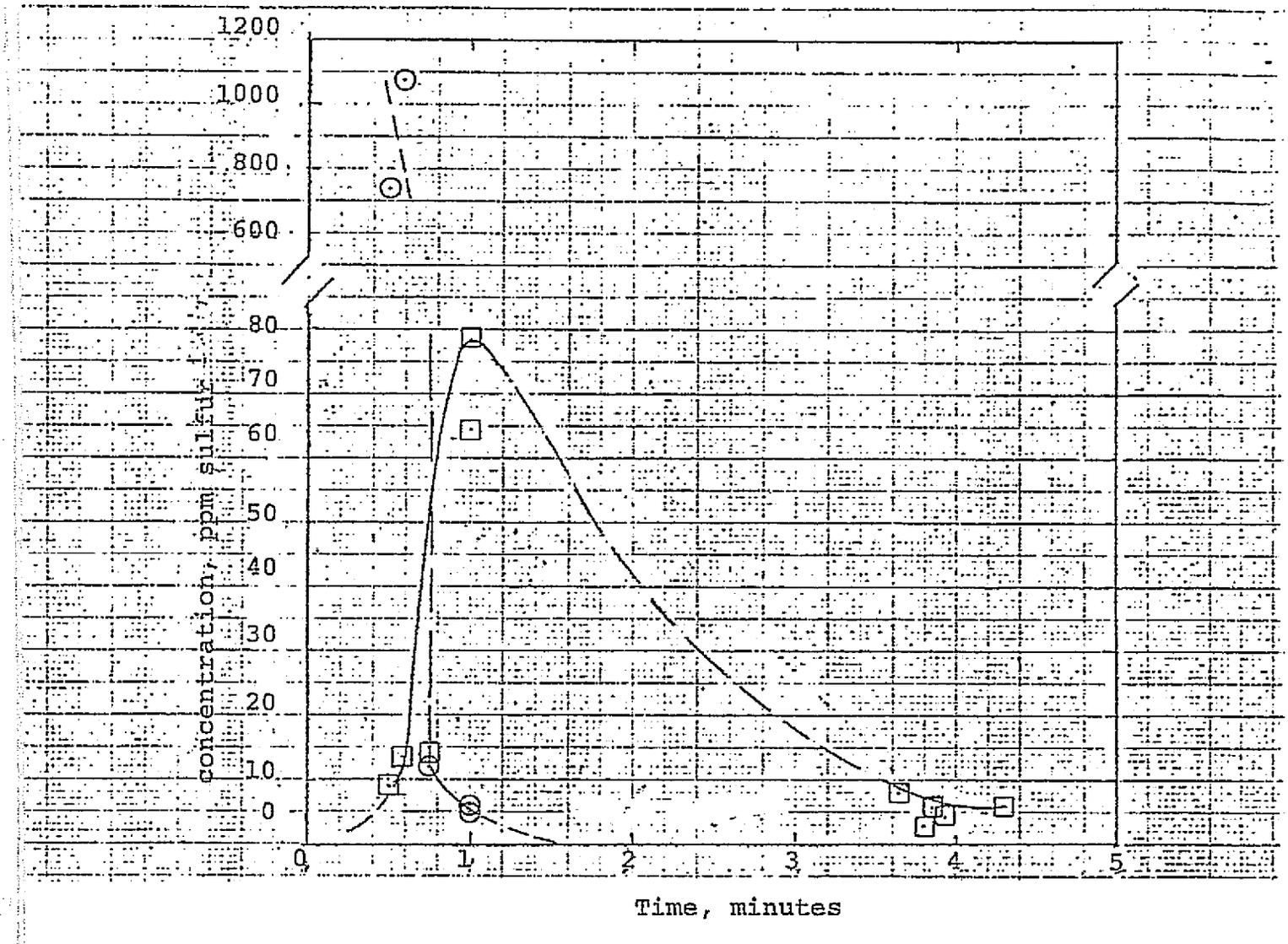

Figure 40 Oxidation of a 15.1 μ mole hydrogen sulfide injection over 1.11 grams of the γAl_2O_3 catalyst support. Reaction temperature was 211.0-212.2°C, residence time was 2.81 minutes. Steady state input of hydrogen sulfide in air was 1.2 ppm. Symbols: sulfur dioxide; hydrogen sulfide.

Appendix 9.

Diffusion Limitations

The symbols and pellet dimensions* used in the diffusion calculations are:

average pellet radius	0.19 cm
R, equivalent active pellet radius	0.15 cm
S, surface area	120 m^2/g
ρ_p, pellet density	0.51 g/cm^3
θ, porosity	0.85
D_{eff}, effective diffusivity of the pellet	0.11 cm^2/sec

η, effectiveness factor

k_w, intrinsic catalytic first order rate coefficient, $cm^3/(sec \cdot g)$

Θ_s, Thiele diffusion modulus for a spherical catalyst pellet

Θ_L, h_o Thiele diffusion modulus for a spherical catalyst pellet

The Thiele diffusion modulus for a sphere, first order reaction is $\Theta_s = R\sqrt{k_v/D_{eff}}$ (28). In terms of the experimental data reported in this work $\Theta_s = R\sqrt{\rho_p \cdot k_w/D_{eff}}$. For isothermal pellets the Thiele model predicts no diffusion limitations when $\Theta_s \leq 1$. Calculations showing the pellets

*The surface area, S, used in these calculations is that measured on the first catalyst load in this work. Other reported physical dimensions are those of the unimpregnated γAl_2O_3 catalyst base as measured by Masaharu Komiyama, a graduate student working in this laboratory.

to be effectively isothermal under the steady state conditions used in this work are presented in another appendix.

Two quantities, R and D_{eff}, must be approximated to calculate the diffusion modulus. The assumptions in their calculation are presented below.

(1) effective pellet radius, R.

Because the center of the pellet is not impregnated the active pellet geometry is a spherical shell. To compensate for this the length used in the definition of θ_L or $\theta_s/3$ since $\theta_s = 3\ \theta_L$ should be the ratio of the volume of the shape to the surface are through which reactants flow into the volume. Aris (29) has shown that the maximum error in this approximation for a spehre vs a flat plate is at $\theta_L \simeq 1$, here η(flat plate) exceeds η(sphere) by only 0.09. This definition translates to an equivalent spherical pellet radius equal to the actual pellet radius times the ratio of impregnated alumina to bulk alumina.

(2) calculation of the effective diffusivity, D_{eff}.

The effective diffusivity of the pellet is given by the equation, $D_{eff} = D\ \theta/\tau$. The tortuosity factor, τ, is assumed to have value of 1.0. In the calculation of D, the diffusion coefficient, it turns out that assuming either extreme Knudsen or bulk diffusion does not result in a large error because of the large catalyst pores. Using the Chapman Enskog equation (22) the effective bulk diffusion coefficient is estimated to be 0.13 cm^2/sec at 260°C. Equating the

pellet diffusion process to Knudsen diffusion in a cylinder and using a mean pore radius given by the equation, $r = 2\theta/S\rho_p$, the effective Knudsen diffusion coefficient is calculated to be 0.096 cm^2/sec at 260°C.

Given the criterion that $\theta_s \leq 1$ for insignificant diffusion limitations the equivalent rule for the Arrhenius plot is $\ln k_w \leq \ln(D_{eff}/R^2 \rho_p)$. Assuming an average D_{eff} of 0.11 cm^2/sec the predicted intrinsic diffusion limitations are at the Arrhenius coordinate of $\ln k_w = 2.26$. The linearity of the Arrhenius plot of the first catalyst load and the nonlinearity of the Arrhenius plot of the second load suggests this prediction is somewhere between the two cases observed.

Correlations of the effectiveness factor of the Thiele model by Weisz (30) afford a simple calculation of the deviation of the apparent E_a. Assuming the predicted value of $\theta_s = 1$ at $\ln k_w = 2.26$ the apparent E_a at 310°C is ∿20 kcal/mole. Although there is some scatter in the data neither the slope of the Arrhenius line nor the predicted value of the apparent rate coefficient k_w apparent = (k_w intrinsic) x (0.68) fit the assumption of $\theta_s = 1$ at $\ln k_w = 2.26$. The error is most likely introduced in the active pellet radius, the catalytically active metal distribution in the pellet is not known, it is only assumed from the visible Pd impregnation.

Wheeler (25) has shown that with a sufficiently large diffusion modulus a small amount of pore mouth poisoning results in severe mass transfer limitaitons, accordingly intrinsic kinetics will not be observed after the first introduction of poison.

That increased diffusion resistance caused by pore mouth poisoning did not affect the reaction rate at 256°C on the first catalyst load can be seen by the following argument. The onset of significant intrinsic diffusion limitations is at a diffusion modulus $\theta_s = 1$. The linear Arrhenius plot of the first catalyst prior to poisoning would put the maximum value of $\theta_s = 1$ at the high end of the temperature range investigated ∿310°C. Assuming this then the maximum value of θ_s at 256°C can be calculated since $\theta_{s_{310°C}} = 1$, $\theta_s \propto \sqrt{k}$ then

$$\theta_{s_{256°C}} = \exp E_a/(R \cdot 2)\ [1/T_{310°C} - 1/T_{256°C}] = 9 \times 10^{-2}$$

Wheeler's model predicts the fraction of the activity left after poisoning F, is given by

$$F = \left[\frac{\tanh[h_o(1 - \alpha)]}{\tanh h_o}\right] \left[\frac{1}{1 + h_o}\right]$$

where h_o is the intrinsic diffusion modulus for a cylinder, $h_o = \theta_s/3 = 3 \times 10^{-2}$, and α is the fraction of the pore surface poisoned. Since for $x < 0.3$ $\tanh x \simeq x$ then for small h_o $F \simeq (1 - \alpha)$ which is the result expected since the active surface is uniformly accessible to the reactants at low h_o.

Calculation of the intrinsic activity of the second catalyst load is complicated by the nonlinear Arrhenius plot. Assuming the Arrhenius plot represents intrinsic mass transfer limitations the intrinsic activity can be estimated from the onset of the 13-14 kcal/mole phenomena at $1/T \times 10^5 = 189°K^{-1}$. Weisz (30) has calculated that the transition to an apparent E_a about 1/2 of the intrinsic E_a occurs at about $\theta_s = 20$, $\eta = 0.14$. Knowing the η at the transition temperature allows an estimation of the assumed intrinsic pre-exponential. It is $k_w = 2.9 \times 10^{12}$ $cm^3/(sec \cdot g)$.

Appendix 10

Reaction Heating of Catalyst Pellets

The following symbols are used in the calculations below:

ΔT max, maximum temperature difference between the center and outside of a catalyst particle °C.

ΔH, heat of reaction, ethane oxidation value 3.4×10^6 cal/mole.

Deff, effective diffusivity ≈ 0.11 cm^2/sec.

C_s, ethane concentration at the pellet surface 30 ppm at 1 atm, 200°C $= 7.7 \times 10^{-10}$ moles/cm^3.

λ, effective pellet thermal conductivity $\approx 0.53 \times 10^{-3}$ cal/(sec cm °C) (assumed).

E_a, apparent activation energy for reaction, 27×10^3 cal/mole.

T_o, pellet surface temperature, °K.

R, gas constant, 1.987 cal/mole °K.

δ, isothermal criteron $|\delta| \leq 0.3$.

Damkohler's equation (31) relating the maximum temperature difference between the surface and center of a catalyst particle is:

$$\Delta T \text{ max} = \frac{\Delta H \text{ Deff } C_s}{\lambda}$$

Prater (32) has shown this equation applies to any kinetics or particle geometry. A maximum temperature difference ΔT max of 0.54°C is predicted by the above equation.

The pellets are non-isothermal, however Peterson's criterion (26) can be used to show that the non-isothermal effects are insignificant. The criterion is that $|\delta| \leq 0.3$ where δ is defined by:

$$\delta = \frac{E_a \ -\Delta H \ D_{eff} \ C_s}{R \ T_o^2}$$

At 200°C, 30 ppm ethane $|\delta| = 0.03$. The prediciton is that at concentrations below ~300 ppm insignificant non-isothermal effects will result.

The concentration transients used in the non-steady state reaction order runs on the second catalyst load exceed this steady state criterion. In the three runs reported, fig. 7, $|\delta| = 0.3$ occurs at ln (mole fraction) = -8.0 to -7.7. Thus ~ 80% of the data lies below this value. This criterion is applied to the non-steady state concentration runs only to show that the heating effects are small throughout ~80% of the data.

Appendix 11.

Description of Catalyst and Gases

The catalyst was in the form of spherical, roughly 1/8 inch in diameter, gamma alumina pellets, "Purzaust Base," impregnated with pallidium at a concentration of 0.5 wt%. The catalyst source was the Universal Oil Products Research Laboratory, lot #2787-66, "Uniform Impregnation."

Pre-mixed hydrocarbon reactant gases were supplied by Liquid Carbonic. They were custom gas mixtures prepared with 20-30 ppm hydrocarbon in zero grade* air.

The pre-mixed sulfurons gases used in calibrating the sulfur dectector, ppm of hydrogen sulfide and sulfide dioxide in zero grade nitrogen, were supplied by Matheson Gas.

The purity and sources of gases used for injections into the reactor, for catalyst preparation, and for adsorption experiments are given in the table below.

---

*Zero grade is a specification for low hydrocarbon content, usually less than 1.0 ppm of methane equivalent hydrocarbon content.

Gas	Purity	Source
Ethane	99.97%	Phillips Petroleum Lot #1197
Diethyl Ketone	95% Practical Grade	Eastman Kodac Lot #711-1B
Hydrogen Sulfide	99.6% C.P. Grade	Matheson Gas
Freon 22	99.9%	Matheson Gas
Gentron 142B	98.0%	Matheson Gas
Carbon Monoxide	99.5% C.P. Grade	Matheson Gas
Hydrogen	99.9%	Liquid Carbonic
Helium	99.995%	Liquid Carbonic
Nitrogen	99.996%	Liquid Carbonic
Air	Breathing Air Grade E	Ohio Medical Products

Appendix 12.

Gas Chromatograph Data

Symbols and abreviations used:

FPD = flame photometric dectector

FID = flame ionization dectector

AH2S = FPD hydrogen sulfide peak area

ASO2 = FPD sulfur dioxide peak area

AE = FID ethane reactor effluent peak area

AEO = FID ethane reactor feed peak area

AM = FID methane reactor effluent peak area

AMO = FID methane reactor feed peak area

Atten = gas chromatograph attenuator setting times the recorder setting in mV

Tr = reactor temperature, °C

T = room temperature, °C

f = volumetric flowrate feeding the reactor recycle loop, cc/min.

[dc/dt = 0] = amount of time in minutes after the poison injection when the data was taken.

Injection loop volumes, cm^3: #10 = 4.822; #20 = 0.4856; #500 = 10.085.

The ethane injections mentioned below were injections of pure ethane at room temperature. The DEK injections were injections of air DEK mixtures obtained by slowly passing air through a DEK bubbler packed with glass beads. At equilibrium this procedure should result in approximately 4 volume % DEK in the injection.

The gas chromatograph operating parameters used in this work were similar to those used by Rabb (2) and a detailed description is given in his thesis.

Gas chromatograph peak areas were obtained from a Disc Instruments Series 200 disc integrator installed in a Hewlett-Packard model 7100-B dual pen strip chart recorder. Since only one channel of the recorder was equipped with an integrator when simultaneous FID and FPD peaks were recorded a plain meter was used on the FPD peaks.

Figure 3

197°C run inlet conc. 21.0 ppm ethane

	AE	AEO	AM	AMO	Tr	T	f
1st Day							
4:30 pm	0.64	14.56	0.62	0.17	196.5	25.0	1.71
8:40 pm	1.36	14.61	0.83	0.23	201.0		1.71
2nd Day							
10:05 am	8.50	13.47	0.30	0.25	195.0		27.8
12:10 am	10.07	12.83	0.26	0.22	194.5		40.3
3:21 pm	10.07	13.57	0.27	0.20	194.7		40.3
4:53 pm	10.83	13.51	0.30	0.22	196.5		48.8
6:44 pm	11.41	13.26	0.24	0.21	196.9		60.6

Figures 3 and 4 (data plotted on both figures 3 and 4)

198°C run inlet conc. 21.6 ppm-ethane

	AE	AEO	AM	AMO	Tr	T	f
1st Day							
7:38 pm	8.83	14.83	0.93	0.39	198.0	23.5	4.79
10:16 pm	6.97	14.73	1.39	0.30	198.5		2.73
2nd Day							
1:29 am	5.85	14.79	1.91	0.32	198.0		1.41
3:43 am	4.45	14.76	2.30	0.34	198.9		0.61
7:16 am	7.84	14.47	1.90	0.32	198.8		2.73
10:43 am	13.81	14.59	0.42	0.34	194.7		57.5
3rd Day 227°C run							
2:10 am	5.58	14.61	1.07	0.32	226.3	24.0	15.3
4:36 am	10.04	14.48	0.76	0.34	228.0		57.3
6:23 am	7.46	14.35	0.88	0.27	229.1		29.9
9:44 am	6.64	14.30	0.89	0.32	229.1		21.4
11:44 am	3.59	14.65	1.39	0.37	226.7		7.0
2:02 pm	11.62	14.70	0.45	0.30	225.9		97.3
5:28 pm	6.10	15.21	1.02	0.28	226.3		15.3
4th Day 248°C run							
11:38 am	4.27	12.17	0.95	0.26	245.6	24.0	15.8
2:27 pm	8.72	12.12	0.52	0.23	245.8		122.4
5:18 pm	6.13	11.79	0.75	0.28	249.0		55.1
7:45 pm	7.45	12.02	0.64	0.27	250.0		92.0
11:07 pm	4.85	11.91	0.80	0.20	250.8		36.8

Figures 3 and 4 (continued)

	AE	AEO	AM	AMO	Tr	T	f
5th Day							
1:31 am	1.79	12.04	1.25	0.23	248.8	24.0	9.09
4:23 am	3.12	12.34	1.14	0.25	249.8	24.0	15.8
271°C run							
3:30 pm	6.07	11.94	0.87	0.19	266.3	25.2	102.3
5:50 pm	7.54	11.72	0.62	0.21	269.3		185.8
8:19 pm	6.56	11.96	0.82	0.25	270.7		159.0
11:38 pm	4.01	11.99	1.15	0.29	271.9		64.3
6th Day							
1:21 am	1.88	11.86	1.07	0.26	273.0		31.3
3:55 am	4.91	12.71	1.01	0.31	271.9		85.3
5:47 am	4.73	11.75	0.80	0.19	271.4		102.3
7th Day	301°C run						
11:07 am	5.10	14.19	0.99	0.20	297.7	25.8	374.7
1:36 pm	6.39	14.27	0.97	0.30	297.9		311.1
4:00 pm	6.73	14.02	0.88	0.29	296.9		335.3
6:01 pm	6.78	14.07	0.85	0.23	301.0		300.6
7:58 pm	3.89	14.05	1.10	0.23	303.9		185.2
10:17 pm	2.26	14.16	1.19	0.23	305.8		90.91
12:19 pm	4.65	14.11	1.17	0.19	306.5		374.7

Figure 5 inlet conc. 30.0 ppm ethane

	AE	AEO	AM	Tr	T	f
1st Day						
9:34 am				215.0	23.0	22.5
9:37 am	Inject #20					
10.59 am	7.28	9.19	0.07	210.2		96.0
11:03 am	Inject #20					
12:11 am	7.69	9.24	0.07	212.0		96.0
12:17 am	Inject #20					
2:42 pm	7.93	9.39	0.06	209.8		94.0
4.56 pm	4.56	9.25	0.18	2.219		15.8
6:46 pm	1.00	9.26	0.06	261.0		77.6
8:59 pm	1.57	9.37	0.01	312.5		537.0
9:38 pm	Inject #20 twice					
12:48	5.13	9.41	0.18	205.2		16.1
3rd Day	On steam at Tr = 205 since 12:48 pm, 1st day					
2:38 pm	6.78	9.50	0.09	205.3	22.7	19.6
3:48 pm	Inject #20					
6:17 pm	2.71	9.36	0.15	231.0		34.8
6:50 pm	Inject #20					
9:23 pm	3.83	9.39	0.10	253.8		140.0
10:23 pm	Inject #20					
11:37 pm	1.62	9.36	0.01	296.0		303.0
4th Day						
2:48 am	3.75	9.38	0.15	200.2		23.3
10:58 am	4.22	9.33	0.15	200.5	23.3	7.8

Figure 5 (continued)

	AE	AEO	AM	TR	T	f
12:17 am	4.24	9.36	0.16	200.5	23.3	7.8
1:26 pm	Inject #20 twice					
2:47 pm	2.54	9.34	0.05	282.5		303.0
3:32 pm	Inject #20 twice					
4:45 pm	5.15	9.35	0.07	257.9		292.0
5:15 pm	Inject #20 twice					
6:57 pm	5.93	9.49	0.08	236.8		110.0
7:40 pm	Inject #20 twice					
9:36 pm	3.92	9.33	0.19	217.6		17.0
5th Day						
11:09 am	2.02	9.61	0.04	299.3	23.4	529.0
12:25 am	Inject #20					
2:30 pm	3.09	9.63	0.06	274.9		309.0
3:26 pm	Inject #20					
4:30 pm	6.67	9.8	0.06	246.3		306.0
5:12 pm	Inject #20					
8:37 pm	5.56	9.52	0.11	230.7		71.7
9:45 pm	Inject #20					
10:46 pm	3.08	9.66	0.06	279.6		320.0
12:25 pm	Inject #20					
12:40 pm	1.85	9.76	0.01	319.2		505.0

Figure 6 Data of R. Vincent

	AE	AEO	Tr	T	f
1/30					
10:30	10.85	12.50	210	24.0	8.5
1:00	11.10	12.20	207		
3:30	10.40	11.95	210		
1/31					
10:45	8.30	10.25	210		
3:45	5.45	10.40	242		
2/1					
1:40	3.95	10.40	269		8.0
2:50	5.40	10.40	273		19.0
3.50	5.65	10.40	269		31.5
2/13					
11:00	3.40	8.20	269		16.0
1:00	2.83	8.00	268		7.8
2:30	4.70	8.00	269		19.3
2/19					
5:15	8.70	14.33	269		26.0
2/20					
10:15	5.65	14.05	298		30.5
12:40	5.2	14.20	296		25.8
2/26					
4:20	4.60	13.15	296		24.0
5:30	5.08	16.20	295		19.3

Figure 6 (continued)

	AE	AEO	Tr	T	f
2/27					
9:30	4.57	14.13	296	24.0	22.8
1:45	2.31	9.90	293		15.0
3:15	4.0	12.50	296		25.7
5:30	4.80	14.60	296		23.8
9:20	4.87	12.60	296		23.3

Figure 7

230°C run

ethane FID calibration: 30 ppm = 7.17 at atten of 8

Time, Minutes	AE	Atten
1.39	6.69	256
2.52	9.76	128
6.05	6.64	128
8.27	9.05	64
11.42	12.74	32
14.94	8.42	32
17.74	12.24	16
20.60	8.74	16
23.34	6.33	16
26.12	8.99	8
29.71	12.00	4
32.42	8.88	4
35.50	5.98	4
38.08	8.95	2
40.81	6.39	2
43.41	10.10	1
46.31	6.24	1
49.15	4.58	1
52.03	3.37	1

261°C run

ethane calibration: 30 ppm = 7.16 at atten of 8

0.98	6.95	512
4.09	9.15	256
7.22	5.92	256
10.60	7.21	128
13.34	9.65	64
16.35	6.39	64
19.78	6.55	32
22.67	10.14	16

Figure 7

261°C run (continued)

Time, Minutes	AE	Atten
25.69	6.39	8
31.62	10.09	4
34.92	5.99	4
38.21	6.98	2
40.60	4.96	2
44.32	5.25	1
47.12	4.15	1

284°C run

ethane calibration: 30 ppm = 7.29 at atten of 8

0.76	6.48	512
3.67	4.85	256
6.55	6.80	64
9.06	5.19	32
11.90	6.93	8
14.27	5.67	4
16.85	4.10	2
19.17	3.01	1

Figure 8

time, hr.	effluent	feed	f	Tr	T
93.6	33.03	74.59	36.4	137.3	24.0
121.6	40.18	76.50	36.4	136.8	
156.3	36.98	66.57	36.4	137.6	
326.2	36.19	56.18	37.2	137.9	
370.0	41.01	62.83	37.2	137.3	

Figure 9

	effluent	feed	f	Tr	T
1st Day					
5:07 pm	28.24	66.57	16.2	138.6	240
9:40 pm	26.96	65.79	16.2	139.7	
4th Day					
3:41 pm	16.54	68.51	5.20	138.3	
8th Day					
10:21 am	36.19	56.18	37.2	137.9	
11th Day					
9:42 am	41.01	62.83	37.2	137.3	

Figure 10

	effluent	feed	f	Tr	T
1st Day					
6:17 am	Inject #10 22 times				
1:14 pm	38.84	62.62	18.6	113.0	24.0
2nd Day					
5:50 am	29.73	60.33	17.8	125.8	
10:02 am	25.95	64.21	17.8	139.0	
1:02 pm	21.31	63.10	17.8	149.3	
3:14 pm	16.76	64.45	17.8	156.2	
9:44 pm	36.95	65.48	76.3	159.0	
3rd Day					
12:15 am	35.19	72.00	77.1	165.4	
3:06 pm	29.95	67.40	77.1	172.7	
5:30 pm	28.59	66.37	129.7	184.5	
10:20 pm	15.47	48.97	193.0	198.6	
5th Day					
	Inject #10 30 times at 115°C, f = 9.7				
6th Day					
12:02 am	32.41	62.24	32.4	108.7	
3:06 pm	39.77	60.36	71.3	114.9	
5:34 pm	35.61	58.06	70.5	123.3	
8:14 pm	32.14	59.61	70.5	132.5	
10:36 pm	29.05	59.61	93.3	144.5	
7th Day					
2:12 am	28.53	58.30	144.3	156.7	
9:18 am	28.09	63.43	180.0	167.6	
11:19 am	23.65	62.27	192.2	192.5	
11:30 am	Inject #10 30 times at 110°C, f = 10.9				
10:38 pm	17.34	70.82	10.9	109.2	

Figure 11

H_2S μmoles	AE	AEO	AM	Tr	T	f	dc/dt = 0	Procedures and Comments
	First catalyst load 1.1 grams First injection series							
0	4.74	8.56	0.06	255.8	21.4	269.9	-	
10.0	5.64	↓	0.07	254.4	21.2	301.2	30	
20.4	5.30	↓	0.09	259.0	↓	298.2	60	
30.6	5.76	↓	0.09	256.3	↓	294.4	70	
40.8	5.82	↓	0.10	257.1	21.4	292.2	40	
51.0	6.15	8.43	0.09	254.6	↓	295.1	50	
								outgas CO-H_2-CO ads.-des.
51.0	4.00	8.36	0.14	255.5	23.4	126.1	-	
								wait 15.5 hrs to start 2nd injection series
	Second injection series							
51.0	3.70	8.49	0.12	255.2	23.4	129.7	-	
61.3	3.95	↓	0.15	↓	↓	↓	60	
71.6	4.15	↓	0.14	↓	↓	↓	60	
81.9	4.38	↓	0.15	↓	↓	↓	60	
92.2	4.59	↓	0.15	↓	↓	↓	60	
102.5	4.59	↓	0.15	↓	↓	↓	60	
112.8	4.89	8.60	0.15	255.6	↓	129.9	90	
								outgas CO ads.-des.

Figure 11 (continued)

H_2S μmoles	AE	AEO	AM	Tr	T	f	dc/dt = 0	Procedures and Comments
	Third injection series							
112.8	3.93	8.18	0.13	254.3	23.6	125.0	-	
171.8	4.60	↓	0.11	↓	↓	↓	80	
230.8	4.60	↓	0.10	↓	↓	↓	100	
289.8	4.88	↓	0.09	↓	↓	↓	130	
348.8	5.03	8.19	0.09	253.9	23.5	↓	270	
								Outgas CO ads.-des.
	Fourth injection series							
348.8	4.32	8.16	0.14	254.2	24.0	126.1	-	
532.9	4.98	↓	0.03	↓	23.7	↓	180	
717.0	4.83	8.29	0.04	254.4	24.4	↓	310	
								Outgas
717.0	5.48	8.16	0.39	250.0	24.2	216.5	-	
								High temperature O_2 treatment
717.0	4.39	8.02	0.61	251.9	22.8	144.7	-	
								CO ads.-des.

Figure 12

Four H_2S injections, 59.0 μ moles each
113-349 μmoles on figure 11.

30 ppm ethane feed no methane feed
ethane FID calibration 30 ppm = 8.18
sulfur FPD calibration 3.0 ppm SO_2 = 8.0 at atten of 32*

Time min.	AH_2S	ASO_2	(FPD atten)	AE	AM	T	Tr	f
First injection								
0	-	-	-	3.93	0.13	23.6	254.3	125.0
0.42	0.20	(lost)	1024	3.93	0.13			
2.42	0			4.69	0.13			
4.51				5.76	0.12			
5.67		23.8	1024					
7.23		30.2	512	6.18	0.11			
10.56		6.7	512	6.21	0.10			
13.00		1.4	128	5.98	0.10			
18.58		3.4	16	5.59	0.11			
22.67		12.5	2	5.40	0.11			
26.72		14.4	1	5.26	0.13			
30.67		10.5	↓	5.18	0.11			
34.63		7.5	↓	5.00	↓			
38.32		5.6	↓	4.89	↓			
42.16		12.6	0.32	4.90	↓			
45.67		8.6	↓	4.81	0.12			

*Two integrators were used for the FPD (sulfur) peaks on this run, a disc integrator and a plainmeter. The FPD peak areas are recorded to the first decimal point whereas disc integrator areas are recorded to the second decimal point. The ratio of the relative areas for this experimental run is disc/plainmeter = 1.1625.

Figure 12 (continued)

Time Min.	AH_2S	ASO_2	($^{FPD}_{atten}$)	AE	AM
50.02		5.6	0.32	4.77	0.11
53.89		3.4	↓	4.77	0.12
61.11		1.4	↓	4.73	0.11
76.50		1.0	↓	4.77	↓
72.97		0.4	↓	4.62	↓
78.37		0.1	↓	4.66	↓
83.68		0	↓	4.60	↓
95.91				4.60	↓
Second injection 100.0 minutes					
100.5	11.7	16.6	1024	4.73	0.12
105.61	0	40.2	512	6.61	↓
109.70		10.3	512	6.61	↓
114.42		2.2	128	6.28	↓
118.83		8.6	8	6.11	↓
123.92		15.9	2	5.76	↓
129.85		19.5	1	5.54	↓
136.09		13.9	↓	5.35	↓
143.66		9.6	↓	5.17	↓
151.09		19.5	0.32	5.08	↓
161.14		9.6	↓	5.09	↓
170.67		3.8	↓	4.93	↓
177.25		2.0	↓	4.94	↓
183.62		1.0	↓	4.89	↓
190.64		0.5	↓	4.93	↓
196.29		0.2	↓	4.88	↓

Figure 12 (continued)

Time Min.	AH_2S	ASO_2	FPD ($_{atten}$)	AE	AM
201.38		0.1	0.32	4.82	0.12
206.25		0.1	↓	4.88	↓
Third injection 210.0 minutes					
210.50	11.3	17.3	1024	4.76	0.09
214.99	0	41.3	512	6.31	0.09
219.38		14.3	512	6.73	0.10
223.24		3.2	256	6.62	0.11
227.54		2.9	64	6.47	0.10
231.39		10.3	8	6.12	
236.10		13.5	4	5.93	
239.85		19.6	2	5.78	
244.23		15.3	2	5.63	
249.74		25.5	1	5.49	
254.11		20.6		5.43	
258.84		18.0		5.27	
263.41		10.2		5.35	
275.45		6.3		5.13	
Start using disc integrator					
283.66		3.15		5.07	
288.30				5.11	
292.31		4.45	0.32	5.03	
296.65		3.03		4.94	
301.32		2.12		5.05	
306.51		1.48		4.95	0.09

Figure 12 (continued)

Time Min.	AH_2S	ASO_2	(FPD atten)	AE	AM
312.56		0.91	0.32	5.07	0.09
317.70		0.60	↓	5.11	↓
322.87		0.53		4.92	
333.86				5.13	
336.32				5.02	↓
Fourth injection 340.0 minutes					
340.75	10.0	24.1	1024	4.95	0.10
344.71	0	21.3	1024	6.24	0.10
349.41		17.1	512	7.0	0.09
Start using disc integrator					↓
353.88		7.44	256	6.81	
358.06		7.21	64	6.64	
362.21		12.62	16	6.42	
366.43		16.29	8	6.22	
370.58		25.88	4	6.02	
374.75		21.73	↓	5.85	
380.16		18.19		5.71	
386.02		15.31		5.48	
392.08		11.85	↓	5.35	
397.46		17.97	2	5.33	
403.17		12.76	2	5.28	
409.91		14.75	1	5.14	
416.61		7.55	1	5.04	
422.08		13.64	0.32	5.09	
427.29		7.55	↓	5.05	
432.16		5.24		5.06	↓

Figure 12 (continued)

Time Min.	AH_2S	ASO_2	$(^{FPD}_{atten})$	AE	AM	T	Tr	f
436.71		3.39	0.32	5.03				
441.26		2.62	↓	4.93				
446.19		1.92		5.14				
451.17		1.05		4.95				
455.76		0.72		4.90				
460.06		0.60		4.94				
464.40		0.42		5.00		23.6	254.3	125.0
610.00				5.03		23.5	253.9	125.0

Figure 13

1 H_2S injection, 184.1 µmoles

349-533 µmoles on figure 11.
30 ppm ethane feed, no methane feed
ethane FID calibration 30 ppm = 8.16
sulfur FPD calibration 3.0 ppm SO_2 = 6.87 at atten of 32

Time min.	AH_2S	ASO_2	($_{atten}^{FPD}$)	AE	AM	T	Tr	f
0.0				4.32	0.14	24.0	254.2	126.1
0.76	11.28	15.58	2048					
2.67				4.86	0.13			
5.10		41.62	1024					
5.50				6.56	0.10			
10.12		33.13	1024	7.75	0.04			
14.46		68.36	512	7.84	0.02			
16.79				8.01	0.02			
19.30		28.37	1024					
21.84				8.06	0.01			
23.86		24.99	1024	8.10				
25.92				8.02				
28.50		18.72	1024	8.05				
30.68				8.08				
33.02		18.95	512	7.86				
35.11				7.92				
37.42		6.05	512	7.73				
40.95		12.64	128	7.51				
45.44		13.28	64	7.50				
50.39		16.10	32	6.99				
54.57		20.80	16	6.70	0.02			
58.58		13.98	16	6.36				
62.90		17.56	8	6.31				
67.07		10.68	8	6.08				
71.29		12.85	4	5.89				
75.70		15.03	2	5.83				
80.21		17.69	1	5.66				

Figure 13 (continued)

Time min.	AH_2S	ASO_2	FPD ($_{atten}$)	AE	AM	T	Tr	f
84.65			1	5.59	0.03			
88.97		22.85	0.32	5.51	0.02			
93.29		15.40		5.42	0.03			
97.53		11.32		5.33				
102.27		7.60		5.27				
106.76		5.93		5.21				
111.30		4.43		5.23				
119.91		2.79		5.23				
124.14		2.18		5.21				
128.36		1.62		5.12				
132.83		1.89		5.10				
137.48		1.30		5.14				
141.89		0.95		5.18				
145.95		0.90		5.12	0.04			
150.73		0.85		5.12	0.03			
160.29		0.49		5.00	0.02			
164.67		0.06		4.99	0.03			
170.77		0.04		5.04				
175.59		0.35		4.98				
180.09		0.35		(lost)				
237.0	Inject 184.1 μ moles (last injection on 1st catalyst load)							
545.0				4.83	0.04	24.4	254.4	126.1

At 545.0 minutes FID calibration was: 30 ppm = 8.29

Figure 14

Cycle #	Strip chart recorder Integration areas, counts		Ambient conditions		He carrier gas flow
	ads	des	T	P, torr	cm^3/min
1	4.10	23.90	25.0	755	178.1
2	7.04	15.52	↓	↓	↓
3	7.10	14.70			
4	8.82	15.86			
5	12.28	21.78			

integration speed = 60/8 counts/(inch min)

pen response from
mV scale setting = 8/5 inches/mV

CO-He calibration curve = 1.16×10^3 mV/volumetric fraction CO

at 6ml/min cell flow
200 mA cell current

volume CO, cm^3, at room T and P $= \left[\frac{60}{8} \quad \frac{8}{5} \quad 1.16 \times 10^3\right]^{-1}$ (178.1) (integration area, counts)

catalyst weight 1.1 grams

assumed CO-Pd surface area calibration $3.1 m^2/cm^3$ (STP)

Figure 15

FPD sulfur dioxide calibration
3.0 ppm = 7.86 at attenuation of 32
heating schedule, 0.11 °C/sec.
He carrier gas flow, 0.40 cm^3/sec.

Tr	ASO_2	atten
256	9.15	0.64
265	2.50	2.56
278	2.36	2.56
299	8.30	1.28
319	10.05	10.24
337	6.00	256
353	12.80	512
365	10.25	1024
376	12.11	1024

Figure 16

FPD sulfur dioxide calibration
3.0 ppm = 10.13 at attenuation of 16
Air flow sweeping catalyst bed, 0.75 cm^3/sec.

Time Min.	Tr	ASO_2	atten
1.57	200	0	
3.68	281	0.38	0.32
5.67	349	2.26	
7.65	409	2.17	
9.65	458	7.06	
11.85	474	7.36	
13.70	526	4.91	16
15.96	548	8.15	32
18.13	567	5.64	64
20.50	582	7.67	64
23.03	592	4.52	128
25.26	599	5.00	
27.57	603	5.06	
30.39	611	4.93	
34.18	614	4.58	
38.56	618	4.19	
42.49	618	3.84	
47.77	620	3.47	
52.77	620	2.95	
58.44	621	2.67	

Figure 16 (continued)

Time Min.	Tr	ASO_2	atten
63.03	621	8.17	32
76.54	621	8.15	↓
74.93	624	7.30	
81.17	↓	6.92	
88.77		5.97	
99.68		5.10	
105.50		4.92	
108.95		4.46	

Figure 17

Data for the initial rate coefficients(steady state) measured along with the unsteady state reaction order runs.

	AE	AEO	AM	Tr	T	f
First day						
10:35 am	1.22	7.58	0.20	227.3	23.0	208.5
10:36 am	inject #500					
11:35 am	5.82		0.02	226.6		
11:42 am	5.60		0.02	226.6		
12:09 pm	4.80		0.03	227.1		86.4
12:25 pm	4.90		0.02	227.1		86.4
12:29 pm	4.40	7.17	0.14	257.1		230.6
12:39 pm	inject #500					
Second day						
1:14 am	4.17		0.14			228.8
7:46 am	4.03	7.29	0.27	279.0	23.6	317.0
7:49 am	inject #500					
8:15 am	4.06	7.29	0.31	279.0	23.6	317.0

Data for two temperature runs.

Third day						
9:32 am	3.37	7.22	0.08	231.1	24.0	38.8
10:20 am	4.08	7.22	0.12	254.9		207.8
11:06 am	3.93	7.32	0.23	275.6		353.1
12:01 pm	3.47	7.28	0.43	310.0		365.0
12:45 pm	3.42	7.28	0.49	316.6		482.7

Figure 17 (continued)

	AE	AEO	AM	Tr	T	f
	Oxidize 9 hr. at 380°C					
Fourth day						
1:00 am	Inject #500					
3:21 am	3.88	7.22	0.05	229.5	24.0	83.8
4:36 am	3.67	7.28	0.19	259.0	↓	200.4
5:38 am	3.53	7.30	0.31	289.0		345.3
6:47 am	2.95	7.30	0.50	305.4		329.2
7:26 am	3.19	7.25	0.51	319.5		449.8

Figure 18

H_2S μ moles	AE	AEO	AM	Tr	T	f	dc/dt = 0	Procedures and Comments
	Second catalyst load 1.66 grams							
	First injection series							
0	2.39	7.95	0.64	309.2	24.4	122.2	-	
58.7	2.65	7.95	0.81	309.2	24.4	121.6	90	
243.0	2.96	7.95	0.92	308.3	24.4	121.6	240	
	Second injection series							out gas CO ads.-des.
243.0	2.77	8.11	0.92	309.8	24.0	124.7	-	
427.4	2.66	8.11	1.06	310.0	24.8	122.9	420	
1753.4	1.52	8.11	1.39	311.0	24.8	120.7	600	
								Out gas CO ads.-des.
	Third poisoning series							
1753.4	2.08	8.05	0.80	248.9	24.4	74.3	-	
1937.3	1.95	8.06	0.85	249.7	24.6	71.2	1410	
3259.3	4.17	7.98	0.59	255.1	24.6	222.6	1200	
								Out gas CO ads.-des.

Figure 19

1 H_2S injection, 1326 μ moles,
427.4-1753.4 μ moles on figure 18.

30 ppm ethane feed, no methane feed
ethane FID calibration 30 ppm = 8.11
sulfur FPD calibration 3.0 ppm SO_2 = 19.93 at atten of 8

Time, min	AH_2S	ASO_2	($^{FPD}_{atten}$)	AE	AM	T	Tr	f
0.0				2.66	1.06	24.8	310.0	122.9
0.68				2.51	1.37			
0.72	0.23	10.35	1024					
4.79	0.45	23.60	1024					
5.81				3.60	0.51			
11.69				3.28	0.30			
11.73		14.6	1024					
14.09				3.89	0.31			
16.73				4.60	0.31			
18.27		29.51	512					
23.31				4.29	0.60			
24.85		48.58	256					
29.88				3.26	0.83			
32.74		31.46	256					
37.03				2.33	0.95			
39.64		19.67	256					
43.11				2.23	1.03			
46.77		12.54	128					
51.38				2.03	1.02			
55.38		18.69						
58.80				2.15	1.07			
62.45		14.73						
65.91				2.02	1.02			
69.91		12.51						
73.15				1.96	1.05			
76.79		10.98						
80.67				1.94	1.06			

Figure 19 (continued)

Time, Min	AH_2S	ASO_2	($^{FPD}_{atten}$)	AE	AM	T	Tr	f
84.36		20.15	64					
88.65				1.85	1.01			
91.92				1.94	1.16			
94.88		17.17						
99.84				1.90	1.15			
106.40		14.91						
120.01				1.94	1.12			
125.38		12.26						
134.70				1.93	1.15			
142.51				1.94	1.23			
152.28		9.04						
170.37		10.01						
184.12		8.24						
187.12				1.95	1.21			
190.47				1.89	1.19			
194.14				1.88	1.19			
197.25				1.91	1.21			
199.94				1.83	1.23			
600				1.52	1.39	24.8	311.0	120.7

Figure 20

30 ppm ethane feed, no methane feed
ethane FID calibration 30 ppm = 8.05
sulfur FPD calibration 3.0 ppm SO_2 = 6.28 at atten of 32

Time, Min	AH_2S	ASO_2	atten	AM	AE	T	Tr	f
0				0.83	2.03	24.4	248.9	74.3
1.0	13.3	18.1	1024	0.83	2.08			
3.33	0	18.9	1024	0.62	4.17			
6.44				0.56	6.06			
8.42		42.14	512					
12.13				0.32	7.02			
15.83		37.52	512					
19.34				0.22	7.55			
22.53		35.71	512					
26.64				0.25	7.90			
30.36		35.49	512	0.19	7.89			
39.53		37.08	512					
43.54				0.10	7.87			
47.61		38.92	512	0.10	7.93			
59.46		40.01	512					
63.50				0.09	7.90			
69.44		40.44	512					
75.17				0.07	7.90			
82.60		41.24	512					
92.47				0.09	7.87			
102.75		40.10	512					
112.90				0.10	7.65			
119.67		37.25	512					
128.02				0.13	7.65			
136.66		34.39	512					
145.79				0.17	7.22			
158.43		29.44	512					
166.53				0.20	7.11			

Figure 20 (continued)

Time, Min.	AH_2S	ASO_2	atten	AM	AE
182.06				0.25	6.72
212.79		13.63	512		
220.50				0.35	6.14
228.34		8.50	512		
239.34				0.36	5.77
256.52		7.81	256		
262.12				0.49	5.25
272.45		8.76	128		
283.60				0.54	4.95
290.87		8.29	64		
303.83				0.60	4.39
317.98		4.58	32		
330.05				0.74	3.91
345.26		6.10	8		
348.68				0.70	3.65
367.60		10.54	2		
371.86				0.82	3.38
388.14		10.55	1		
393.41				0.84	3.12
407.64		5.62	1		
411.02				0.84	3.02
425.06		10.96	0.32		
428.94				0.84	2.93
442.90		8.25	0.32		
448.51				0.87	2.87
458.44		6.32	0.32		
465.96				0.83	2.77
485.95		4.73	0.32		
490.49				0.89	2.65
515.82		2.63	0.32		
536.86				0.89	2.57

Figure 20 (continued)

Time, Min.	AH_2S	ASO_2	atten	AM	AE	T	Tr	f
556.32		3.14	0.32					
568.38				0.91	2.47			
579.22		2.79	0.32					
583.53				0.87	2.39	24.5	249.5	74.5
1406				0.85	1.93	24.6	249.7	71.2